National Library of Canada

Acquisitions and Bibliographic Services Branch

395 Wellington Street
Ottawa, Ontario
K1A 0N4

Bibliothèque nationale du Canada

Direction des acquisitions et des services bibliographiques

395, rue Wellington
Ottawa (Ontario)
K1A 0N4

Your file Votre référence

Our file Notre référence

NOTICE

The quality of this microform is heavily dependent upon the quality of the original thesis submitted for microfilming. Every effort has been made to ensure the highest quality of reproduction possible.

If pages are missing, contact the university which granted the degree.

Some pages may have indistinct print especially if the original pages were typed with a poor typewriter ribbon or if the university sent us an inferior photocopy.

Reproduction in full or in part of this microform is governed by the Canadian Copyright Act, R.S.C. 1970, c. C-30, and subsequent amendments.

AVIS

La qualité de cette microforme dépend grandement de la qualité de la thèse soumise au microfilmage. Nous avons tout fait pour assurer une qualité supérieure de reproduction.

S'il manque des pages, veuillez communiquer avec l'université qui a conféré le grade.

La qualité d'impression de certaines pages peut laisser à désirer, surtout si les pages originales ont été dactylographiées à l'aide d'un ruban usé ou si l'université nous a fait parvenir une photocopie de qualité inférieure.

La reproduction, même partielle, de cette microforme est soumise à la Loi canadienne sur le droit d'auteur, SRC 1970, c. C-30, et ses amendements subséquents.

Canada

Auto-ignition of Liquid Droplets of Single and Two Component Fuels under Pressure

Titus S. Chen

A thesis submitted to the School of Graduate Studies and Research

in partial fulfilment of the requirements for the degree of

MASTER OF APPLIED SCIENCE

in the Department of Chemical Engineering,

University of Ottawa

April 1995

ISBN 0-612-04939-6

Canada

UNIVERSITÉ D'OTTAWA
UNIVERSITY OF OTTAWA

Abstract

Property characterizations and chemical interaction of combustible fuels are important parameters for Diesel engine designers. A simplified approach to gain more insight into this area is to examine ignition of static fuel droplets under physical conditions similar to those experienced in a Diesel engine.

Experimental measurements and model predictions of ignition delay times for single component and two-component liquid fuels are presented. The methodology used is the suspended-droplet/moving-furnace technique, in which a droplet of fuel is suspended from the tip of a thin quartz fibre. A preheated electric furnace moves towards and encompasses the droplet locality, producing a sudden rise in ambient temperature, and thus initiating the ignition process. The entire apparatus is enclosed in a pressure vessel and is remotely operated.

Data were collected for pressures up to 18 atm absolute and in a temperature range of 773 K to 973 K. Physical constraints prevented measurements beyond this pressure limit. Fuels tested comprised *n*-paraffins (decane, dodecane, and hexadecane), aromatics (mesitylene, *o*-xylene, and isobutylbenzene) and a cycloparaffin (decalin), as well as selected binary combinations: *n*-decane/*n*-dodecane, *n*-dodecane/*n*-hexadecane, *n*-decane/decalin, *n*-decane/isobutylbenzene, *n*-decane/mesitylene, and *n*-decane/*o*-xylene. Paraffin measurements at low pressures and high temperature revealed a monotonic decrease in ignition times with increasing pressure. However, higher pressure ignitions at lower temperatures showed more complex behaviour by the measurement of two or "twinned" ignition times for the same pressure and temperature condition, indicating a

change in reaction mechanism, possibly from one-stage to two-stage ignition. Aromatic fuels did not show "twinned" ignition time behaviour and responded with a slight increase in ignition times with inreasing pressure, owing to a weaker reaction rate dependence on pressure. The cycloparaffin behaved analogously to the *n*-paraffin family. The behaviour of mixtures was largely controlled by the more volatile component.

Attempts to model the data were made using a full numerical model of the processes of ignition. Two chemical reaction models were tried out in this model. The first was a single-step reaction model, and the second was a simplified version of a four-step model for *n*-heptane. Although both models could roughly represent some of the trends in the measurements, neither model was capable of being fitted to the complex behaviour of much of the data.

Acknowledgements

The author would like to express his deepest appreciation to several people that made this research possible. Special thanks are owed to the technical professionals at the Department of Mechanical Engineering Technical Shop at the University of Ottawa. The gentlemen are: Mr. Madan Masakare, Mr. Michael Burns, Mr. Kola Porubovic, Mr. Greg Duchesne, and Mr. George Spak. Their laborious work and incomparable craftsmanship provided a functional apparatus, and they were prepared for solutions when maintenance problems arouse.

Finally thanks are extended to contract monitor Dr. Gaston Verville at the Department of National Defence for their financial support and encouragement, and also to my research supervisor Dr. William Hallett for his strong leadership and guidance.

Nomenclature

a	-	fuel concentration exponent
b	-	oxygen concentration exponent
m	-	stoichiometric carbon number
n	-	stoichiometric hydrogen number
A	-	WD pre-exponential factor, units of rate equation in terms of kg, kmol, and cm^3
A_1	-	MPL pre-exponential factor 1, s^{-1}
A_2	-	MPL pre-exponential factor 2, $\frac{cm^3}{gmol \cdot s}$
A_{2OVL}	-	MPL 2nd-order overall pre-exponential factor *2*OVL, $\frac{cm^6}{gmol^2 \cdot s}$
A_{3f}	-	MPL pre-exponential factor 3f, $\frac{cm^3}{gmol \cdot s}$
A_{3b}	-	MPL pre-exponential factor 3b, s^{-1}
A_4	-	MPL pre-exponential factor 4, $\frac{cm^3}{gmol \cdot s}$
E	-	activation energy, $\frac{J}{gmol}$
$E_1/\tilde{R}$	-	MPL activation temperature 1, K
$E_2/\tilde{R}$	-	MPL activation temperature 2, K
$E_{2OVL}/\tilde{R}$	-	MPL second-order overall activation temperature *2*OVL, K
$E_{3f}/\tilde{R}$	-	MPL activation temperature 3f, K
$E_{3b}/\tilde{R}$	-	MPL activation temperature 3b, K
$E_4/\tilde{R}$	-	MPL activation temperature 4, K

F	-	fuel species
I, X	-	intermediate species
k	-	rate constant, s^{-1}
m	-	mass, kg
$\dot{m}$	-	mass flow rate, $\frac{kg}{s}$
M	-	mixture molecular weight, $\frac{kg}{kgmol}$
M_F	-	molecular weight of fuel, $\frac{kg}{kgmol}$
M_O	-	molecular weight of oxygen, $\frac{kg}{kgmol}$
O	-	oxygen
P	-	product species
p	-	pressure, atm
ρ	-	mixture density of fuel and air, $\frac{kg}{m^3}$
$\tilde{R}$	-	gas constant, $\frac{kJ}{kgmol \cdot K}$
r_1, r_2, r_{3f}, r_{3b}, r_4	-	MPL global reaction rates, $\frac{kg}{m^3 \cdot s}$
r_{fuel}	-	overall reaction rate of fuel, $\frac{kg}{m^3 \cdot s}$
r_1	-	reaction rate of fuel component 1, $\frac{kg}{m^3 \cdot s}$
r_2	-	reaction rate of fuel component 2, $\frac{kg}{m^3 \cdot s}$
t	-	time; ignition delay time, s
t_{corr}	-	corrected ignition delay time, s
T	-	temperature, K
T_{lig}	-	chamber liquid temperature, K
X	-	molar fraction, $\frac{kgmol_{fuel}}{kgmol_{mix}}$
y	-	mole fraction, $\frac{kgmol_{fuel}}{kgmol_{mix}}$

Y	-	mass fraction, $\frac{kg_{fuel}}{kg_{mix}}$

Nomenclature subscripts

F	-	furnace
V	-	vessel
F	-	fuel
O	-	oxygen
1	-	fuel species 1
2	-	fuel species 2
1	-	first-order MPL model subscript
2OVL	-	second-order overall MPL model subscript
corr	-	corrected measurement
meas	-	experimental measurement
model	-	model prediction
model@40°C	-	model prediction at 40°C chamber temperature

Table of Contents

List of Figures

List of Tables

CHAPTER ONE

Introduction

The use of unconventional or off-specification fuels, such as tar sands fuels or alcohols, in Diesels and gas turbine engines requires, among other things, knowledge of how the fuel properties will affect ignition behaviour. The ignition delay in a Diesel can strongly influence engine power, efficiency, and vibration; in a gas turbine, flame stabilization and re-light can be affected. The future use of alternative fuels may be mandated by environmental considerations (for example, alcohols for bus engines to meet particulate emission standards) or by future supply considerations (tar sand products as substitutes for dwindling conventional petroleum reserves). Unfortunately, the literature shows that the conventional method of assessing the ignition quality of Diesel fuel - the cetane number - does not work well for unconventional fuels, especially those of low ignition quality (Ryan and Stapper, 1987; Pischinger *et al.*, 1988). This is a problem with tar sands derivatives, and even more so with alcohols, and it is becoming clear that alternative means of predicting ignition behaviour are required.

The research presented here is a further step in developing models of the chemical and physical processes of ignition for liquid fuels under Diesel and gas turbine conditions, with the long-term goal of being able to predict the effects of fuel physical properties (in particular the boiling range) and chemical composition of the fuel on ignition performance. It is expected to ultimately benefit the fuel supply industry as well

as fuel users. The ability to predict the ignition behaviour of fuels would allow producers to assess the effects of feedstocks, blending, additives, and process changes on the product quality, while for the user it would give guidance in fuel selection and specification.

1.1 Auto-ignition

The ignition process of fuel and oxygen involves chemical reaction accompanied by rapid evolution of heat and emission of light. Auto-ignition refers to self- or spontaneous ignition when the combustible is exposed to air at a temperature above its spontaneous ignition temperature under a given set of experimental conditions, without the assistance of a spark or flame (Mullins and Penner, 1959). Even though induced or forced ignition is dissimilar from auto-ignition, both processes require some form of mixing between fuel and oxidant before full-fledged combustion occurs.

Auto-ignition has direct applications in Diesel engines and gas turbines, in which fuel properties can affect ignition delay and flame stabilization. Diesels are more efficient, powerful, and require a lower quality of refined fuel than their gasoline counter-parts.

Gas turbines are exclusively used to power all new commercial airplanes, as well as some ships, trains, and electric power generators and gas pipeline compressors (Bathie, 1984). The turbine basically consists of a gas generator, comprising a compressor and a combustion chamber, together with a power turbine. Hot gases are produced in this combustion chamber and by recirculating these burned gases back to the incoming fuel-air mixture, sustaining the ignition of fuel. This process is termed flame stabilization and the arrangement results in a high temperature and high pressure gas within and at the exit of the combustor (Bathie, 1984).

By studying fuel properties and how fuels ignite in Diesels and in gas turbine engines one can greatly influence engine performance, fuel economy, and pollution emissions.

1.1.1 Description of Diesel ignition

Figure 1.1 shows the processes of a typical four stroke cycle in an automotive Diesel. The first process is the air intake stroke in which air is drawn in by the downward motion of the piston as the intake valve opens. In the compression stroke, the air is compressed in the combustion chamber to very high pressures, ≈60 atm. This process occurs almost adiabatically, causing the internal gas temperature to rise to about 700°C. Towards the end of the stroke, fuel is introduced into the chamber by a high pressure fuel injector. The fuel enters at large velocities relative to the air from several small nozzles. This disintegrates the fuel jet into very fine droplets, forming a spray (Benson, 1979). The droplets evaporate and the fuel vapours mix with the air through swirl, diffusion, turbulence, and forced convection. Ignition does not proceed immediately because the mixing process is occurring simultaneously with chemical reaction. Reaction is initially slow, which allows an appreciable amount of fuel vapour to become premixed with oxygen. As mixing proceeds to near stoichiometric proportions at the reaction zone, ignition in a particular region occurs and initiates reaction in other parts of the mixture. Soon full combustion proceeds and combustion is sustained by the rate of fuel injection and by the rate of diffusion. Given the very short time allotted for fuel injection during the compression stroke, the fuel must be able to ignite under the conditions of high pressure and temperature. Thus, the ignition delay of fuels becomes a very important parameter for modelling the processes that occur inside a Diesel.

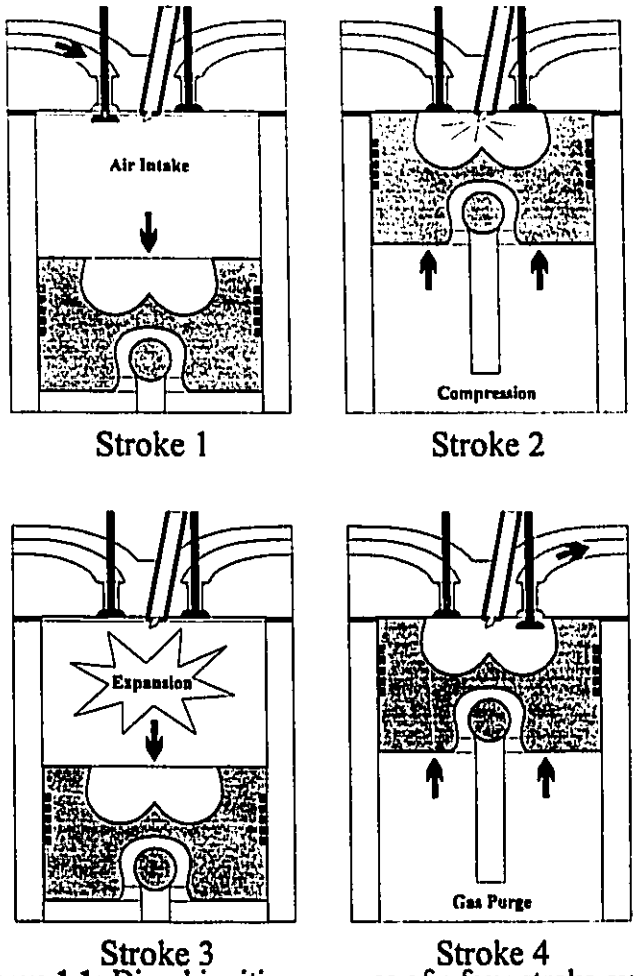

Figure 1.1: Diesel ignition process of a four-stroke cycle.

1.1.2 Description of gas turbine ignition

The combustor "can" is essentially a straight duct with a perforated liner. This liner not only provides recirculatory flow for re-light and flame stability, it also admits unconsumed air downstream to mix with the burned combustion products and thereby reduce the temperature to a value that is acceptable to the turbine. The combustion of gases takes place in three zones, all located downstream in series from the fuel nozzle. The first is the primary combustion zone, followed by the intermediate combustion zone and the dilution zone. Most of the ignition and combustion of the fuel-air mixture occurs in the primary zone, and the perforated shell anchors the flame and provides sufficient residence time, turbulence, and high temperatures to essentially produce complete

combustion of fuel (Lefebvre, 1983). The intermediate zone is present for conditions where low pressures exist. Under low pressures, the rate of reaction in the primary zone is slower, owing to lower concentrations of fuel and air, and the combustion is far from complete at the exit of this zone. The function of the intermediate combustion region is simply to serve as an extension to the primary zone, by providing added air and increased residence time at high temperatures that are necessary to complete the reaction. The last region is not a combustion zone but rather a gas dilution zone that serves to cool the gas to an acceptable level.

1.2 Description of droplet ignition under pressure

The modelling of Diesel engine and gas turbine ignition can be very complicated because it involves detailed descriptions of spray mechanics, forced convection, diffusion, heat transfer, and chemical reaction. An understanding of single static droplets of fuel exposed to high temperature and pressure is required before exploring more complex ignition processes. In this work we focus on droplet ignition, because a droplet is the basic unit in a fuel spray, and we gain insight by studying the auto-ignition of pure hydrocarbons and their two-component mixtures under high pressures and temperatures. The need to study mixtures of fuels is significant because typical Diesel fuel and jet fuel blends contain many heavy paraffins, olefins, and aromatics, and ignition is governed primarily by the chemical nature and boiling points of the most volatile constituents of the fuel (Hallett and Ricard, 1992).

Three processes occur when a liquid fuel droplet is exposed to high temperatures and pressures: evaporation, diffusion, and chemical reaction. Figure 1.2 shows the fuel diffusing out radially from the droplet surface, driven by the concentration gradient of fuel. As the droplet is heated by heat conduction and convection from the hot surrounding air and by radiation from surrounding walls, the fuel begins to evaporate and diffuse

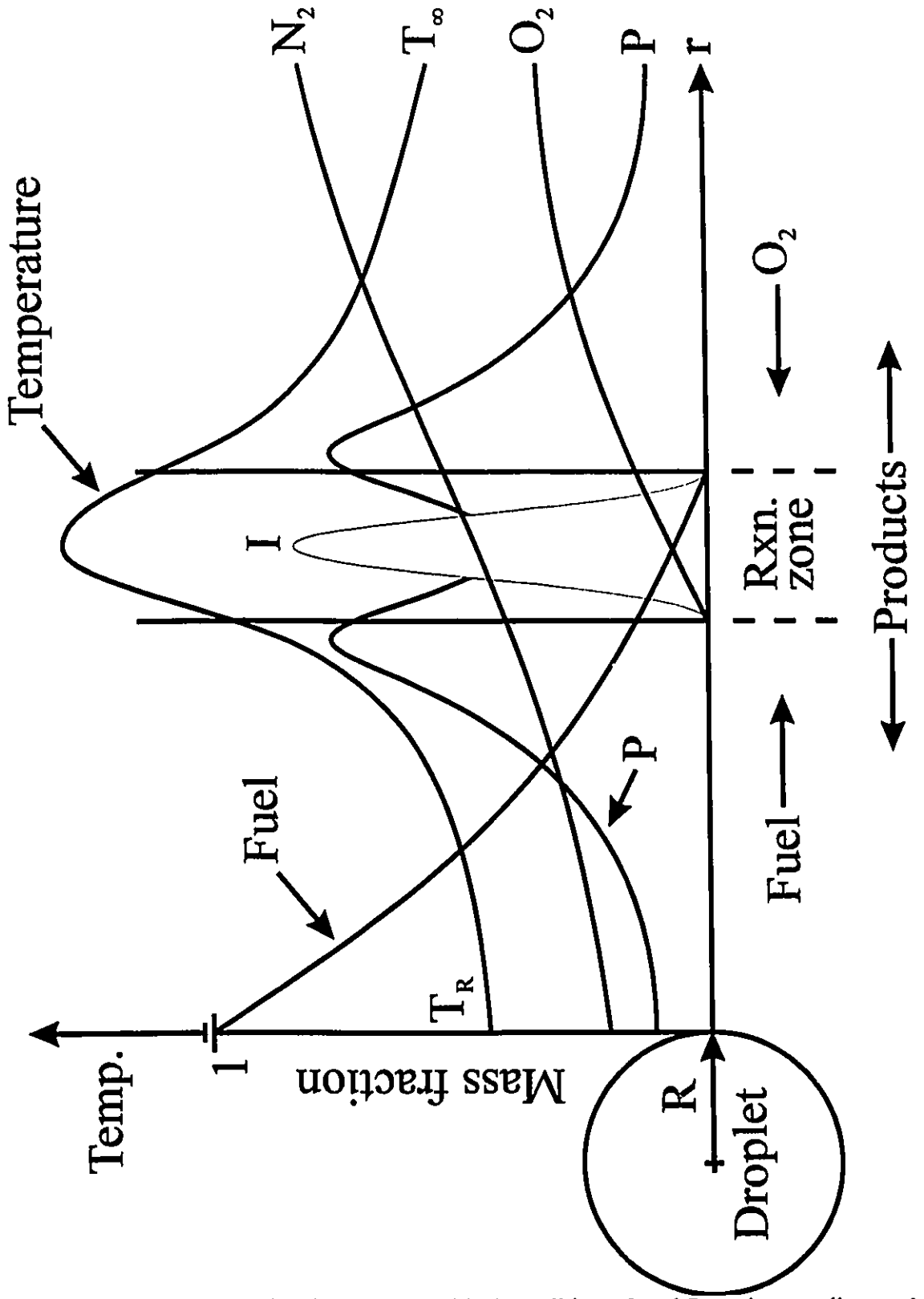

Figure 1.2: Droplet combustion for sub-critical conditions. I and P are intermediate and product species, respectively.

outward and the amount of fuel vapour present is dependent on the rate of evaporation and diffusion. Since oxygen and nitrogen molecules completely surround fuel molecules, they also diffuse towards and into the droplet surface, by means of the concentration gradients. Both air and fuel diffusion are accelerated by high pressures. Diffusion can also be affected by natural convection, which is driven by the density difference between fuel vapour and air. Free convection can also contribute to further mixing of fuel and air.

Chemical reaction can occur wherever fuel vapour and oxygen meet. This intersection region is the incipient reaction zone, which will later be the flame front once ignition occurs. At time zero (as the fuel is first exposed to high temperature and pressure), chemical reaction is initially slow and contributes little to raising the reaction zone temperature. As more and more fuel molecules collide with oxygen the reaction accelerates, which raises the temperature further, until thermal runaway occurs - this is ignition.

A rapid rise in temperature at a particular point encompassing the droplet surface, signals ignition of a small volume of fuel-air mixture. As the reaction progresses it is sustained by the rate of diffusion of both fuel and oxygen. Intermediate and product species evolve from the flame zone and they diffuse outwards and towards the evaporating droplet. The flame zone is the area where temperatures are greatest.

1.3 Objectives

The goal of the present research was to investigate droplet ignition under pressure by measuring ignition delay times of droplets of selected pure hydrocarbons and two-component mixtures with respect to temperature and pressure. Numerous data are available for droplet vaporization of pure hydrocarbons under pressure. However, only one publication, by Kadota and Hiroyasu in 1976, has dealt with single droplet ignition under pressure.

A second objective of the work was to explore the use of two different simple reaction kinetic schemes in an existing numerical model of droplet ignition, and if possible to fit their reaction rate parameters for different fuels.

1.4 Method

The approach used was the suspended-droplet/moving-furnace technique, in which a droplet of fuel is suspended from the tip of a thin quartz fibre and a preheated electric furnace moves towards and encompasses the droplet region, producing a sudden rise in temperature. The entire apparatus was enclosed under pressure and was operated remotely.

1.5 Outline

The thesis begins with a literature survey, followed by methodology, experimental procedures, results and discussion, conclusions and recommendations, and finally appendices. Sample and property calculations are presented in the appendices.

CHAPTER TWO

Literature Survey

Past research into droplet ignition has been focused on single droplets suspended on a fibre or thermocouple, or on free drops falling through hot air, in order to gain fundamental insight into ignition, combustion, and evaporation processes which can then be applied to sprays. Most published information to date on droplet ignition has been concerned with experiments done at atmospheric pressure; at high pressure little ignition data are available, not for a lack of motivation or intent, but rather because of the experimental difficulties involved. Most of the high pressure literature deals therefore with evaporation and combustion of droplets rather than ignition.

2.1 Experimental studies

Two main experimental techniques are used to explore droplet ignition, evaporation, and combustion: the suspended-droplet method and the free-falling droplet method. The suspended-droplet technique is simple to employ and allows events to be easily observed. A fuel droplet is hung from the tip of a fibre of an inert material (usually quartz) on which a rounded bead is formed to support the droplet. Sometimes a chromel-alumel thermocouple is used instead of a quartz filament, so that the liquid temperature can be recorded. The suspended droplet is subjected to a sudden rise in temperature by moving a preheated hot furnace into a position surrounding the droplet, heating the droplet and

beginning the auto-ignition process. Ignition at a particular point in the fuel-air boundary layer then spreads to other parts.

The free-falling droplet technique allows a fuel droplet to fall freely through a hot air column, leaving behind a trail of vapour which mixes with the air, producing combustible mixtures. If conditions are suitable, ignition occurs in this mixture in the wake of the droplet (Satcunanathan, 1970). This geometry of ignition was explored by Satcunanathan and others. The method can eliminate the effects of natural convection and droplet distortion from spherical symmetry, but at the expense of introducing forced convection and a different ignition mechanism.

A third experimental technique is that of using a porous sphere to study purely steady state droplet evaporation and combustion (Canada and Faeth, 1972, 1974), but this is not suited to ignition. The porous sphere, usually a catalyst support pellet (containing many micro-pores), is affixed permanently to the tip of a hypodermic needle or syringe, such that the tip resides in the centre of the sphere. As fuel is injected, it channels through the pores and wets the entire surface. The sphere is usually ignited by a hot wire ignitor or subjected to a flow of hot gases, and evaporation rates and flame sizes are investigated with steady flows of fuel to the sphere surface.

2.1.1 Droplet ignition at atmospheric pressure

Not all the work on droplet ignition at atmospheric pressure is reviewed in this section. Only those of most interest were selected. A more detailed review is presented by Bergeron and Hallett (1989b).

Faeth and Olson (1968) ignited suspended hydrocarbon droplets, using a quartz fibre for droplet support. The sudden rise in ambient temperature was achieved by means of a preheated furnace which approached the droplet from above. In order to investigate the effects of natural convection, some runs were performed under reduced gravity by allowing the whole apparatus to free-fall 16' into a tub of styrofoam. Fuel vapour, being

heavier than air, normally produces a downward net convective flow around the droplet; this could be virtually eliminated in this way. Ignition delay times were measured as a function of droplet diameter and temperature by a 16 mm camera. Faeth and Olson concluded that droplet diameter had little or no effect on ignition delay under zero and natural gravity conditions. Ignition delay times increased very slightly with increasing droplet diameter, but decreased slightly with the effect of natural convection. More information on natural convection is presented in section §2.3. Times also decreased monotonically with increased temperature. Bergeron and Hallett (1989b) also measured the ignition times of liquid hydrocarbon fuels as single droplets suspended from a quartz fibre. Ignition times decreased with temperature and an identification of a kinetic two-stage ignition was observed at high temperatures.

Hall and Diederichsen (1953) were among the first researchers to investigate free-falling single droplets of fuel in air. Kerosene fuel was injected onto the centre of a rotating metal disc. The centrifugal force caused the fuel to migrate towards the edge of the disc upon which fuel would accumulate over time. When sufficient fuel was present a droplet would form by agglomeration and leave through a stationary narrow slit. The slit acted as a heat shield and protected the fuel droplet from convective hot air flow. Released droplets were immediately exposed to a heated column of air at 710°C and the combustion burn times, with respect to droplet diameters, were recorded. Burn times increased logarithmically with increasing droplet size. Satcunanathan (1970) chose a slightly different fuel delivery system, releasing droplets individually from a fine hypodermic needle that was fed from a burette of fuel. The fuel drops, some paraffins and kerosene, were allowed to fall through a heated tube furnace and the ignition phenomena recorded by a 16 mm ciné-camera. A shutter covered the furnace orifice to minimize the heat losses. Ignition delay times decreased logarithmically with increasing temperature. Satcunanathan concluded that ignition delay times for various pure hydrocarbon fuels are

strongly dependent on the physical properties of these fuels, and that the effect of pressure on ignition delay needs investigation.

Free-falling ignition delay times of droplets tend to be much shorter than suspended ignition delay times. This is due to the markedly different mechanism of ignition, the former being ignition in the vapour trail of the droplet's wake and the latter in the boundary layer around the evaporating droplet, termed "envelope" ignition (Drisdelle, 1990).

El-Wakil and Abdou (1966) suspended *n*-paraffin hydrocarbon droplets from a fine-wire thermocouple. The droplet was exposed to a hot air stream from below. Atmospheric pressure experiments were conducted for a temperature range from 785°C to 980°C and ignition delay times, burning phase times, liquid temperature histories, flame size and droplet diameters were recorded with thermocouples and rapid cinematography as a function of air temperature, droplet diameter, and air flow velocity past the droplet. The ignition delay time is defined as the time taken between the initial exposure to the hot ambient gas to the time droplet ignition occurs, and the burning phase time or droplet lifetime is defined as the time between the start of induced ignition to the disappearance of the visible flame. El-Wakil and Abdou discovered that ignition delay times decreased with increasing temperature, at a constant air velocity and droplet size. This experimental study combines elements of the suspended-droplet and falling-droplet techniques because the suspended droplets were exposed to a forced convective stream of hot air, which may have produced similar characteristics to wake ignition. This consolidation of methods makes it difficult to classify and compare these results with those of other researchers.

2.1.2 Ignition, combustion, and evaporation under pressure

Only one paper reports droplet ignition under pressure, that of Kadota *et al.* (1976). They followed Faeth and Olson's methodology of the suspended-droplet/moving-furnace technique, with the preheated furnace falling freely by its own weight over a quartz

suspended fuel droplet. However, Kadota *et al.* decided not to use their apparatus in free fall because of Faeth and Olson's conclusion that natural convection did not appreciably affect the ignition delay of hydrocarbons. They were able to conduct ignition experiments using *n*-paraffin fuels for pressures up to 41 atm, but at the relatively low temperature ranges: 220°C-345°C @41 atm, 320°C-480°C @21 atm, and 425°C-700°C @1 atm. These are well below the temperatures encountered in Diesels and gas turbines. The light emission from ignition was detected by a photo-transistor, which was connected to an oscilloscope. Kadota *et al.* concluded that for *n*-paraffin hydrocarbons ignition delay times decreased logarithmically with increasing pressure, ignition times decreased with carbon number, and under pressure droplet diameter had little effect on ignition. Today, their experiments remain the only published data on high pressure ignition of suspended fuel droplets.

For free-falling experiments, Goodger and Eissa (1987) used apparatus similar to Satcunanathan (the Cranfield pressure rig) to record spontaneous ignition delays of a paraffin, an olefin, and kerosene for pressures up to 30 atm. Unlike Satcunanathan, the Cranfield pressure rig did not have a furnace shutter covering the top opening of the furnace column, and thus had natural convective air flows from the furnace. The droplet was shielded by a shutter prior to its release, but once exposed to the furnace column it was subjected to the convective flow. Under the influence of pressure, free-falling droplet ignition delay times were again shorter than those for suspended droplet methods.

Other past research on suspended and free-falling droplets under pressure has focused on combustion and evaporation, and deals with quasi-steady burning and evaporation rates, burning times, and flame size measurements. Hall and Diederichsen (1953) studied the combustion of single fuel droplets of furfuryl alcohol, tetralin, decane, and amyl acetate, and measured the total burning times over a pressure range from one atmosphere to twenty atmospheres, as determined by high speed direct ciné-photography of the combustion event. The droplets were hung from a quartz filament and were ignited

by a small coal gas diffusion flame. Faeth *et al.* (1969) and Lazar and Faeth (1970) observed burning rates and combustion lifetimes of *n*-paraffin hydrocarbons under zero gravity conditions in a free-fall apparatus for pressures up to 2.5 times the critical pressure of the fuels. Suspended droplets were hung from a thermocouple and were ignited by a hot wire electric ignitor. Droplet photographs were recorded by high speed photography at a rate of 100 frames per second. Kadota and Hiroyasu (1980) measured combustion lifetimes of paraffin hydrocarbons at up to three times the critical pressure of the fuels by modifying the existing apparatus of Kadota *et al.* (1976) to include a resistance coil ignitor. All the above combustion researchers found that for paraffin hydrocarbons the burning lifetimes decreased and the burning rates increased with increasing pressure and droplet diameter.

Savery and Borman (1970) followed El-Wakil and Abdou with similar experiments using suspended droplets of Freon 13 refrigerant and *n*-heptane on a thermocouple bead with a uniform upward hot air flow flowing pass the droplet region. However, they did not investigate combustion, unlike their predecessors, but rather droplet evaporation at low temperatures (35°C to 150°C). The experiments were conducted for pressures up to 100 atm and it was found that evaporation rates increased with pressure. Matlosz *et al.* (1972) had similar results from investigations of high pressure evaporation of *n*-hexane droplets, suspended on a chromel-alumel thermocouple, for pressures up to 102 atm at 275°C.

A porous sphere study was conducted by Canada and Faeth (1972), who investigated the steady-state burning rates of fuels for pressures up to 100 atm. The evaporating fuel was ignited by a hot wire ignitor and data was collected by means of cinematography. In another geometry, Canada and Faeth (1974) ignited the spheres in the hot gases of combustion products to observe combustion behaviour (burn rates) that would be analogous to gas turbine combustion. Experiments were conducted using some short chained alcohols and some *n*-paraffin hydrocarbons to pressures of 40 atm.

2.1.3 Comparison of experimental techniques

The main advantages of the suspended-droplet technique are:

- the generation and observation of droplets is simple, as the droplets are fixed in space;
- the construction of apparatus, particularly for experiments under pressure, is simple;
- the process taking place can be reasonably approximated by a spherical symmetry symmetrical model, and the relative simplicity of such a model allows attention to be focused on the fundamental processes involved.

However, some drawbacks of the method, not present for falling droplets, are the effects of fibre disturbances that can cause distortions of the droplet shape, the possibility of heat conduction through the support fibre[1], and the need to use larger droplets than would be normally formed in a spray.

The principle advantages of the free fall method are that smaller droplet sizes can be studied without interference from the suspension support, and that the droplets are reasonably spherical. Drawbacks of the approach stem from complications with ciné-photography, to the convective air flow (forced convection), to experimental complexity, and to difficulties with modelling free-fall or wake ignition (Drisdelle, 1990).

Porous spheres are useful for detailed studies of flame geometry and stability, and for comparison with numerical descriptions. However, the large apparent droplet size leads to greater natural convection, and transient processes, such as ignition, cannot be simulated at all.

[1]The use of a thermocouple rather than quartz as a support fibre has the disadvantage of high thermal conductivity from the thermocouple casing, which can accelerate the droplet transient heating process.

2.2 Effects of natural convection

A difficult problem with all droplet ignition investigations is the effect of natural convection, because evaporating fuel vapour is heavier than air and tends to flow downward from the droplet region. Natural convection may change the site of stoichiometric reaction and can lead to stochastic variation in recorded ignition times.

Faeth and Olson (1968) and Sangiovanni (1978) have both looked into the effect of natural convection on droplet ignition. Faeth and Olson discovered from their experimental results that the effect of natural convection under atmospheric pressure was negligible in contributing to the overall ignition delay of the fuel. However, they suggested that natural convection may have greater influence at higher pressures. Sangiovanni (1978) performed a numerical study into the unsteady ignition and combustion of a fuel droplet with and without convection. His calculations revealed that predicted ignition delay times were 6 and 12% lower with free and forced convection respectively than with pure diffusion. He also concluded that droplet vaporization and liquid temperature were nearly independent of the mode of gas-phase heat and mass transfer.

Sato *et al.* studied the effects of natural convection on droplet combustion at elevated pressure using a free-falling apparatus similar to that of Faeth and Olson (1968). They found that natural convection increased the droplet burning rate by 37% at atmospheric pressure, by 260% at the critical pressure, and by 290% at 1.4 times the critical pressure; natural convection decreased the burning lifetime by 38% at atmospheric pressure, by 68% at the critical pressure, and by 73% at 1.6 times the critical pressure. However, the main reason for this was that natural convection caused the flame to move much closer to the droplet, greatly increasing heat transfer rates to the surface. For droplet evaporation without combustion or for ignition the absence of a flame would considerably reduce the effect of convection, as shown by Faeth and Olson and Sangiovanni.

2.3 Models of droplet behaviour at high pressure

A realistic high pressure droplet ignition model must consider the physical and chemical processes contributing to ignition, but also the non-ideal vapour-liquid equilibrium behaviour, the penetration of air into the liquid, and the increasing role of transient processes as the gas becomes denser at higher pressure.

Since modelling is not the main subject of this work, only a brief review of models will be given. For a more complete review, refer to Ruszalo and Hallett (1992). This section refers to high pressure numerical models; atmospheric pressure models will not be mentioned, even though many past studies have been conducted, such as those of El-Wakil and Abdou (1966) and Faeth and Olson (1968). A more detailed review is given by Bergeron and Hallett (1989b).

2.3.1 Ignition delay models

Only two models for droplet ignition at high pressure are present in the literature. Kadota *et al.* (1976) fitted a simple correlation to their high pressure ignition data; this did not include a complete physical description of the process, but was merely an empirical equation to relate ignition delay time to pressure and temperature. Ruszalo and Hallett (1992), developed the droplet model used for this study, basically extended the earlier atmospheric pressure model of Bergeron and Hallett (1989b) to include high pressure effects of liquid phase diffusion, air penetration, and a Peng-Robinson equation of state for the vapour-liquid equilibrium (*VLE*) approximation. Bergeron and Hallett had devised numerical solutions to the continuity, diffusion, energy, and chemical reaction equations, coupled with energy and mass balances on the droplet. This gives a complete transient description of droplet ignition.

2.3.2 Droplet evaporation and combustion models

The other models reviewed here are for pure evaporation or fully-developed combustion rather than ignition.

2.3.2.1 Quasi-steady models

One of the earliest physical descriptions of droplet processes is to approximate droplet combustion and evaporation as quasi-steady (*QS*). This theory assumes uniform properties, reaction stoichiometry, and a spherically symmetric fuel droplet evaporating radially outward into a large static gas reservoir of air. The main feature of this model is the omission of transient terms from the governing equations, which is justified by the assumption that the rate of change of droplet radius is slow compared to other processes; thus, the $\partial/\partial t$ terms are neglected. Spalding (1959) used a quasi-steady model along with a transient model he developed, so as to compare the predicted fuel burn times. Wieber (1963), Rosner (1967), and Lazar and Faeth (1970) developed a form of quasi-steady theory. Manrique and Borman (1969), Savery and Borman (1970), and Kadota and Hiroyasu (1976) have examined quasi-steady state droplet vaporization at high pressures. Quasi-steady models approximate the transient process by slowly varying the sequence of steady states (Rosner and Chang, 1973). Generally, it was discovered that the quasi-steady theory agreed reasonably well at low pressures, but at pressures approaching or above the critical pressure of the fuel, deviations from theory clearly occurred.

2.3.2.2 Transient models

Transient effects tend to dominate the burning processes at high pressures, and this motivated Spalding (1959) to abandon the quasi-steady model and to adopt a new theory to include the transient terms. Spalding's theory comprises of two parts, with the first part establishing the mixture composition with respect to space and time, and the second part making the distinction between fuel fraction and mass fraction of unburned fuel.

Comprehension of reaction stoichiometry allows the first part of the theory to be used to predict the transient burn rate of the fuel. This model treats the liquid phase as a denser gas and predicts the burn times and flame radius of fuel droplets at supercritical pressures only.

Much more realistic models have been contrived recently, such as those of Rosner and Chang (1973), Lee and Fernandez-Pello (1986), Shuen *et al.* (1992), and Curtis and Farrell (1992). They all have looked at vaporization and combustion of droplets at high pressures, either by extending the *QS* theory to estimate droplet lifetimes (Rosner and Chang, 1973), or by developing complete solutions of the governing equations of diffusion, energy and mass (Lee and Fernandez-Pello (1986), Shuen *et al.* (1992), and Curtis and Farrell (1992)). Some of these models have used the Redlich-Kwong equation of state (*EOS*) to approximate the vapour-liquid equilibrium, while others have used the Peng-Robinson *EOS*.

2.4 Multi-component models

Commercial liquid fuels are not pure hydrocarbons but mixtures, usually with hundreds of components. In view of this, efforts have been made recently to extend droplet theories to mixtures. Most of the literature on the subject deals with simple binary mixtures. The main issue is the state of mixing in the liquid phase, which controls the liquid composition at the surface and hence the vapour flux and composition. Two limiting cases exist: the well-mixed liquid, in which the liquid composition is assumed uniform and evaporation proceeds as a batch distillation; and the diffusion-limited liquid, in which molecular diffusion is the only transport process within the droplet. Real droplet behaviour falls between these limits.

All real droplets exhibit some degree of internal circulation. This problem was investigated by Tong and Sirignano (1986) and Talley and Yao (1986). Tong and Sirignano stated that in the absence of internal circulation, only diffusion transport takes

place inside the droplet. However, this condition is unrealistic, so they developed their numerical model to include internal circulation by assuming the existence of a Hill's spherical vortex inside the droplet. More will be said about droplet internal circulation for two-components in section §4.3.

Talley and Yao (1986) showed that the effects of internal circulation on evaporation could be approximated by radial diffusion of components with the value of diffusivity enhanced to account for the more rapid mixing. This results in a much simpler, yet reasonably accurate, treatment of liquid phase processes and has been the model used in most multi-component droplet calculations since then.

A study of mixture ignition at high pressure is present, that of Ruszalo and Hallett (1992), who extended their numerical model for pure fuels by including liquid-phase diffusion in the manner of Talley and Yao (1986). Bergeron and Hallett (1989a) and Hallett and Ricard (1992) investigated droplet mixture ignition at atmospheric pressure. Other recent works have examined evaporation without reaction at high pressure. Jin and Borman presented evaporation models which coupled the transport properties to form a simple quasi-steady description, while Hsieh *et al.* (1988) developed a two-component vaporization model which include a full transient solution of state equations, using the Redlich-Kwong *EOS* for the *VLE*.

To date no mixture ignition experiments have been published at high pressure.

CHAPTER THREE

Experimental Apparatus and Techniques

This chapter focuses on the techniques used to conduct the experiments. It reports all aspects involved in the measuring the ignition delay times of fuel droplets, which includes a detailed description of the apparatus and experimental procedure, and some experimental limitations and maintenance procedures.

3.1 Suspended droplet/moving furnace method

For reasons cited in the literature survey (§2.1.3), the experimental method of choice was the suspended droplet/moving furnace technique, even though the falling droplet method may more closely resemble the processes that occur in some sprays. Because of their importance, the arguments cited in §2.1.3 will be briefly summarized here. Suspended droplets offer simple generation and observation because the droplets are static in space. The difficulty of apparatus construction, particularly for experiments under pressure, is reduced. Finally, the physical process can be approximated by a spherically symmetric model, thus allowing one to focus on the fundamental processes involved. However, some drawbacks stem from the effects of fibre disturbances such as thermal conduction through the support fibre, distortions of the droplet shape from spheroidicity, larger droplet sizes than would normally appear in a spray, transient convective flow from the

moving furnace, and the presence of natural convection (which can only be eliminated by the use of a free falling apparatus). The possible effects of these will be discussed later in §3.4.

The disadvantages of the suspended droplet technique might suggest that the other method (free falling droplets) would be better. However, the free fall technique has greater disadvantages due to the difficulties involved with the ciné-photography of free falling droplets, the experimental complexity of the apparatus, and the completely different mode of ignition (by forced convection) known as wake ignition. Wake ignition is an arduous task to model, requiring solution of the fluid flow about the droplet in addition to heat and mass transfer; moreover, this must be done in two dimensions in the fairly complex geometry of the droplet wake. This makes it difficult to focus attention on the fundamental processes. The last consideration negates any other advantages the method may possess.

3.2 Experimental apparatus

Figure 3.1 shows a cross-section of the experimental apparatus. A liquid fuel droplet is hung on a bead at the tip of a quartz fibre (1) supported from a stationary steel rod (2). A fuel droplet, supplied from a pressurized fuel reservoir, is placed on the fibre by transfer from a fuel injector probe (3) by orienting the injector tip towards the fibre shaft.

The furnace (4) is preheated to a desired temperature, as indicated by a fixed thermocouple (5), and is raised by the furnace air cylinder (6) to a position such that the centre of the droplet bead is in the centre of the furnace cavity. A shutter (7) which is actuated by a lever riding in a guide rail (8) keeps the furnace opening closed until the droplet is just about to enter. A photo-diode array (9) monitors the light intensity around the droplet region inside the raised furnace. Light is focused onto the diode array by means of two lenses (10), and the diodes are connected to a digital storage oscilloscope (11) which records the signal. The oscilloscope is triggered by a micro-switch (12) that is

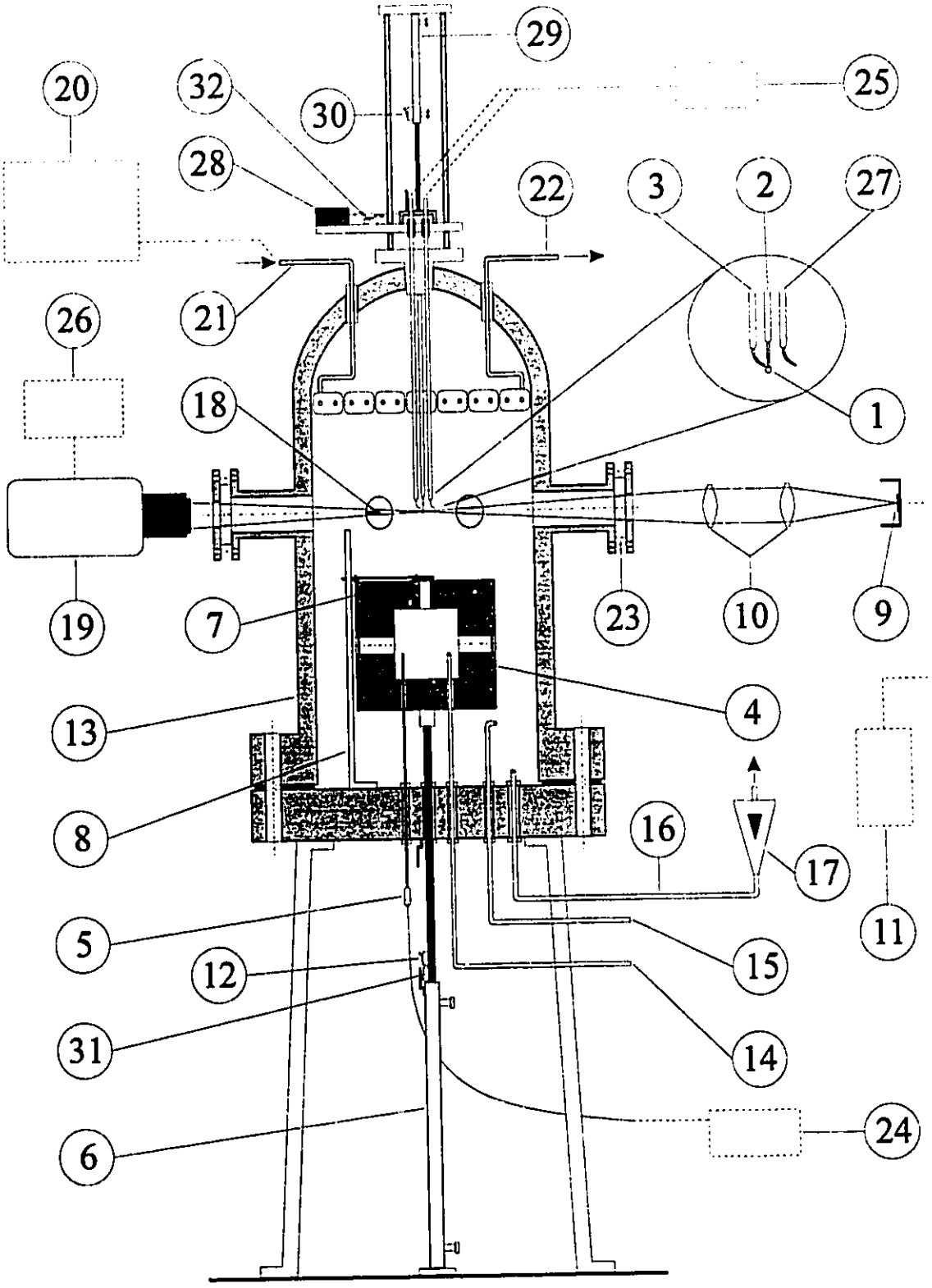

Figure 3.1: Cross-section of experimental apparatus. Part numbers are keyed to description in text.

activated upon impact with a strike plate as the furnace drive cylinder approaches the top of its travel. The switch timing coincides with the moment the droplet is entering the hot environment. When ignition occurs, emission of light from the flame causes the oscilloscope trace to rise suddenly, as indicated by Figure 3.2, and the ignition delay time can be measured. The term ignition delay time is defined as the time elapsed for a fuel droplet to auto-ignite or spontaneously ignite, from the time of initial droplet exposure to the hot environment to the time when ignition is first detected.

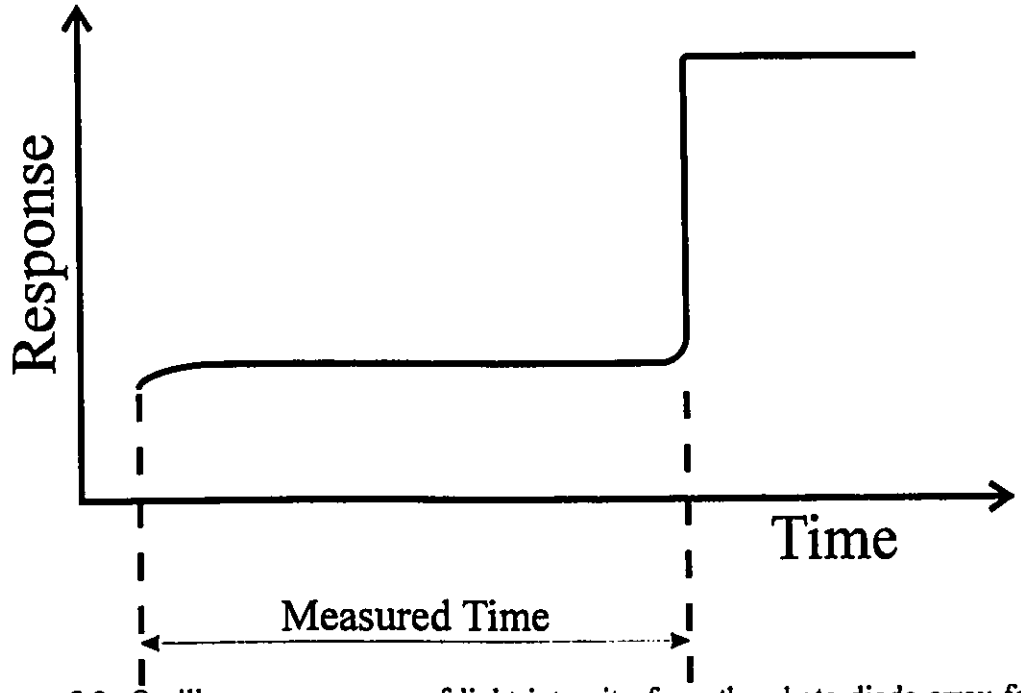

Figure 3.2: Oscilloscope response of light intensity from the photo-diode array for the measurement of ignition delay time.

The furnace is composed of high density refractory, Nichrome resistance heating wire, and a ceramic core. The refractory is a high density fibre board called cristobalite Fiberfrax Duraboard® from Carborundum Co. This crystalline silica insulation was chosen for its refractory properties, durability, and lightness. Figure 3.3 shows four 2" discs that are stacked to form the furnace refractory. A 19 gauge (AWG) (0.91 mm)

Nichrome wire is wrapped around a corrugated ceramic Norton Alundum® tube to form the furnace element.

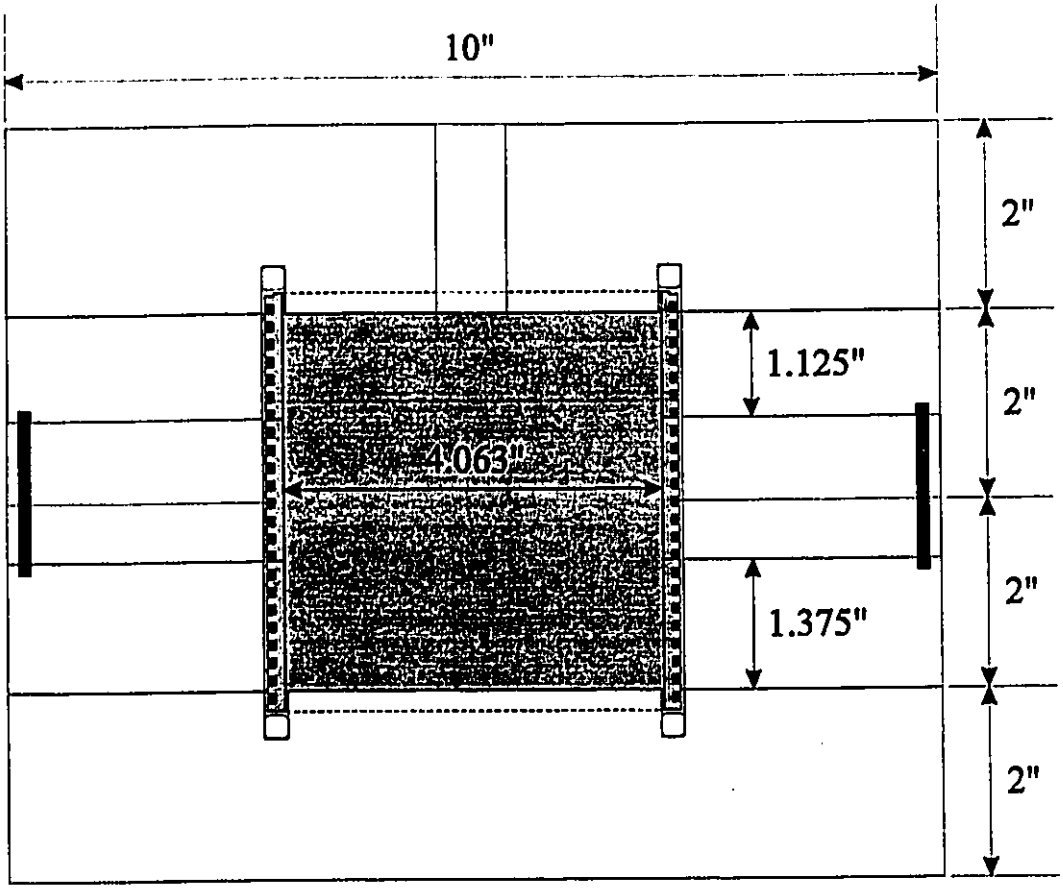

Figure 3.3: Furnace components and dimensions. Dimensions shown are exact specifications.

The wire ends are connected to a power transformer and heat is produced by the wire's electrical resistance to power.

A considerable amount of detail is shown on the furnace parts to demonstrate its relative size compared to the droplet of fuel and to reveal the amount of refractory used. The internal volume is 850 cm^3 of air. Past literature surveys of furnaces used by other researchers show that the current furnace is one of the largest of its kind, and that the furnace walls are some 30-40 droplet diameters away from the static droplet.

Secondary refractory paper, also a Fiberfrax® product, was placed around the ceramic core inside the donut hole and also on the top and bottom between the discs and the core to prevent the heating element from movement. Any movement of furnace components would lead to premature erosion of furnace refractory. The refractory paper also helped minimize the heat losses from the furnace.

The chamber (13) is pressurized with breathing quality bone dry compressed air from three tanks of 8000 standard litre STP capacity. A separate single tank supplies air for the various air cylinders. The chamber air enters through two purge tubes. The first (14) protrudes into the furnace cavity when the furnace is in its down position, and the second (15) is at the base of the chamber, with a slightly bent tip so as to produce some gas swirl during purging of product gases. After each ignition event of a fuel droplet, the air in the furnace cavity is purged, followed by purging of chamber gases.

Another tube (16), located beside the chamber purge, connects to a relief valve to maintain the chamber pressure at a set level, followed by a rotameter (17) which is used to monitor the purge air flow rate. A thermocouple (18) in one of the six side ports indicates chamber air temperature prior to ignition. A video camera (19) is present to allow the experimenter to control the release of the droplet and view the ignition event. Heat lost from the furnace is removed by a cooling system (20), from which ethylene glycol antifreeze is pumped into the cooling coils at (21) and out at (22). Key number (23) is a quartz glass port window, and (24) is a thermocouple junction box.

The fuel injector produces a droplet by displacing fluid from the chamber of a small needle valve located on a control panel (25). The entire fuel line, from the reservoir to the tip of the injector probe, is completely filled with fuel and contains no air pockets. Figure 3.4 shows the arrangement of two ball valves and one needle valve, positioned between the reservoir and the injector probe. The three valves work in conjunction to serve as a miniature piston pump for releasing the fuel droplet.

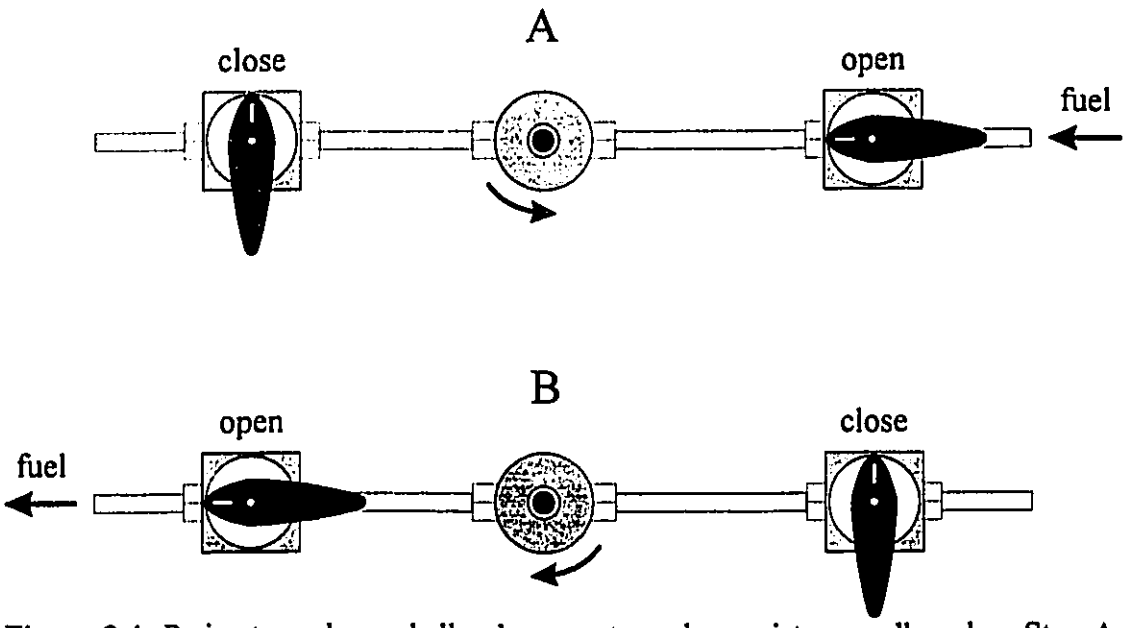

Figure 3.4: Perimeter valves - ball valves, centre valve - piston needle valve. Step A: opened piston valve - fuel enters chamber. Step B: closed piston valve - fuel displaced from chamber.

The scheme is as follows: Step A: With the upstream ball valve opened and the downstream ball valve closed, the needle valve is opened by rotating the knob counter-clockwise, which allows the pressurized fuel to fill the valve chamber. Step B: The upstream ball valve is then closed and the downstream ball valve is opened. Fuel is displaced from the needle valve chamber by rotating the knob slowly clockwise. The droplet evolves from the small diameter tip of the probe through fluid displacement and rests against the fibre shaft. When the probe moves away, the droplet falls under gravity and positions itself around the fibre bead. Droplet diameter is determined and adjusted by viewing a grid transposed on the screen of a video monitor (26). A second adjacent injector probe (27) is provided to produce an alcohol droplet which can be ignited after an experiment to burn off residual soot from the fibre. The alcohol is also supplied from an alcohol reservoir, located adjacent to the fuel supply next to the control panel.

Several interlocks are provided to prevent operation of the controls in any way that might damage the equipment. Once the fuel droplet is released, both probes are

rotated to a parallel orientation by an actuator motor (28). This activates a micro-switch which in turn operates a solenoid valve, allowing air to pressurize an air cylinder (29) at the top of injector assembly which raises the probes out of the path of the furnace. Two probe ball valves on the control panel control the flow of air to and from the solenoid valve. When the probes are in the raised position, another micro-switch (30) actuates another solenoid valve that prevents the furnace drive cylinder from lifting the furnace when the probes are not in the raised position. A bottom micro-switch (31) control prevents the probes from being lowered when the furnace is in the raised position. This safety arrangement is present to prevent mishaps due to errors in judgement when manipulating ball valves which control the air flow to the solenoid valves. A final micro-switch (32) is present to signal the operator that both injector probes are in proper alignment for raising.

Two bourbon test gauges exist for accurate measurement of chamber pressure. One is a low pressure gauge that records gauge pressure from 0 to 100 ± 0.5 psi and the other is a high pressure gauge with a range of 0 to 550 ± 2 psi.

3.3 Experimental procedure

The apparatus is allowed to warm up to thermal equilibrium before any experimental run can be conducted. This time, usually 2 hours, allows the furnace to reach the desired temperature under the given voltage supply. When the chamber is pressurized slightly longer times are required for the ambient air temperature to reach thermal equilibrium with the cooling system, owing to the greater mass of air that must be heated.

The fibre support assembly and the fibre itself are cleaned with a cloth and alcohol to remove unburnt soot left behind from previous runs. This procedure is usually done at least once after a change in fuel. When a fuel is changed, the fuel line is completely purged by running air through it, to ensure that all the old fuel has been removed. New fuel is then purged through the line before beginning experiments.

The vessel and furnace must be purged with fresh air to maintain a uniform air quality between repeated experiments. After burning a droplet, it is essential to purge both the furnace and the vessel with fresh air to remove the products of combustion. To determine the quantity of air required after each ignition event, a simple theory has been used to develop a purging schedule for the apparatus, and calculations were made to determine the purging time required for various pressures and purge flow rates. The rotameter on the exhaust from the vessel monitored the air flow through the two purge lines. Refer to appendix B for a purge calculation.

After purging, the furnace temperature drops, and one must wait for the temperature to rise back to the desired temperature. The power input to the furnace is adjusted so that the furnace temperature is nearly in equilibrium - only changing very slowly - at the time that the next run is made.

Operating variables (for example air regulator pressure to furnace drive cylinder, furnace power) can change with pressure. Therefore, it is important to monitor the furnace traverse time, defined as the time required for the furnace to move from the moment the scope is triggered to the time it reaches its final resting position. This was measured to be around 100 milliseconds, corresponding to a furnace velocity of about 1.5 m/s. To maintain consistent experimental conditions, the air pressure to the furnace air cylinder is adjusted as the chamber pressure is varied such that the traverse time remains roughly constant. The limited speed of the furnace makes the observation of ignition times below 0.1 seconds impossible.

Both the fuel and alcohol injector probes are prone to clogging due to small suspended particulates in the lines. When these probes are plugged they are replaced with new ones and the old probes are either unplugged (if possible) or discarded. The particulates are suspected to come from metal burrs on pipe linings and connections.

Quartz fibres are also replaced after extended use, soot accumulation, or breakage.

3.3.1 Choice of fuels

High carbon number *n*-paraffin hydrocarbons (listed in Table 3.1) were chosen as fuels because of their presence in commercial Diesel fuel blends, as also were aromatics, and a cycloparaffin. However, the present study did not test olefin hydrocarbons, as these are not present in significant quantities in Diesel fuel.

The fuels were selected based on their normal boiling point. The *n*-paraffins were chosen to roughly cover the boiling point range of Diesel fuel, while decalin, isobutylbenzene, and mesitylene have boiling points that are nearly identical to *n*-decane. This allowed two-component mixtures to be produced which separated the effects of component boiling point and component chemical structure.

Table 3.1: List of hydrocarbon fuels that were tested, with the purity and normal boiling points as given by the supplier. All fuels were supplied by Aldrich Chemical Company.

Fuel	Purity (%)	Boiling Point (°C)
n-decane	99	174
n-dodecane	99	216
n-hexadecane	99	287
o-xylene	98	143 - 145
1,3,5-trimethylbenzene (mesitylene)	98	162 - 164
isobutylbenzene	99	170
decahydronaphthalene (mixture of cis/trans-decalin)	99	189 - 191

3.3.2 Quartz filament fabrication

Filaments are fabricated by holding a solid 8 mm OD Pyrex quartz rod (45 cm long) by the ends and subjecting the middle of the rod to an acetylene torch. Only about 3 cm of the rod is heated. As the hot flame slowly melts the centre section, the ends of the quartz are twisted and manœuvered to obtain a feel for a desired softness. When this softness is

achieved, the rod is removed from the flame and the ends are quickly pulled apart. Instantly, the hot glowing section, which was once 8 mm OD, becomes approximately 0.3-0.5 mm OD. This stretched filament of quartz is detached and the two remaining segments are fused together for another heat and pull. Since the fibres are held by a 23.8 mm long (min. 0.39 mm ID) 304 stainless steel tube support, filament OD's must not be greater than 0.4 mm OD. Manufactured fibres having a diameter greater than the specified tolerance are discarded.

All fibres with the correct tolerances have a round bead formed in one end by placing the tip of the filament over the acetylene flame and rotating the fibre until a small spherical ball is formed. The fibre bead was typically 1.0 mm, with a shaft thickness of 0.4 mm.

3.4 Sources of error

3.4.1 Suspension fibre

The main source of error due to the suspension fibre is an increase in heat transfer to the droplet caused by heat conduction along the fibre; this in turn would cause faster droplet heating and ignition. A rough estimate of this effect can be made as follows: The thermal conductivity of quartz is 1.4 W/m·°C (Weast and Astle, 1982), while for liquid hydrocarbons at 20°C it is around 0.14 W/m·°C. Quartz therefore conducts about 10 times faster, but the fraction of the droplet surface area occupied by the fibre is only

$$\frac{\pi r_{\text{fibre}}^2}{4\pi r_{\text{droplet}}^2}$$

which with r_{fibre} = 0.19 mm and r_{droplet} = 0.75 mm gives 1.6% of the surface area or 10 × 1.6% = 16% of the heat transfer. This estimate assumes that the temperature gradient along the fibre is the same as that in the adjacent gas phase, whereas in reality the much higher conductivity of the fibre will reduce the gradient and the heat transfer through the

fibre. In addition to this, roughly one-half of the heat transfer to the droplet is by radiation, which is not affected by the fibre at all (Bergeron and Hallett, 1989b). This conclusion was reached by running the model. These considerations would reduce the increase in heat transfer due to the fibre to about 5%. Kumagai (1956) found that a 0.2 mm fibre increased the evaporation rate of a *burning* droplet by 10%, but the absence of a flame should make this effect much smaller for a droplet which is igniting or evaporating without combustion. Lafrenière (1989) found that increasing fibre diameter from 0.2 to 0.3 mm decreased the ignition time by less than 2% at an ambient temperature of 760°C.

Measured ignition times under pressure are faster than at atmospheric pressure, so the error would be even smaller for these experiments. In any case, the quartz fibre is manufactured to as small a size as possible, yet must maintain its rigidity, durability, and longevity.

3.4.2 Natural convection errors

As cited in §2.2, the effect of natural convection on droplet ignition is small at atmospheric pressure (Faeth and Olson, 1968 and Sangiovanni, 1978). The measurements of Sato *et al.* (1990) indicate an increasing role for natural convection as pressure increases, but there are no data in the literature which allow this to be quantified for ignition. Until ignition experiments can be performed at high pressure in microgravity, this must remain an open issue.

3.4.3 Limitations of the apparatus

At high pressures, heat losses from the furnace increase and one needs more furnace power to compensate for them - eventually one reaches the point where the furnace winding burns out. Thus experiments were not possible at conditions above 973 K and 13 atm, 873 K and 17 atm, and 773 K and 20 atm. Any attempts to exceed these limits by increasing the power would endanger the Nichrome heating wire.

CHAPTER FOUR

Mathematical Modelling

4.1 Numerical model: single-component fuel

Numerical predictions of ignition delay times are made with an existing numerical model developed by Ruszalo and Hallett (1992). In order to reduce the complexity of calculation, some basic assumptions were made: spherical symmetry was assumed, natural and forced convection were neglected, the effects of chemical reaction on species concentration were neglected (a common assumption in ignition models, since reactions are slow until the moment of ignition), transport properties were assumed uniform in space, and the droplet liquid temperature was assumed uniform. The model gives transient solutions for concentration and temperature fields as well as chemical reaction in the gas phase using finite volume techniques with hybrid differencing, and couples these to mass and energy balances on the droplet to account for transient heating and evaporation. Included in the model are detailed vapour-liquid equilibrium calculations using the Peng-Robinson equation of state (*EOS*) and the effects of air penetration into the liquid. The literature review concluded that the Peng-Robinson *EOS* has been accepted as the best overall cubic *EOS* to date by most researchers. The advantage of a cubic equation of state is that it can be solved analytically. More accurate and rigorous *EOS*s are available, but they require iterative solution, and the gain in accuracy is not worth the extra computational effort. Therefore, the Peng-Robinson *EOS* was adopted as

the *EOS* of choice for the current numerical model. The liquid phase concentration and temperature are assumed uniform - i.e. a well-mixed phase. For further information on the numerical analysis, readers are encouraged to refer to Ruszalo and Hallett (1992).

4.2 Chemical reaction modelling: single-component fuel

The numerical modelling of the physical processes of droplet ignition was not changed from earlier work (Bergeron and Hallett, 1989b and Ruszalo and Hallett, 1992). However, some modifications were required in modelling the chemical reaction, in particular to account for the effects of pressure on reaction. Two different reaction models were employed.

4.2.1 Single-step global reaction model

The first rate equation used was a single-step reaction equation developed by Westbrook and Dryer (WD) in 1981, originally used for predicting laminar flame speeds in flame propagation experiments. The reaction is an overall description of conventional hydrocarbon oxidation:

$$C_m H_n + \left(m + \frac{n}{4}\right) O_2 \overset{r_{fuel}}{\Rightarrow} m\,CO_2 + \frac{n}{2} H_2O \qquad [1]$$

This model was chosen for its simplicity, because a single global reaction is often a convenient way of approximating the effects of the many elementary reactions which actually occur. The overall rate r_{fuel}, Equation [2], must represent the combined effects of all the individual reaction rates involved (Westbrook and Dryer, 1981)

$$r_{fuel} = -\rho^{a+b} M_F \left(\frac{Y_F}{M_F}\right)^a \left(\frac{Y_O}{M_O}\right)^b A \exp\left(-\frac{E}{\tilde{R} \cdot T}\right) \qquad [2]$$

This is the rate equation which has been used in earlier work with this model. Experiments on suspended droplet ignition at atmospheric pressure were used by Bergeron and Hallett (1989b) to predict the pre-exponential factor A and the activation

energy E for each of the hydrocarbons they tested, giving values somewhat different from Westbrook and Dryer's determinations. The Westbrook and Dryer reaction constants were fitted to reproduce experimental laminar flame speeds; their choice of E was more or less arbitrary, affecting only the flame thickness in their calculations. However, previous work on droplet ignition by Bergeron and Hallett (1989b) at atmospheric pressure had shown that it was necessary to modify Westbrook and Dryer's required E to reproduce the measured dependence of ignition time on temperature, which in turn required changing the value of A as well.

The Bergeron and Hallett model represented the data well for *n*-paraffin hydrocarbons using the prescribed fuel and oxygen exponents of $a = 0.25$ and $b = 1.5$ as suggested by Westbrook and Dryer. However, they discovered that Westbrook and Dryer's exponents for aromatic fuels gave unrealistic results for atmospheric pressure droplet ignition. Thus, the aromatic fuel and oxygen exponents were modified to $a = 0.30$ and $b = 1.4$, respectively. Since a and b in [2] directly determine the influence of pressure, these parameters will have to be modified to represent the experimental data of this thesis. In other words, the reaction rate parameters E, A, a, and b would have to be modified for pressure dependence.

4.2.2 Four-step global reaction model

The experimental data presented later in this work for *n*-paraffin hydrocarbons indicate the presence of two different reaction processes occurring at certain pressures or temperatures. Bergeron and Hallett (1989b) also observed this phenomenon experimentally at high temperatures, and they attributed the change to a sudden shift[2] in chemical kinetics from two-stage to single-stage ignition. These results, together with

[2]More information on the observed ignition shift will be presented in the discussion section of chapter five of this report.

deficiencies in the model representing the data with the Westbrook and Dryer model, suggested that a more complicated multi-step reaction model would be required. Therefore, a four-step global reaction model was investigated.

This ingenious yet simple model was developed by Müller *et al.* (MPL) in 1992 for predicting ignition delay times of *n*-heptane at pressures up to 40 atm. Müller *et al.* were able to reduce a full kinetic mechanism for *n*-heptane, comprising 1011 elementary reactions with 171 chemical species, down to 4 global reaction steps and just 5 chemical species, without great loss in accuracy.

The four reaction steps are grouped into two temperature branches:

$$\text{high T} \begin{cases} \mathrm{F} \overset{r_1}{\Rightarrow} \mathrm{X} & \text{[R1]} \\ \mathrm{X} + x \cdot \mathrm{O_2} \overset{r_2}{\Rightarrow} \mathrm{P} & \text{[R2]} \end{cases}$$

$$\text{med. T} \begin{cases} \mathrm{F} + y \cdot \mathrm{O_2} \underset{r_{3b}}{\overset{r_{3f}}{\Leftrightarrow}} \mathrm{I} & \text{[R3]} \\ \mathrm{I} + z \cdot \mathrm{O_2} \overset{r_4}{\Rightarrow} \mathrm{P} & \text{[R4]} \end{cases}$$

The rates r_1, r_2, r_{3f}, r_{3b}, and r_4 are global descriptions of reaction rates, with pre-exponentials that were fitted by Müller *et al.*'s data their *n*-heptane data. Activation energies were obtained from Müller *et al.*, and were kept the same for all *n*-paraffins and the cycloparaffin tested. These rate equations are:

$$r_1 = -A_1 \cdot X_{\mathrm{F}} \cdot \exp\left(-\frac{E_1}{\tilde{R}T}\right) \quad [3]$$

$$r_2 = -A_2 \cdot X_{\mathrm{X}} \cdot X_{\mathrm{O}} \cdot \frac{p}{\tilde{R}T} \cdot \exp\left(-\frac{E_2}{\tilde{R}T}\right) \quad [4]$$

$$r_{3f} = -A_{3f} \cdot X_{\mathrm{F}} \cdot X_{\mathrm{O}} \cdot \frac{p}{\tilde{R}T} \cdot \exp\left(-\frac{E_{3f}}{\tilde{R}T}\right) \quad [5]$$

$$r_{3b} = -A_{3b} \cdot X_{\mathrm{I}} \cdot \exp\left(-\frac{E_{3b}}{\tilde{R}T}\right) \quad [6]$$

$$r_4 = -A_4 \cdot X_1 \cdot X_O \cdot \frac{p}{\tilde{R}T} \cdot \exp\left(-\frac{E_4}{\tilde{R}T}\right) \qquad [7]$$

where $A_1 = 1 \times 10^{10}\ \mathrm{s^{-1}}$,

$A_2 = 2 \times 10^{12}\ \frac{\mathrm{cm^3}}{\mathrm{gmol \cdot s}}$,

$A_{3f} = 3 \times 10^{18}\ \frac{\mathrm{cm^3}}{\mathrm{gmol \cdot s}}$,

$A_{3b} = 4 \times 10^{22}\ \mathrm{s^{-1}}$,

$A_4 = 5 \times 10^{13}\ \frac{\mathrm{cm^3}}{\mathrm{gmol \cdot s}}$,

$\frac{E_1}{\tilde{R}} = 21650\ \mathrm{K}$,

$\frac{E_2}{\tilde{R}} = \frac{E_1}{3\tilde{R}}$,

$\frac{E_{3f}}{\tilde{R}} = \frac{E_1}{\tilde{R}}$,

$\frac{E_{3b}}{\tilde{R}} = 37285\ \mathrm{K}$,

and $\frac{E_4}{\tilde{R}} = 13265\ \mathrm{K}$.

The first pair of these reactions, [R1] and [R2], predominates at high temperatures, and the second set, [R3] and [R4], at lower temperatures. Reaction [R1] in the high temperature branch represents endothermic fuel decomposition into smaller hydrocarbon fragments (species X), [R2] oxidizing the intermediate species to final products. [R2] is fast relative to [R1] at moderate to high temperatures; thus [R1] becomes rate limiting at high temperatures.

The second branch is a moderate temperature regime, for which reactions [R3] and [R4] represent degenerate chain branching mechanisms, and species I is another intermediate. [R3] is in equilibrium, with both forward and backward reactions, and [R4] involves the intermediate species oxidizing to products. The activation energy of the backward step in [R3] is assumed to be large with respect to the forward step, so that at low temperatures (below about 830 K and at 40 atm), the reverse step is negligible

compared to the forward. However, at temperatures above about 830 K, the rate r_{3b} becomes increasingly important and competes with r_{3f}. Less intermediate I would be formed, leading reaction [R4] to become rate limiting. The competition between r_{3f} and r_{3b} results in a slight negative dependence of rate on temperature for temperatures slightly greater than 800 K.

Figure 4.1 shows the individual rates for the reactions [R1], [R2], [R3], and [R4] as plotted by Müller *et al.* for a pressure of 40 atm. Only the rate limiting time scales are of importance and they are r_1 and $k_{2OVL} \cdot X_O^2$, where k_{2OVL} is the overall second-order rate constant. The initial molar oxygen concentration X_O used in the calculations of the rates in the figure is 0.2061 at a pressure of 40 atm. The $k_{2OVL} \cdot X_O^2$ expression represents the net effect of the rates r_{3f}, r_{3b} and r_4 combined. The overall rate expression is determined by whichever rate, r_1 or $k_{2OVL} \cdot X_O^2$, dominates at a particular temperature. At temperatures[3] above about 1180 K, r_1 dominates, while below 1180 K the reverse is true. For low temperatures, the rate of $k_{2OVL} \cdot X_O^2$ decreases as temperature rises. Thus, it was speculated that the shifting of reaction rates from the middle to high temperature regime might reproduce some of the observed ignition delay times.

Using the above arguments, Müller *et al.* were able to formulate an overall rate expression for fuel oxidation, valid for temperatures above about 800 K:

$$r_{fuel} = \rho Y_F \left(-r_1 - k_{2OVL} \cdot X_O^2 \right) \qquad [8]$$

$$\text{where } k_{2OVL} \cdot X_O^2 = A_{2OVL} \cdot \frac{p}{\tilde{R}T} \cdot \exp\left(-\frac{E_{2OVL}}{\tilde{R}T} \right),$$

$$A_{2OVL} = \frac{A_{3f} \cdot A_4}{A_{3b}},$$

$$\text{and } E_{2OVL} = E_{3f} + E_4 - E_{3b}.$$

[3]Using Müller *et al.*'s. pre-exponentials and activation energies for the Arrhenius rate expressions, slightly different values were obtained by the author than reported by Müller *et al.* The temperature shift between two rates was 1180 K for Müller *et al.*, as opposed to our calculated value of 1214 K. The cause of this appears to be a small discrepancy in the numerical value for E_4 given by Müller *et al.*

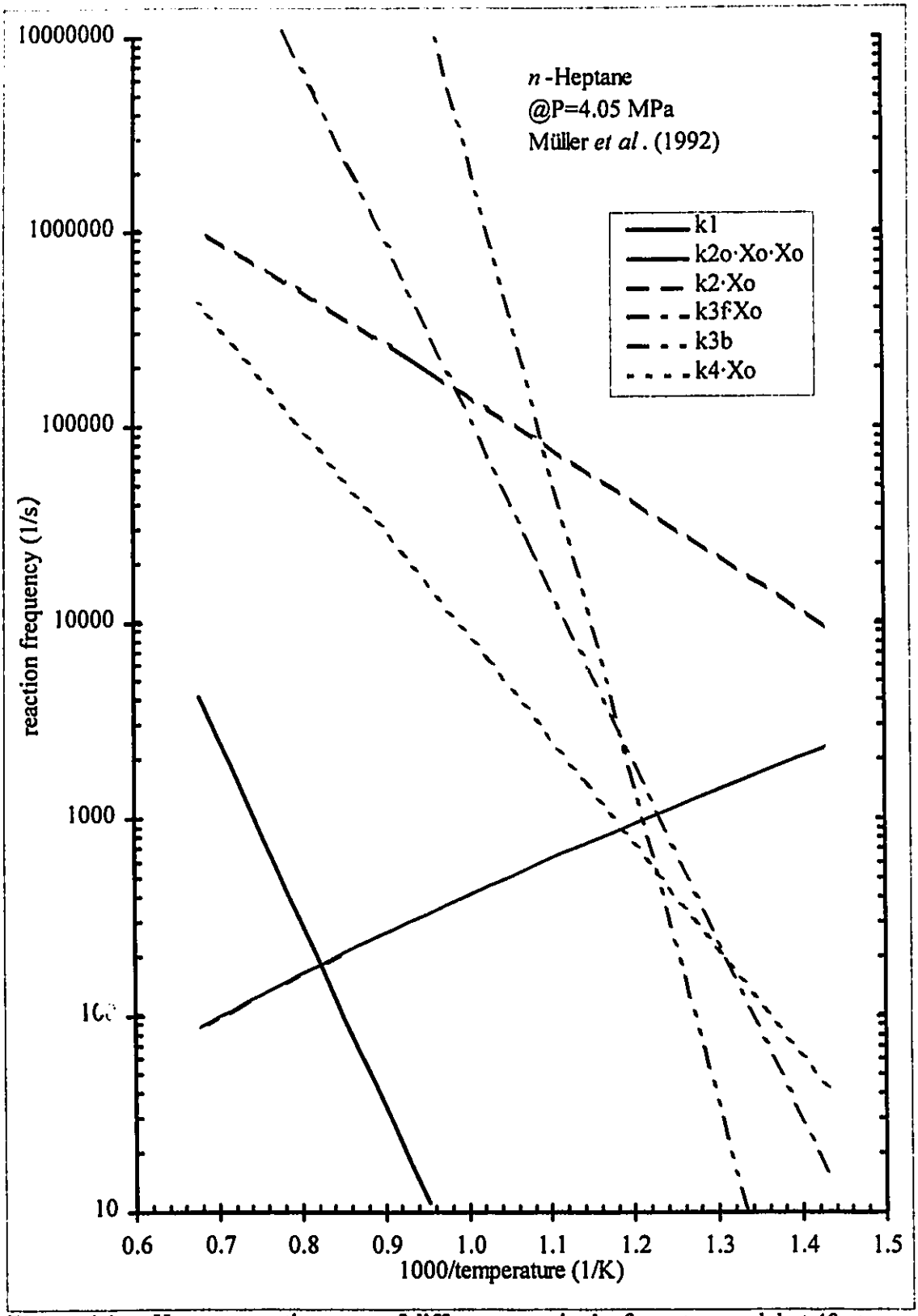

Figure 4.1: *n*-Heptane reaction rates of different steps in the four-step model at 40 atm.

The paper of Müller *et al.* also presented a simplified low temperature equation that was valid for temperatures below 800 K. They hypothesize that for temperatures below 800 K reaction [R3] is no longer in partial equilibrium. Their reasoning was that a two-stage ignition process occurs, where the fuel is partly converted to the intermediate I in the first stage. Since no significant heat release occurs during this stage, the subsequent consumption of I during the second stage is governed by the exothermic reaction [R4]. However, the model they derived for the low temperature branch was only appropriate for a homogeneous gas mixture without diffusion or convection processes. Hence, it could not be applied to the droplet ignition model.

4.3 Numerical model: two-component fuels

The binary mixture droplet ignition model is basically the same as the single component model, incorporating the same type of transient solutions. Two issues were dealt with in the model. The first is the effect of mixing processes within the droplet on ignition. As in earlier work, more rapid mixing in the liquid phase was found to have no significant effect on ignition delay times. The second issue was the combination of component reaction rates to a mixture rate. Bergeron and Hallett (1989a) stated that in extending the model to two components it was necessary to assume that Fick's law held for multi-component diffusion, which is an appropriate approximation for low fuel vapour concentrations. The two-component model can include the effects of liquid phase diffusion of the two fuel components, so that liquid phase concentrations can be non-uniform. However, if desired the droplet concentration can also be considered as "well-mixed" by specifying a high effective diffusivity in the liquid, which would then approximate the "well-mixed" binary scenario.

It must be noted that all real suspended droplets of pure components and mixtures exhibit an internal circulation upon evaporation. In modelling this situation, Tally and Yao (1986) developed a semi-empirical approximation by lumping the effects of internal

circulation into effective thermal and mass diffusivities, giving an enhanced effective radial diffusion rate. Apart from internal circulation, the main issue here is to simply find a practical reaction model for mixtures by combining single component models.

4.4 Chemical reaction modelling: two-component fuels

In formulating a reaction scheme for binary components, Bergeron and Hallett (1989a) developed single step rate expressions similar in form to the original Westbrook and Dryer (1981) description. These rate expressions were also incorporated into the high pressure model by Ruszalo and Hallett (1992).

Two simple models were devised. The first model (denoted as model 1) is a linear combination by mole fraction of the rates that would result if the fuel were one or other of the pure component. The pure component rates would then be

$$r_1 = -\rho^{a_1+b_1} \cdot M_1 \left(\frac{Y_1 + Y_2}{M_1}\right)^{a_1} \left(\frac{Y_O}{M_O}\right)^{b_1} A_1 \exp\left(-\frac{E_1}{\tilde{R} \cdot T}\right) \qquad [9]$$

$$r_2 = -\rho^{a_2+b_2} \cdot M_2 \left(\frac{Y_1 + Y_2}{M_2}\right)^{a_2} \left(\frac{Y_O}{M_O}\right)^{b_2} A_2 \exp\left(-\frac{E_2}{\tilde{R} \cdot T}\right) \qquad [10]$$

and the mixture rate is

$$r_{fuel} = y_1 \cdot r_1 + y_2 \cdot r_2 \qquad [11]$$

The second model (denoted as model 2) is a linear combination by mole fraction of component rate parameters to produce reaction rate parameters for the overall rate expression given by [17].

$$A = y_1 \cdot A_1 + y_2 \cdot A_2 \qquad [12]$$

$$E = y_1 \cdot E_1 + y_2 \cdot E_2 \qquad [13]$$

$$a = y_1 \cdot a_1 + y_2 \cdot a_2 \qquad [14]$$

$$b = y_1 \cdot b_1 + y_2 \cdot b_2 \qquad [15]$$

$$M = y_1 \cdot M_1 + y_2 \cdot M_2 \qquad [16]$$

$$r_{fuel} = -\rho^{a+b} \cdot M \left(\frac{Y_1 + Y_2}{M}\right)^{a} \left(\frac{Y_O}{M_O}\right)^{b} A \exp\left(-\frac{E}{\tilde{R} \cdot T}\right) \qquad [17]$$

For both schemes used the component reaction rate parameters that were previously determined from the single-component model results (Bergeron and Hallett, 1989b).

Model 2 was found in earlier work to be more representative of the data at atmospheric pressure (Bergeron and Hallett, 1989a). The model had demonstrated that the more volatile species dominated ignition under the influence of pressure, and that no model tuning was necessary as all the reaction parameters were obtained from single-component measurements.

The Westbrook and Dryer chemical reaction rate form was applied to the mixture model. No attempt was made to adapt the Müller *et al.* model to mixtures.

CHAPTER FIVE

Results and Discussion

5.1 Correction of experimental data to standard conditions

When experiments were conducted, it was found that increasing the pressure while maintaining a certain furnace temperature would also raise the chamber ambient air temperature, owing to an increase in natural convection heat transfer rates between the furnace exterior walls and the surrounding air. The cooling facility was not able to fully compensate for this, so that the steady ambient temperature which could be maintained within the vessel rose with pressure. Since the droplet liquid temperature before ignition is assumed equal to the ambient temperature in the vessel, it also rises with pressure, reducing the measured ignition times.

To make comparisons of measurements made under different conditions easier, a mathematical model was used to correct for this effect. Since 40°C was about the middle range of the measured chamber temperatures, it was adopted as the standard initial liquid temperature for presenting results, and all data were corrected to this initial liquid temperature. The correction was performed with the single-component model. For a given pressure and furnace temperature, the model was used to predict ignition delay times at the standard liquid temperature of 40°C and at the actual liquid temperature $\left(T_{liq}\right)$. The relative rate of change of ignition time with liquid temperature can be represented as

$$\frac{1}{t}\frac{dt}{dT_{liq}} \approx \frac{t - t_{40°C}}{t\left(T_{liq} - 40°C\right)}, \qquad [18]$$

where t and $t_{40°C}$ are ignition delay times at the actual liquid temperatures T_{liq} and at 40°C respectively. The corrected ignition delay time was found as

$$t_{corr} = t_{meas} + \frac{t_{meas}}{t_{model}}\left(\frac{t_{model} - t_{model@40°C}}{T_{liq} - 40°C}\right)\left(40°C - T_{liq}\right) \qquad [19]$$

by linear extrapolation, where t_{meas} is the original measured time, t_{model} is the computed time, and $t_{model@40°C}$ is the computed time at 40°C. This correction was applied to all experimental points, including data points for mixtures. The data were corrected by first selecting preliminary reaction rate parameters as inputs to the model so as to roughly reproduce measured data. The numerical model was then used to calculate $t_{model}@T_{liq}$ and $t_{model@40°C}$ for each data point and these were inputted into the correction, see Equation [19]. How the corrected time differs from the measured time depends on the difference between the actual liquid temperature and 40°C, and on how ignition delay time for the particular fuel is related to liquid temperature.

5.2 Experimental data: single-component fuels

5.2.1 *n*-Paraffin hydrocarbons

Ignition delay times were measured as a function of pressure and temperature for single-component *n*-paraffins. The fuels tested were *n*-decane, *n*-hexadecane, and *n*-dodecane. The results are presented in Figures 5.1 through 9. Of the fuels, *n*-decane exhibited the fastest drop in ignition times under the influence of pressure, with *n*-dodecane second and *n*-hexadecane third. The monotonic ignition time decrease with increasing pressure on a log-log scale is a representative response for *n*-paraffins at moderate to high temperatures (873 K - 973 K).

For the data at 973 K (Figure 5.1 - 3) and at 873 K (Figure 5.5), at a certain maximum pressure a sudden drop in ignition time occurs to a value lower than can be measured with the current apparatus, which is less than about 0.1 seconds. This is indicated by a vertical dotted line at the highest pressures recorded, which has also been observed in experiments at atmospheric pressure (Bergeron and Hallett, 1989b) and is believed to represent a shift in reaction kinetics from two-stage ignition at lower temperatures and/or pressures to one-stage ignition at higher. (Two-stage ignition comprises a low-temperature ignition process, leading to a barely visible low temperature "cool flame", followed by a further ignition delay period before ignition to full-fledged combustion. The cool flame process disappears with the onset of one-stage ignition.)

The reason for the dotted graphical representation is that no true or actual ignition delay time was recorded because the ignition response of the fuel was below the minimum time, stated previously in §3.3 as the furnace traverse time. The fuel droplet would ignite as soon as it was exposed to the hot environment, prior to the furnace coming to a complete rest.

Some of the data at temperatures below 973 K reveal the presence of a range of pressures for which two distinctly different ignition times were observed (Figures 5.4 to 5.9). The two-ignition or "twinned" ignition times were recorded under the same operating conditions (i.e. pressure and temperature). This appears to be the similar effect just mentioned for data at 973 K, but the lower temperature measurements show two values over a fairly wide range of conditions, while the 973 K data show no regions of overlap between the two types of behaviour. The individual data points at each of these conditions grouped themselves clearly about two different mean values, and the lack of overlap between the error bars show that this grouping is statistically significant. The error bars on all experimental plots shown in this report are of ± one standard deviation wide, and each sample set ranged from 4 to 12 data points.

The explanation which suggests itself for the observation of two distinct values is that they represent two different reaction kinetic paths (probably corresponding once again to two-stage and one-stage ignition), one or other of which can be favoured by slight changes in initial conditions. The brief transient flow of air during entry of the droplet into the furnace and the natural convection about the droplet occurring during the pre-ignition period are subject to some degree of random fluctuation; this may result in local variations in mixture formation and heating and thus affect the reaction pathway taken. Why this should happen more at lower temperatures is not clear, but is probably due to changes in reaction mechanism. This "twinned" data was more evident at higher pressures and lower temperatures. Comparing Figures 5.4 - 6, at 873 K it appears that as the carbon chain length increases from *n*-decane to *n*-hexadecane, the two-ignition phenomenon gradually disappears or shifts to lower temperatures. Data at 773 K, Figures 5.7 - 9 indicates similar results.

Figures 5.10 - 16 are plots of ignition delay times versus the inverse of ambient temperature. Note all *n*-paraffin atmospheric pressure data were taken from Bergeron and Hallett (1989b). The data in all cases show a nearly linear relationship of ignition time on a log scale to inverse temperature. The slope of this relationship represents the effective activation energy for the ignition process. As pressure increases ignition times drop and so do neighbouring data points at lower temperatures (Figure 5.10). The slope inferred from connection of these points indicate a decrease in the effective activation energy for *n*-decane as the pressure rises, suggesting a change in chemical reaction kinetics at higher pressures. At atmospheric pressure, a two-stage ignition is seen for *n*-decane at 1068 K.

A similar but small decrease in activation energy with pressure was recorded for *n*-dodecane and *n*-hexadecane (Figures 5.11 - 16). Figure 5.11 shows *n*-dodecane data plotted at 7.8 atm, which also reveals an effective activation energy decreasing with increasing pressure. These observations hold for pressures below about 10 atm; at higher pressures, the effective activation energy no longer decreases with pressure, as the

example of *n*-dodecane at 12.9 atm (Figure 5.12) reveals. Figures 5.13 - 16 show similar results for *n*-hexadecane, that is effective activation energy decreasing with increasing pressure. It is expected that *n*-paraffins should all behave in a similar fashion and this is born out by these data.

Due to the physical limitations of the apparatus stated in §3.4.3 it was not possible to obtain data beyond 17 atm without the possibility of burning out the furnace windings. Thus, for temperatures of 873 K and 773 K the experimental runs were gathered only to this limit. Higher pressure data may be possible at lower temperatures than 773 K, but this was not investigated.

The only comparable data in the literature was those of Kadota *et al.*, who show substantially shorter ignition times than those reported here (approximating 40% shorter). It was believed that the thermocouple in Kadota *et al.*'s furnace was too close to the proximity of the droplet during the ignition process, creating a "hot spot" which led to premature ignition. This problem was avoided in the present apparatus by having our thermocouple withdraw from the furnace area as the furnace raised, such that the field around the droplet is free from extraneous heat sources during droplet ignition.

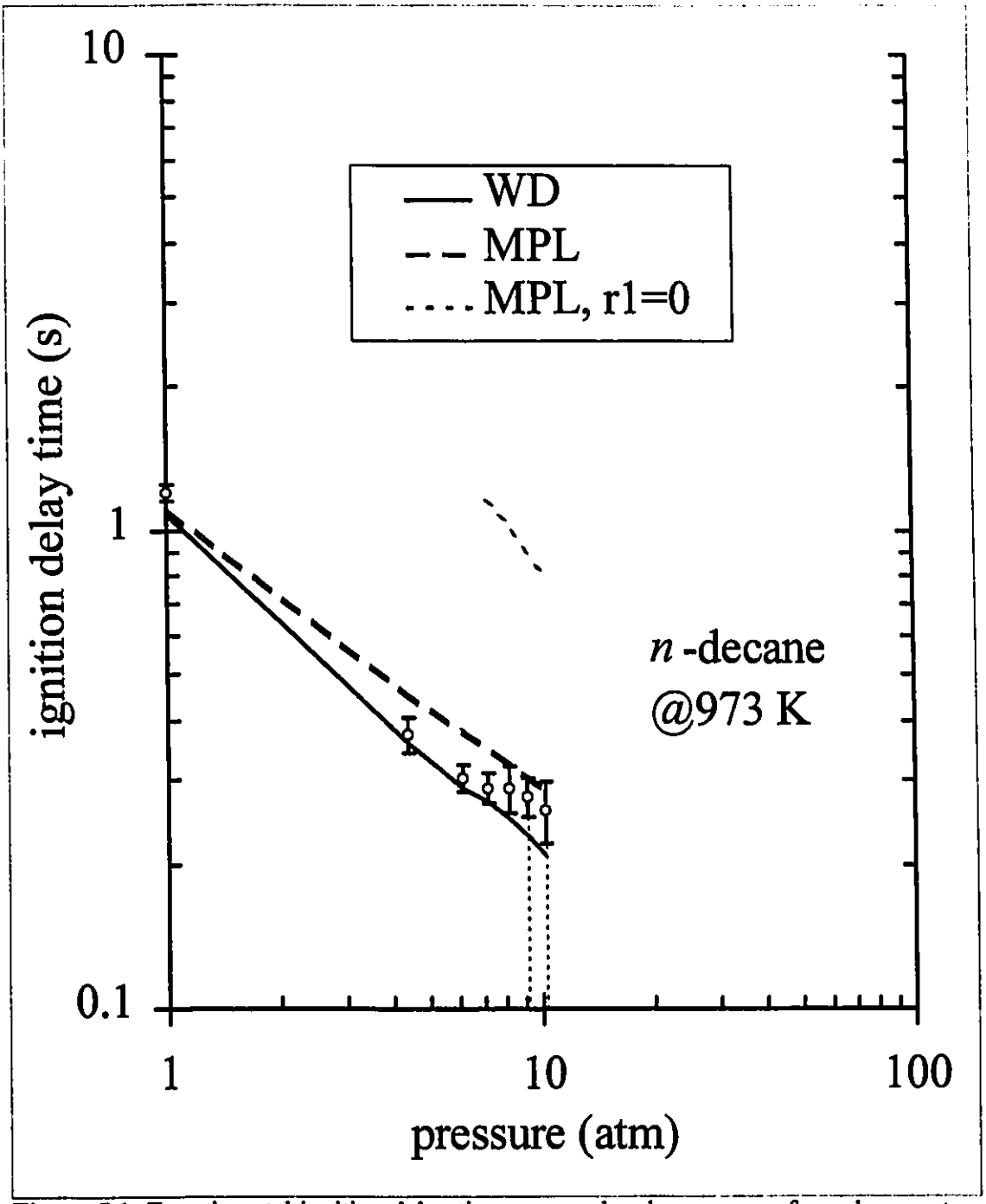

Figure 5.1: Experimental ignition delay time versus chamber pressure for *n*-decane at an ambient temperature of 973 K. Droplet diameter 1.40 mm. All data reduced to a uniform initial liquid temperature of 40°C. The error bars are at ± one standard deviation of the measurements. Solid line represents model predictions with modified Westbrook and Dryer reaction rate parameters: $a = 0.25$, $b = 1.80$, $A = 1.75 \times 10^5$, and $E = 72.80$ kJ/mol. Dashed line represents model predictions with Müller *et al.* reaction rate parameters: $A_1 = 6.00 \times 10^8$ s^{-1}, $E_1 = 180.01$ kJ/mol, $A_{2OVL} = 1.09 \times 10^9$ cm^6/(gmol^2·s), and $E_{2OVL} = -19.71$ kJ/mol.

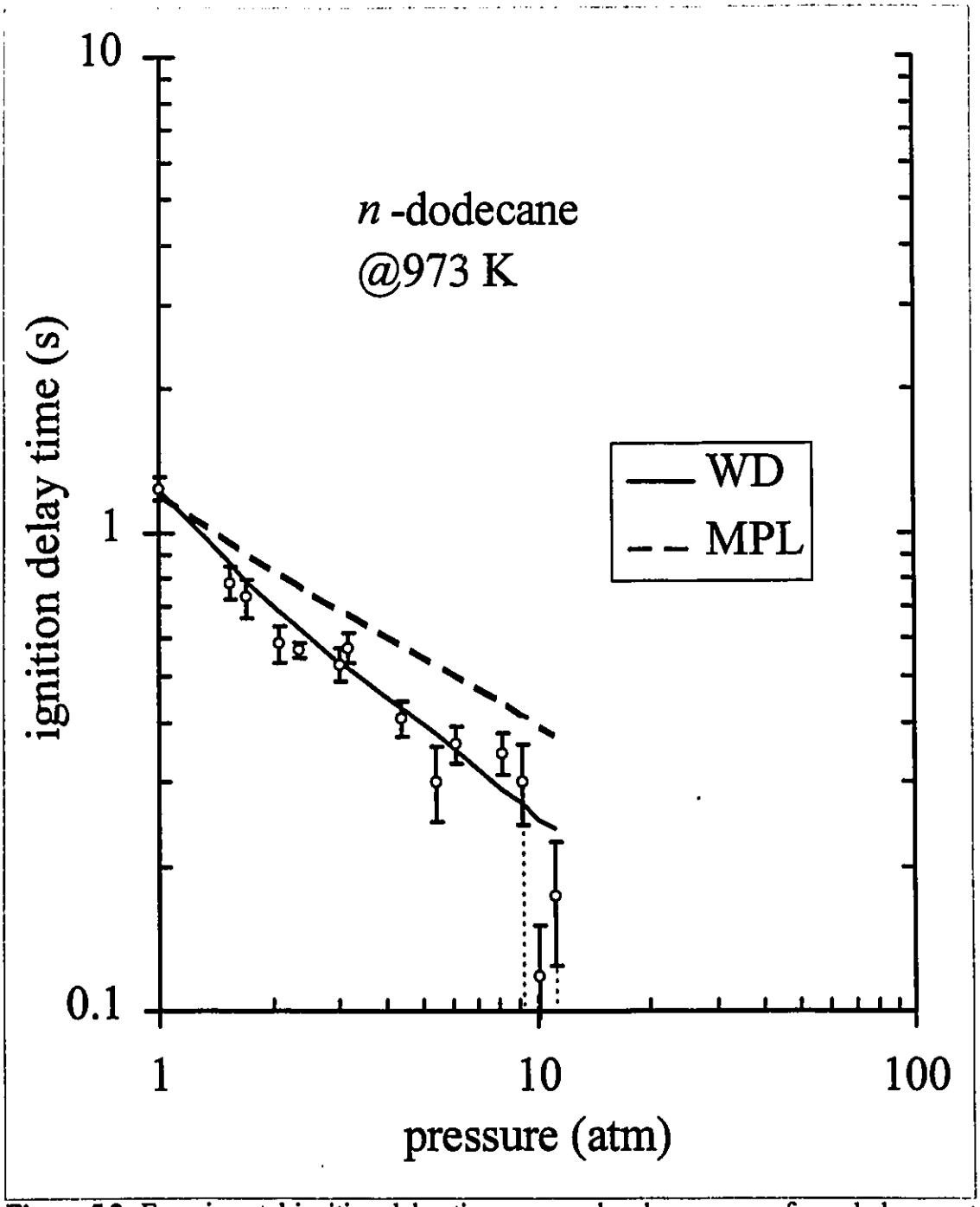

Figure 5.2: Experimental ignition delay time versus chamber pressure for *n*-dodecane at an ambient temperature of 973 K. Droplet diameter 1.40 mm. All data reduced to a uniform initial liquid temperature of 40°C. The error bars are at ± one standard deviation of the measurements. Solid line represents model predictions with modified Westbrook and Dryer reaction rate parameters: $a = 0.25$, $b = 1.90$, $A = 4.05 \times 10^5$, and $E = 76.15$ kJ/mol. Dashed line represents model predictions with Müller *et al.* reaction rate parameters: $A_1 = 7.25 \times 10^8$ s^{-1}, $E_1 = 180.01$ kJ/mol, $A_{2OVL} = 1.24 \times 10^9$ cm^6/(gmol^2·s), and $E_{2OVL} = -19.71$ kJ/mol.

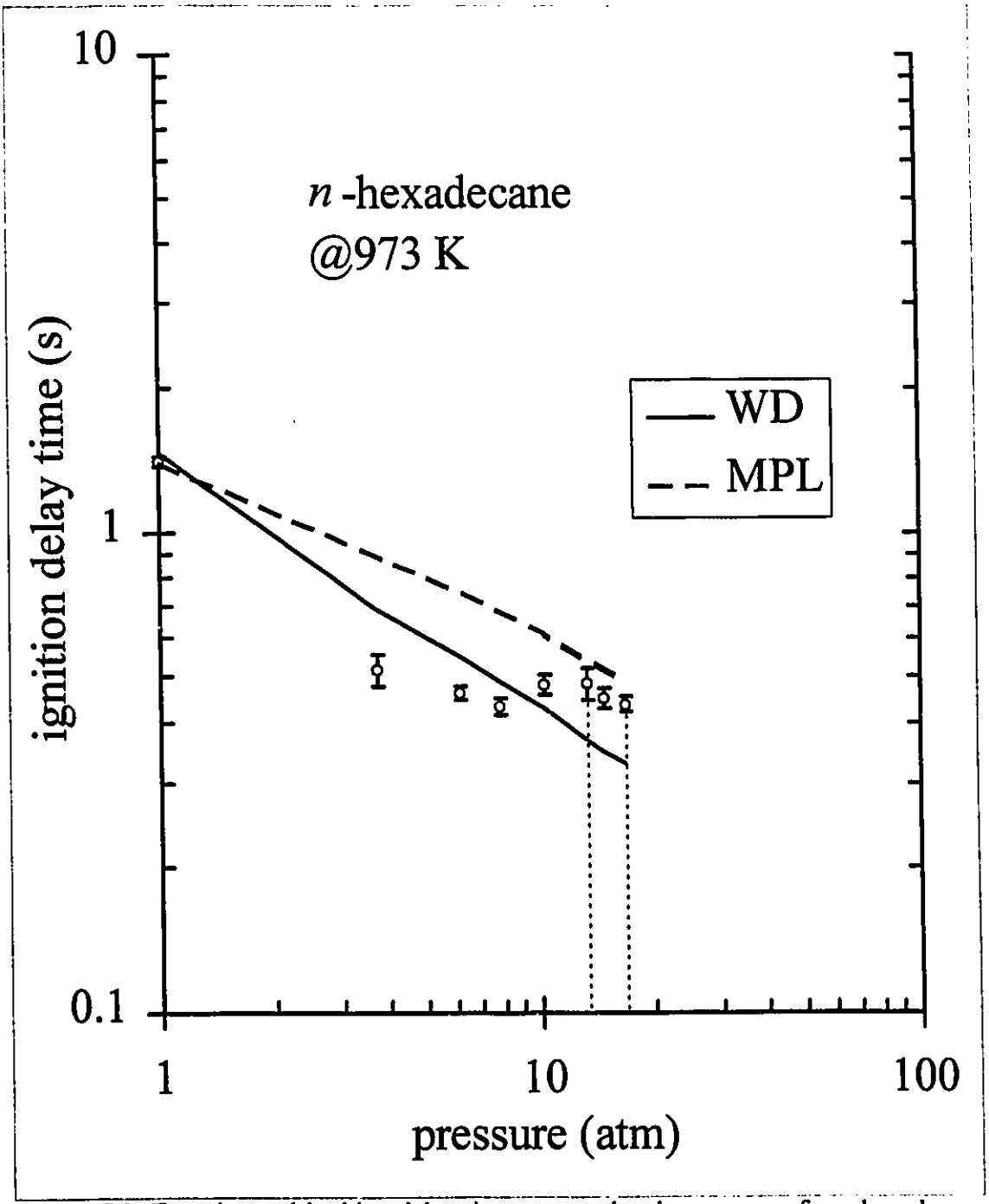

Figure 5.3: Experimental ignition delay time versus chamber pressure for *n*-hexadecane at an ambient temperature of 973 K. Droplet diameter 1.40 mm. All data reduced to a uniform initial liquid temperature of 40°C. The error bars are at ± one standard deviation of the measurements. Solid line represents model predictions with modified Westbrook and Dryer reaction rate parameters: a = 0.25, b = 1.90, A = 4.30 × 10^5, and E = 78.24 kJ/mol. Dashed line represents model predictions with Müller *et al.* reaction rate parameters: A_1 = 9.75 × 10^8 s^{-1}, E_1 = 180.01 kJ/mol, A_{2OVL} = 1.54 × 10^9 $cm^6/(gmol^2 \cdot s)$, and E_{2OVL} = -19.71 kJ/mol.

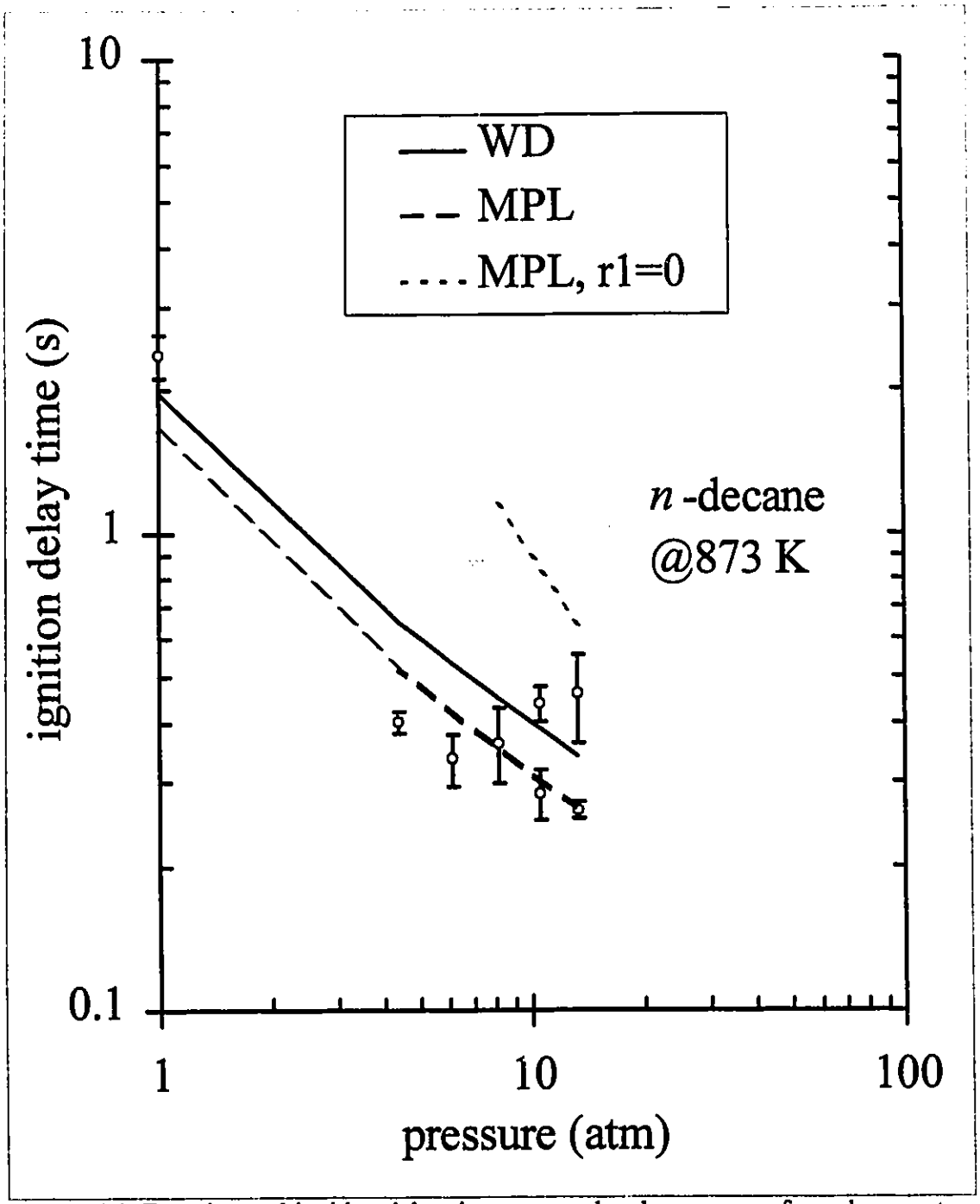

Figure 5.4: Experimental ignition delay time versus chamber pressure for *n*-decane at an ambient temperature of 873 K. Droplet diameter 1.40 mm. All data reduced to a uniform initial liquid temperature of 40°C. The error bars are at ± one standard deviation of the measurements. Solid line represents model predictions with modified Westbrook and Dryer reaction rate parameters: $a = 0.25$, $b = 1.80$, $A = 1.75 \times 10^5$, and $E = 72.80$ kJ/mol. Dashed line represents model predictions with Müller *et al.* reaction rate parameters: $A_1 = 6.00 \times 10^8$ s^{-1}, $E_1 = 180.01$ kJ/mol, $A_{2OVL} = 1.09 \times 10^9$ cm^6/(gmol^2·s), and $E_{2OVL} = -19.71$ kJ/mol.

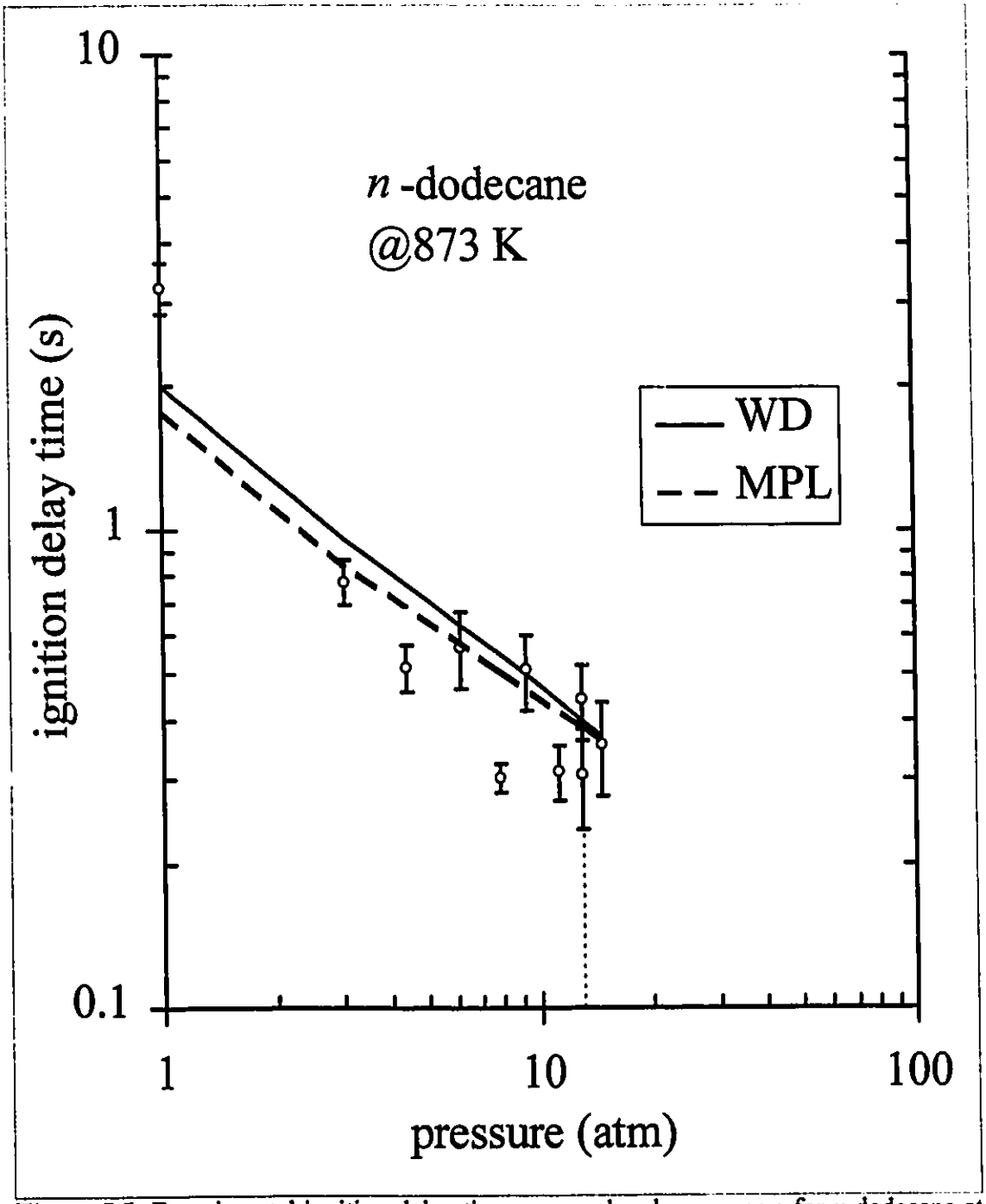

Figure 5.5: Experimental ignition delay time versus chamber pressure for *n*-dodecane at an ambient temperature of 873 K. Droplet diameter 1.40 mm. All data reduced to a uniform initial liquid temperature of 40°C. The error bars are at ± one standard deviation of the measurements. Solid line represents model predictions with modified Westbrook and Dryer reaction rate parameters: a = 0.25, b = 1.90, $A = 4.05 \times 10^5$, and E = 76.15 kJ/mol. Dashed line represents model predictions with Müller *et al.* reaction rate parameters: $A_1 = 7.25 \times 10^8\ s^{-1}$, E_1 = 180.01 kJ/mol, $A_{2OVL} = 1.24 \times 10^9\ cm^6/(gmol^2 \cdot s)$, and E_{2OVL} = -19.71 kJ/mol.

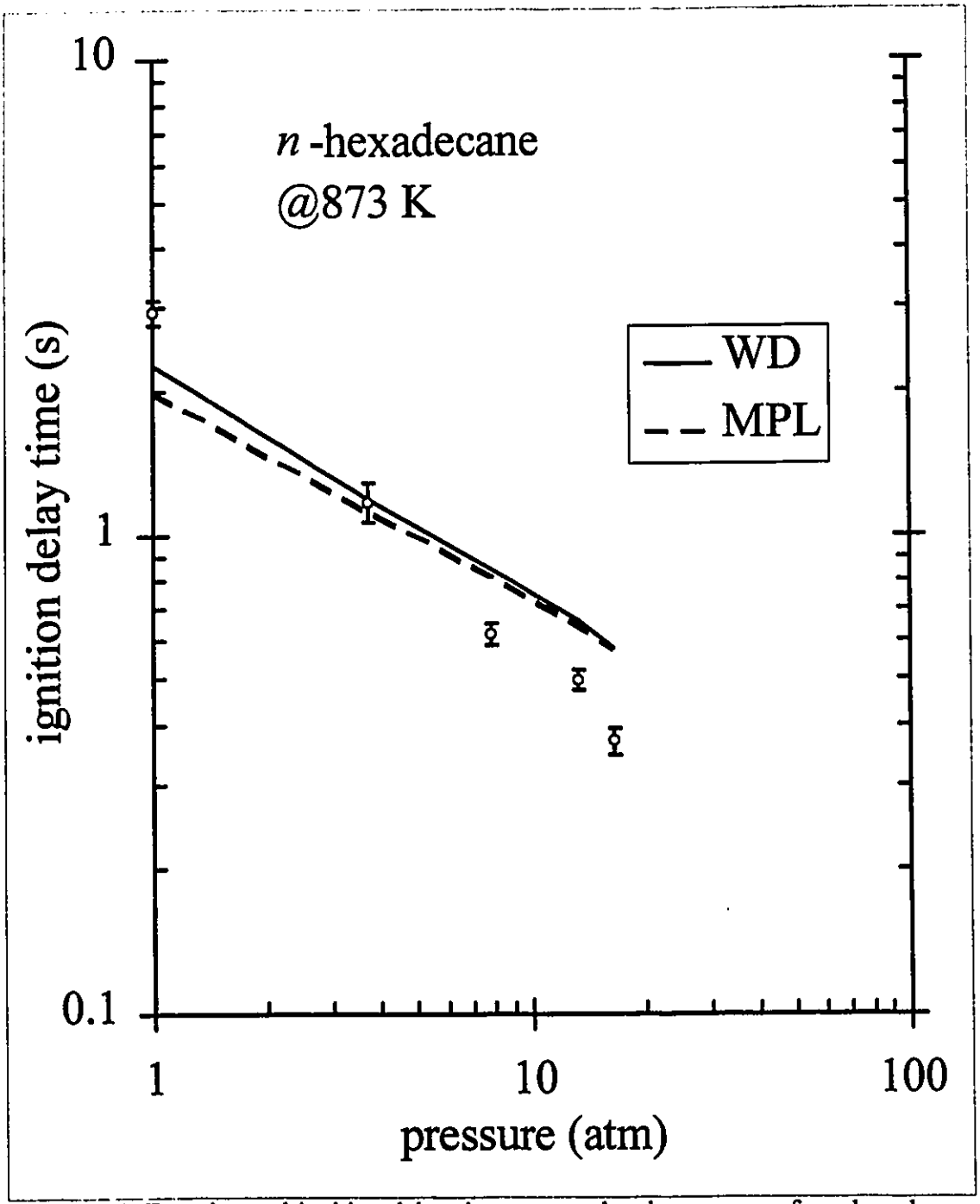

Figure 5.6: Experimental ignition delay time versus chamber pressure for *n*-hexadecane at an ambient temperature of 873 K. Droplet diameter 1.40 mm. All data reduced to a uniform initial liquid temperature of 40°C. The error bars are at ± one standard deviation of the measurements. Solid line represents model predictions with modified Westbrook and Dryer reaction rate parameters: $a = 0.25$, $b = 1.90$, $A = 4.30 \times 10^5$, and $E = 78.24$ kJ/mol. Dashed line represents model predictions with Müller *et al.* reaction rate parameters: $A_1 = 9.75 \times 10^8$ s^{-1}, $E_1 = 180.01$ kJ/mol, $A_{2OVL} = 1.54 \times 10^9$ cm^6/(gmol^2·s), and $E_{2OVL} = -19.71$ kJ/mol.

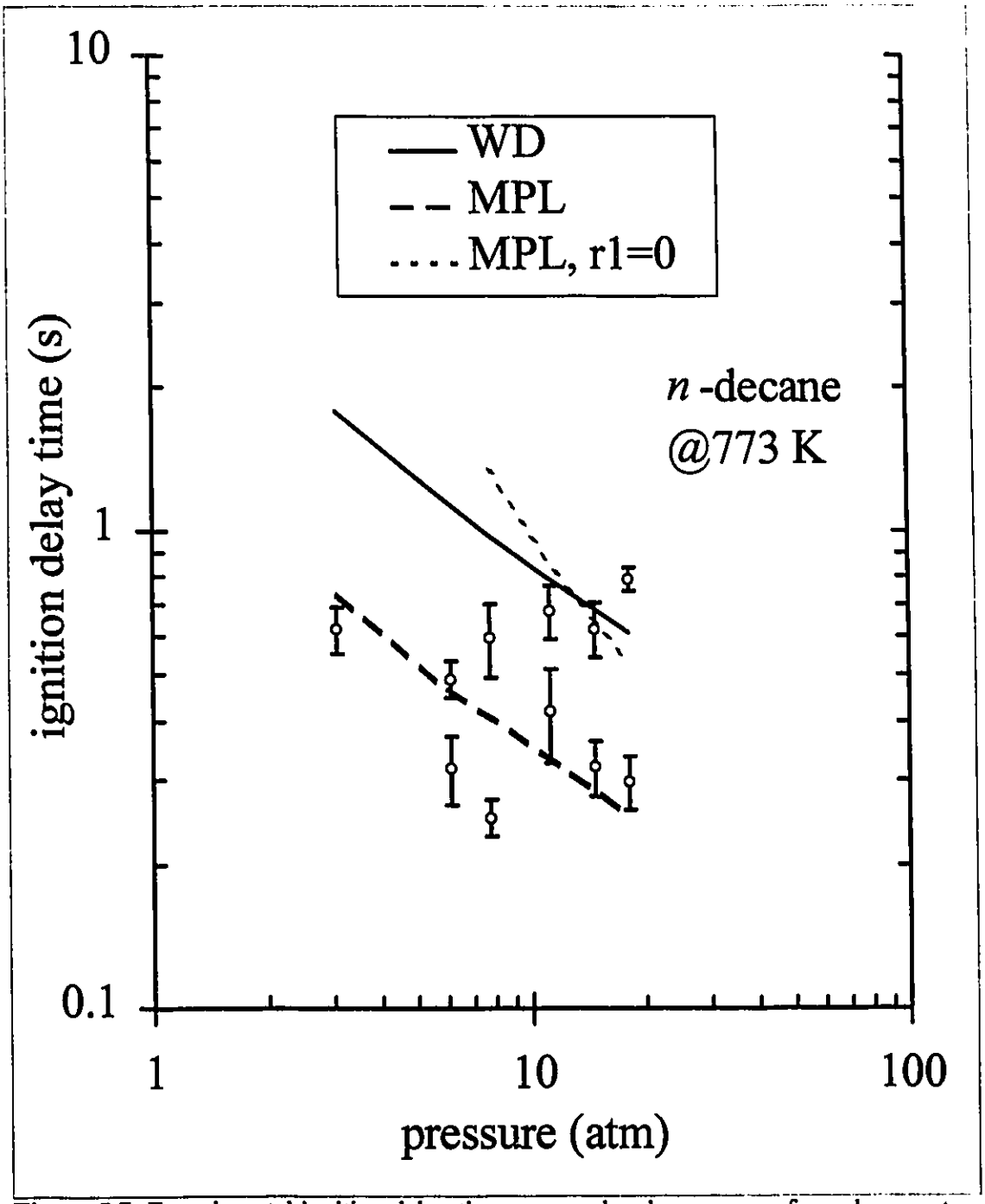

Figure 5.7: Experimental ignition delay time versus chamber pressure for *n*-decane at an ambient temperature of 773 K. Droplet diameter 1.40 mm. All data reduced to a uniform initial liquid temperature of 40°C. The error bars are at ± one standard deviation of the measurements. Solid line represents model predictions with modified Westbrook and Dryer reaction rate parameters: $a = 0.25$, $b = 1.80$, $A = 1.75 \times 10^5$, and $E = 72.80$ kJ/mol. Dashed line represents model predictions with Müller *et al.* reaction rate parameters: $A_1 = 6.00 \times 10^8$ s^{-1}, $E_1 = 180.01$ kJ/mol, $A_{2OVL} = 1.09 \times 10^9$ cm^6/(gmol^2·s), and $E_{2OVL} = -19.71$ kJ/mol.

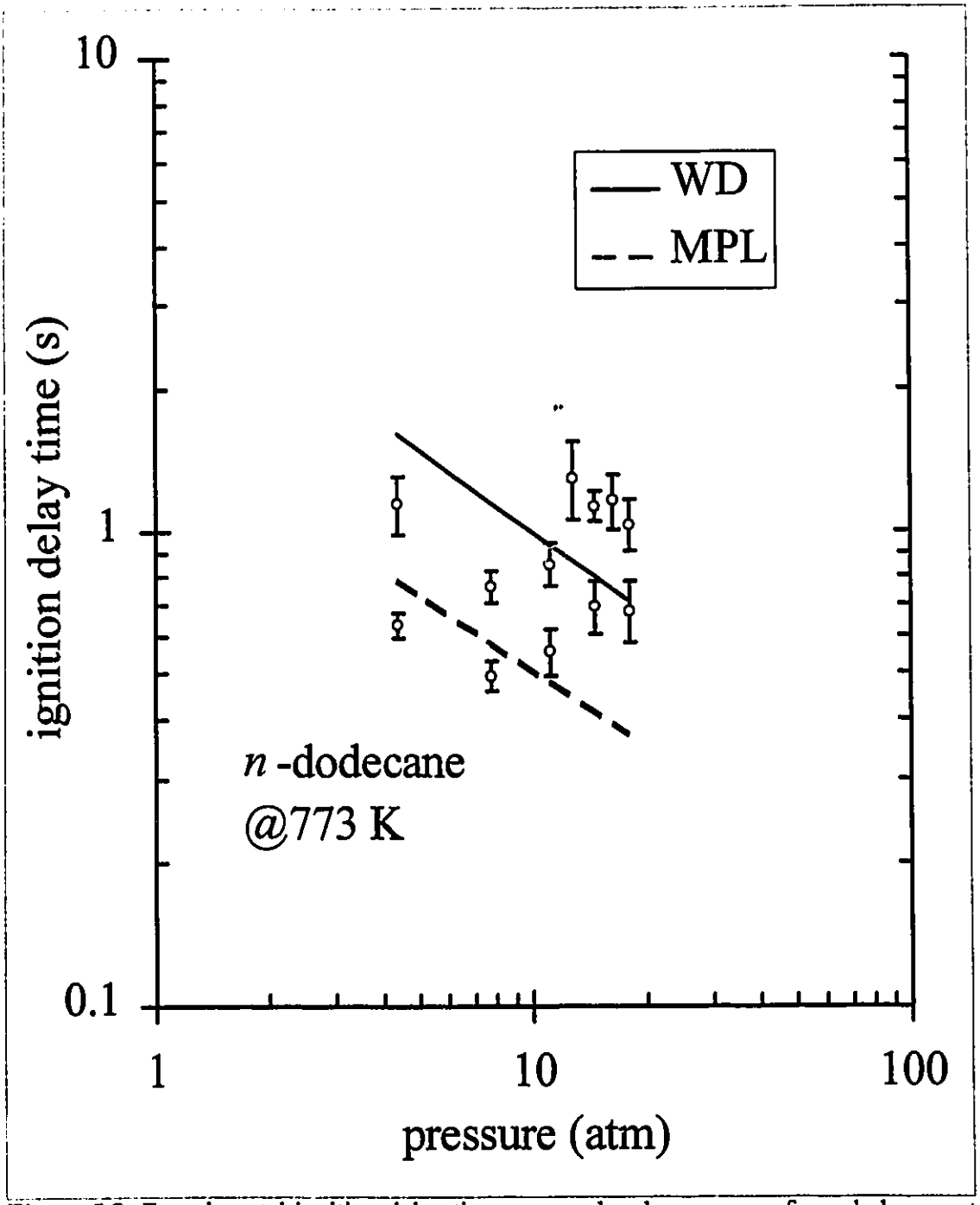

Figure 5.8: Experimental ignition delay time versus chamber pressure for *n*-dodecane at an ambient temperature of 773 K. Droplet diameter 1.40 mm. All data reduced to a uniform initial liquid temperature of 40°C. The error bars are at ± one standard deviation of the measurements. Solid line represents model predictions with modified Westbrook and Dryer reaction rate parameters: a = 0.25, b = 1.90, A = 4.05 × 10^5, and E = 76.15 kJ/mol. Dashed line represents model predictions with Müller *et al.* reaction rate parameters: A_1 = 7.25 × 10^8 s^{-1}, E_1 = 180.01 kJ/mol, A_{2OVL} = 1.24 × 10^9 $cm^6/(gmol^2 \cdot s)$, and E_{2OVL} = -19.71 kJ/mol.

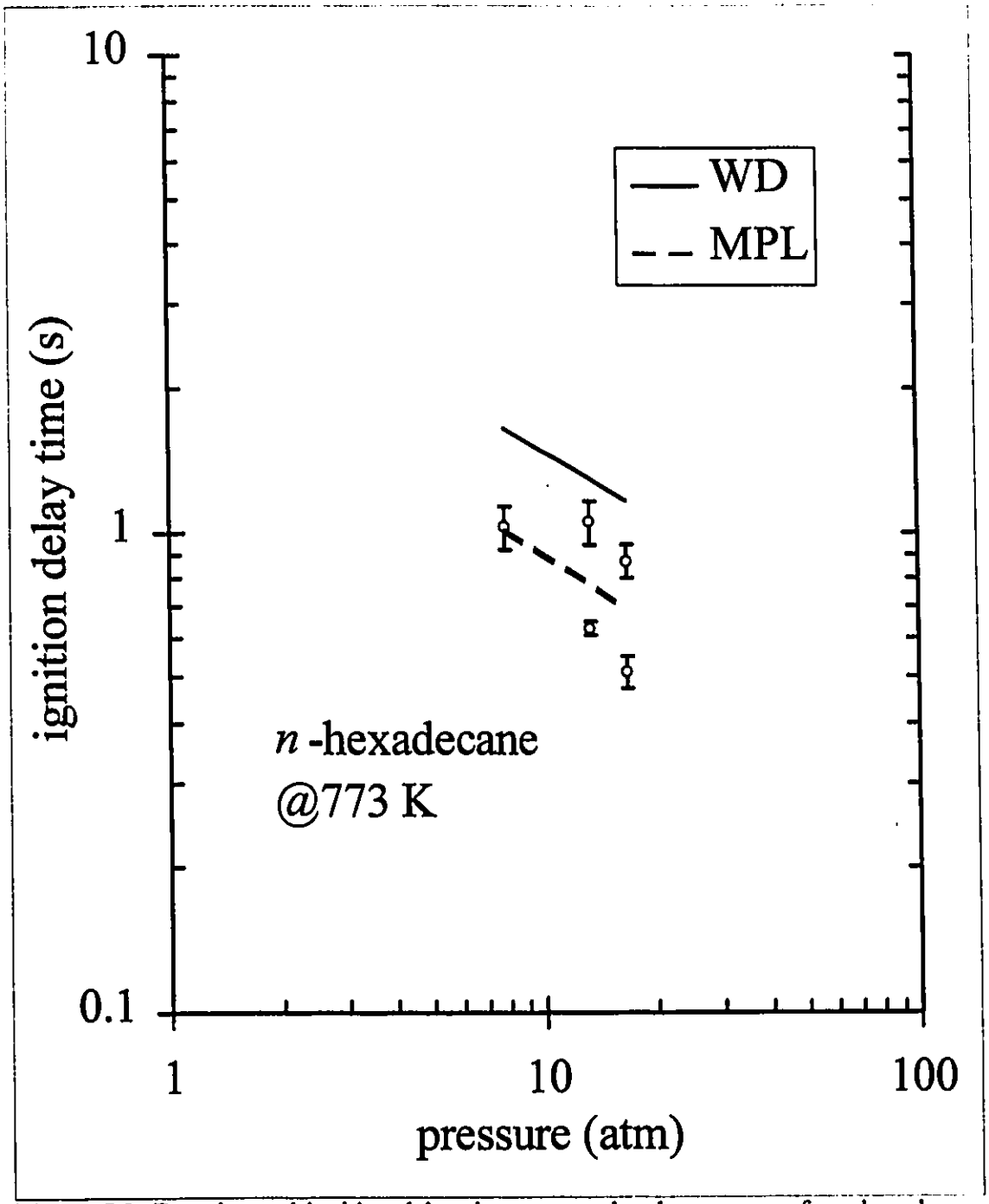

Figure 5.9: Experimental ignition delay time versus chamber pressure for *n*-hexadecane at an ambient temperature of 773 K. Droplet diameter 1.40 mm. All data reduced to a uniform initial liquid temperature of 40°C. The error bars are at ± one standard deviation of the measurements. Solid line represents model predictions with modified Westbrook and Dryer reaction rate parameters: a = 0.25, b = 1.90, $A = 4.30 \times 10^5$, and E = 78.24 kJ/mol. Dashed line represents model predictions with Müller *et al.* reaction rate parameters: $A_1 = 9.75 \times 10^8$ s^{-1}, E_1 = 180.01 kJ/mol, $A_{2OVL} = 1.54 \times 10^9$ cm^6/(gmol^2·s), and E_{2OVL} = -19.71 kJ/mol.

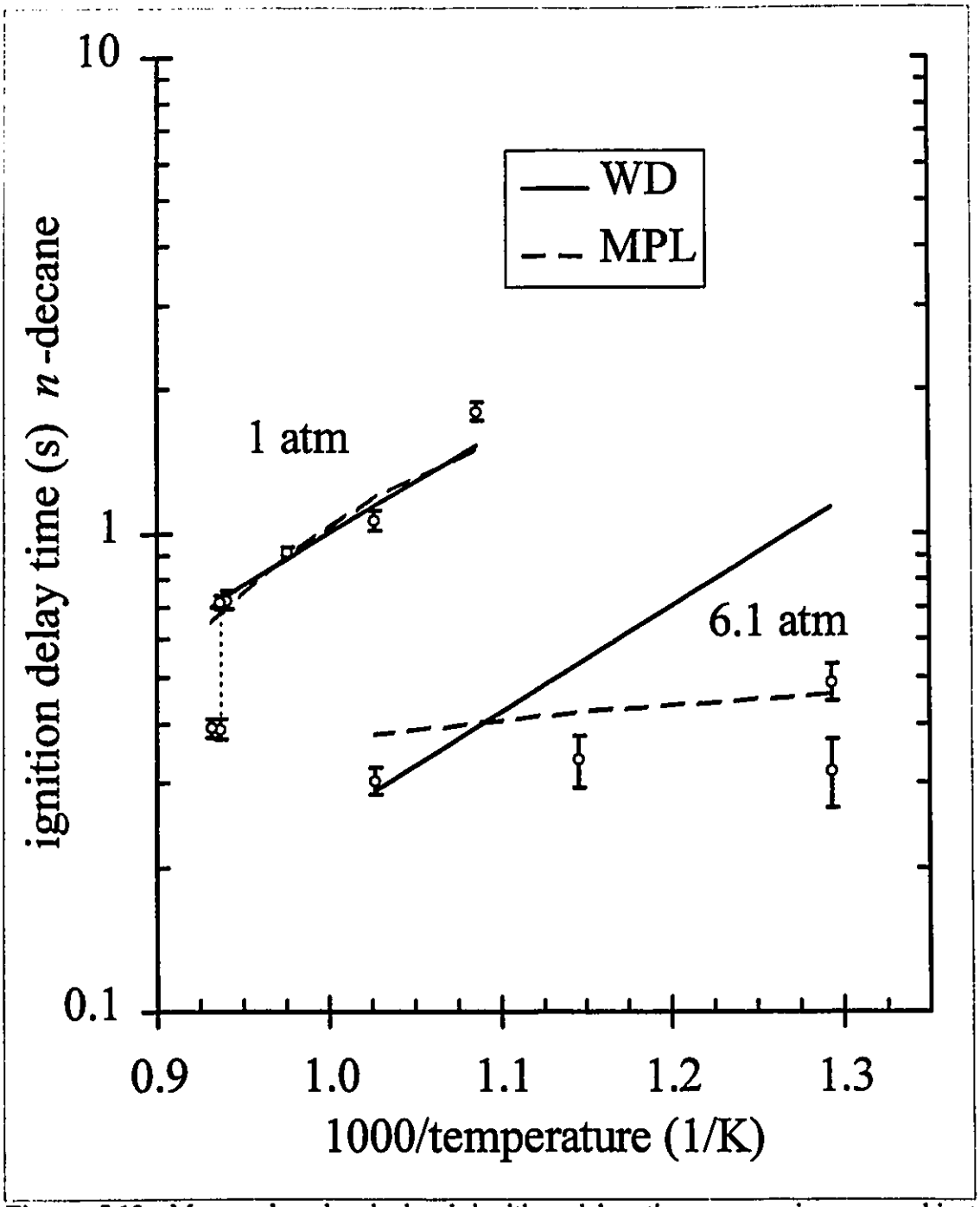

Figure 5.10: Measured and calculated ignition delay time versus inverse ambient temperature for *n*-decane at the chamber pressures of 1 and 6.1 atm. Droplet diameter 1.40 mm. All data reduced to a uniform initial liquid temperature of 40°C. The error bars are at ± one standard deviation of the measurements. Solid line represents model predictions with modified Westbrook and Dryer reaction rate parameters: a = 0.25, b = 1.80, $A = 1.75 \times 10^5$, and E = 72.80 kJ/mol. Dashed line represents model predictions with Müller *et al.* reaction rate parameters: $A_1 = 6.00 \times 10^8$ s^{-1}, E_1 = 180.01 kJ/mol, $A_{2OVL} = 1.09 \times 10^9$ cm^6/(gmol^2·s), and E_{2OVL} = -19.71 kJ/mol.

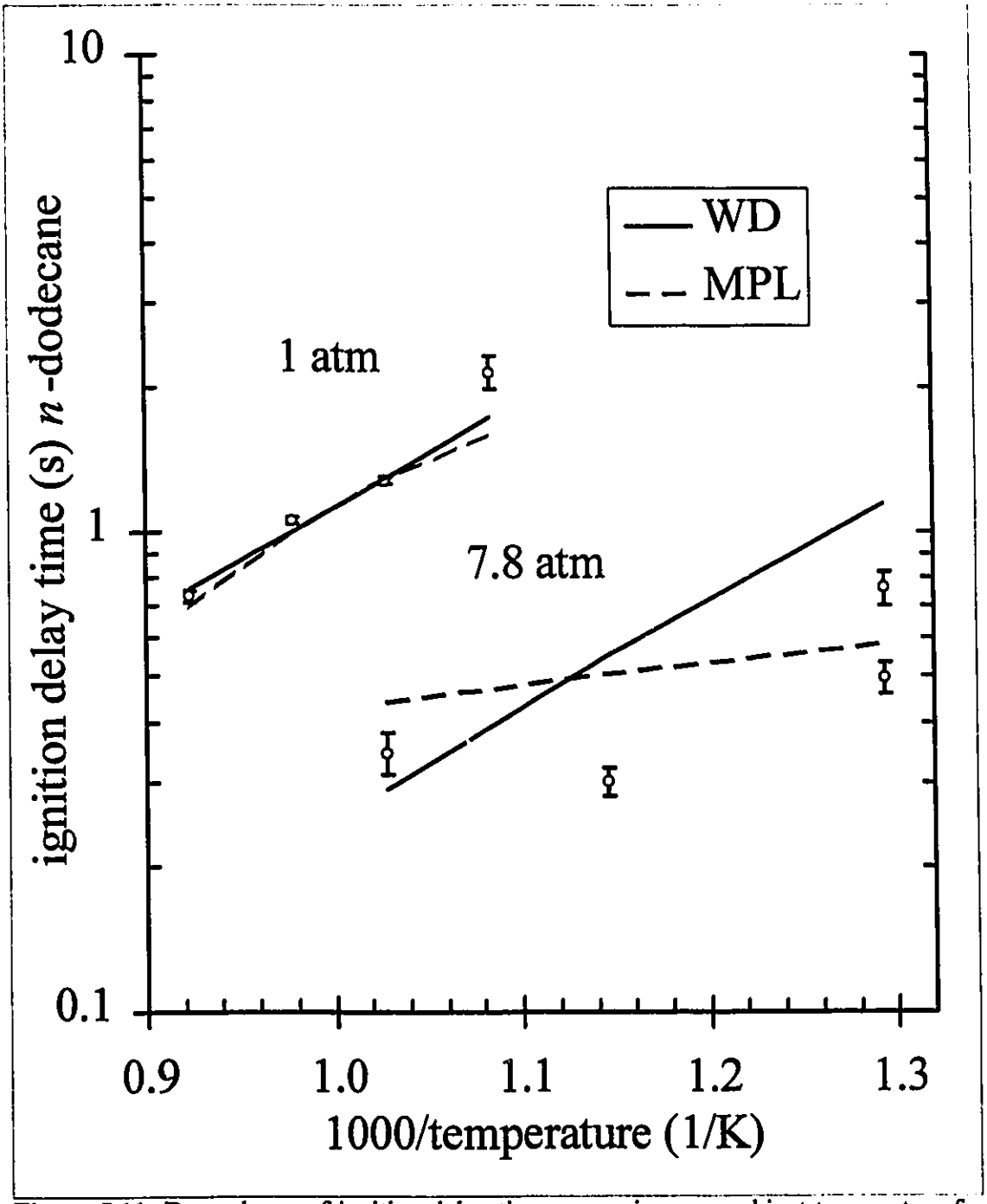

Figure 5.11: Dependence of ignition delay time versus inverse ambient temperature for *n*-dodecane at the chamber pressures of 1 and 7.8 atm. Droplet diameter 1.40 mm. All data reduced to a uniform initial liquid temperature of 40°C. The error bars are at ± one standard deviation of the measurements. Solid line represents model predictions with modified Westbrook and Dryer reaction rate parameters: a = 0.25, b = 1.90, A = 4.05 × 10^5, and E = 76.15 kJ/mol. Dashed line represents model predictions with Müller *et al.* reaction rate parameters: A_1 = 7.25 × 10^8 s^{-1}, E_1 = 180.01 kJ/mol, A_{2OVL} = 1.24 × 10^9 $cm^6/(gmol^2 \cdot s)$, and E_{2OVL} = -19.71 kJ/mol.

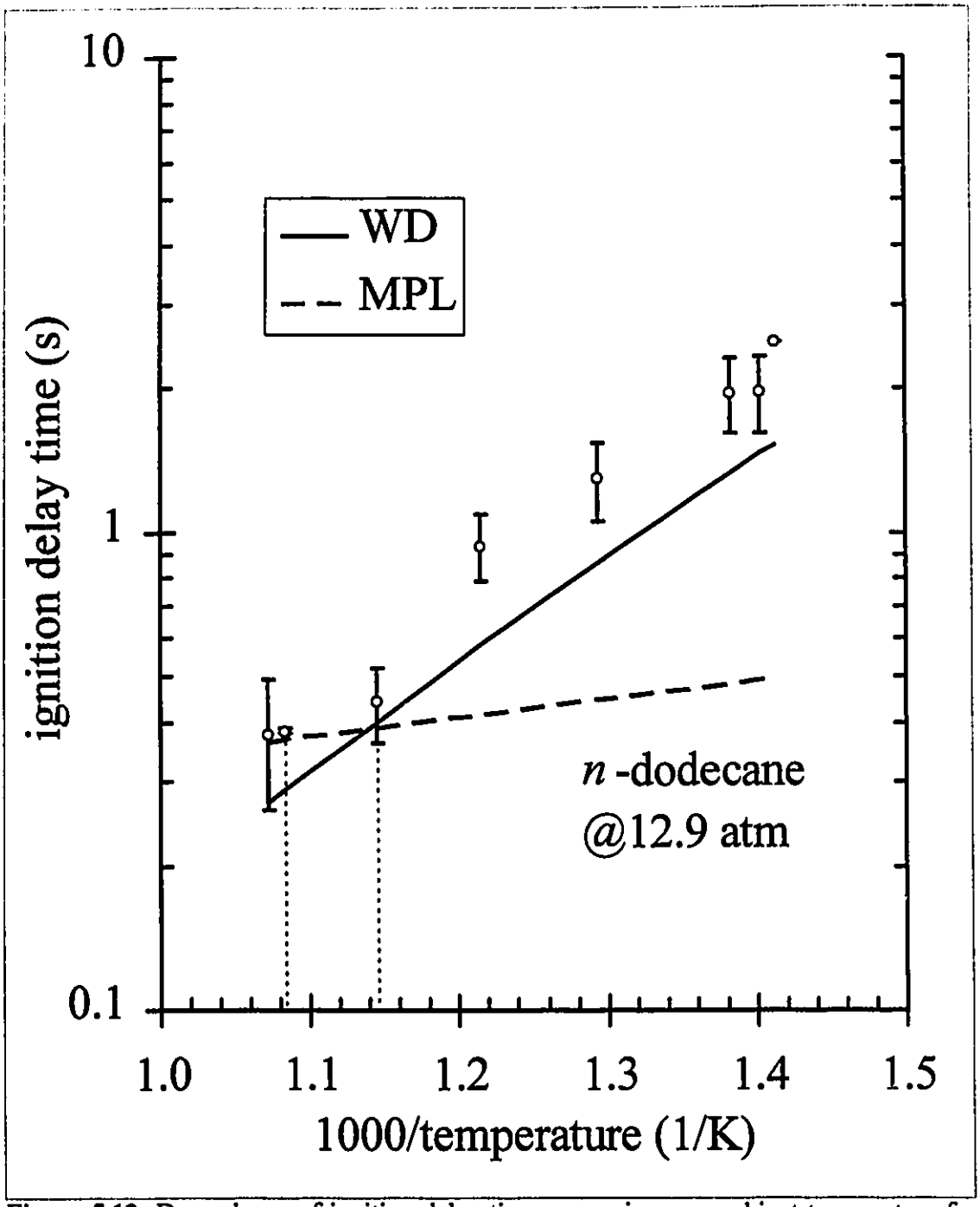

Figure 5.12: Dependence of ignition delay time versus inverse ambient temperature for *n*-dodecane at a chamber pressure of 12.9 atm. Droplet diameter 1.40 mm. All data reduced to a uniform initial liquid temperature of 40°C. The error bars are at ± one standard deviation of the measurements. Solid line represents model predictions with modified Westbrook and Dryer reaction rate parameters: a = 0.25, b = 1.90, A = 4.05 × 10^5, and E = 76.15 kJ/mol. Dashed line represents model predictions with Müller *et al.* reaction rate parameters: A_1 = 7.25 × 10^8 s^{-1}, E_1 = 180.01 kJ/mol, A_{2OVL} = 1.24 × 10^9 $cm^6/(gmol^2 \cdot s)$, and E_{2OVL} = -19.71 kJ/mol.

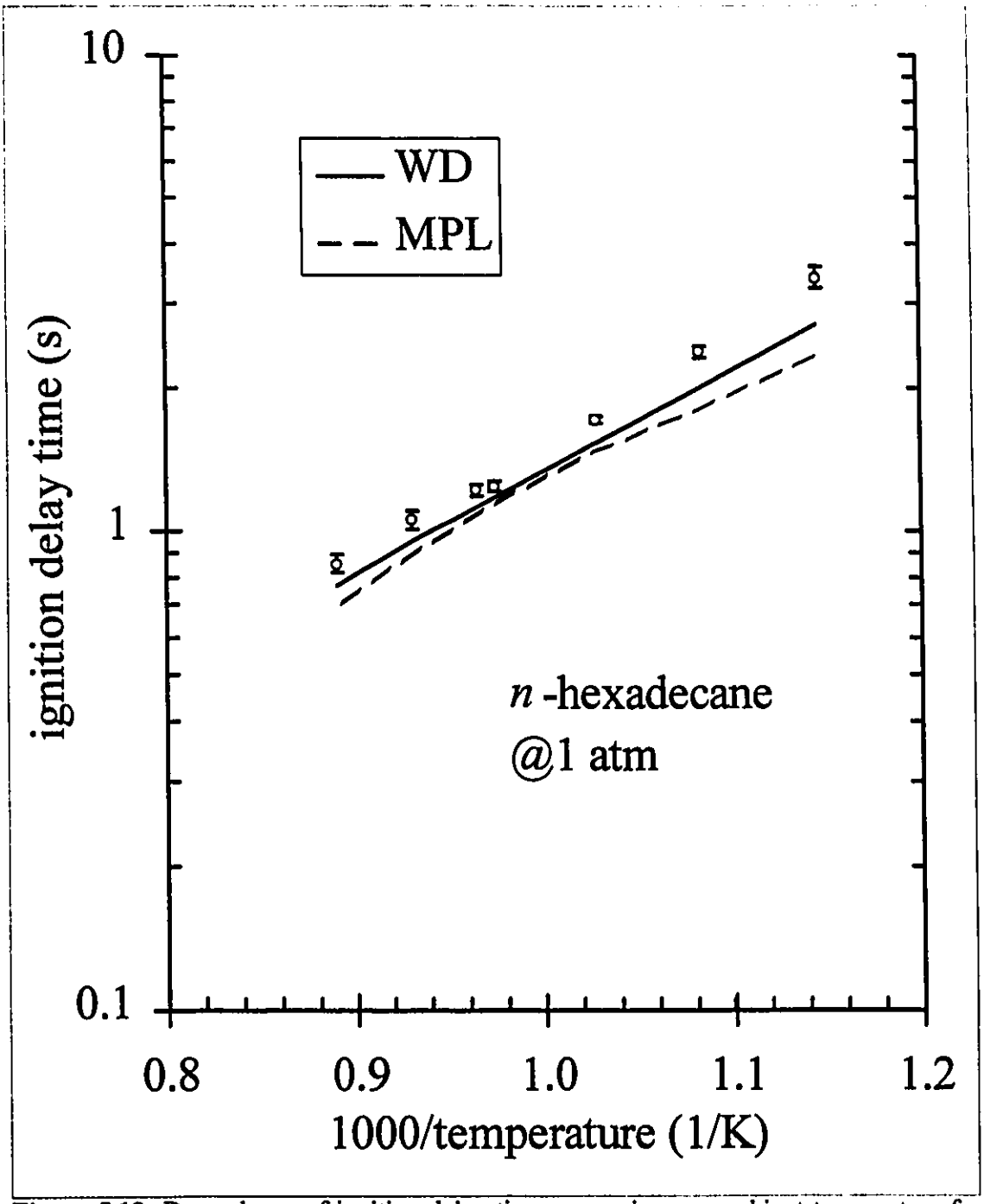

Figure 5.13: Dependence of ignition delay time versus inverse ambient temperature for *n*-hexadecane at a chamber pressure of 1 atm. Droplet diameter 1.40 mm. All data reduced to a uniform initial liquid temperature of 40°C. The error bars are at ± one standard deviation of the measurements. Solid line represents model predictions with modified Westbrook and Dryer reaction rate parameters: $a = 0.25$, $b = 1.90$, $A = 4.30 \times 10^5$, and $E = 78.24$ kJ/mol. Dashed line represents model predictions with Müller *et al.* reaction rate parameters: $A_1 = 9.75 \times 10^8$ s^{-1}, $E_1 = 180.01$ kJ/mol, $A_{2OVL} = 1.54 \times 10^9$ cm^6/(gmol^2·s), and $E_{2OVL} = -19.71$ kJ/mol.

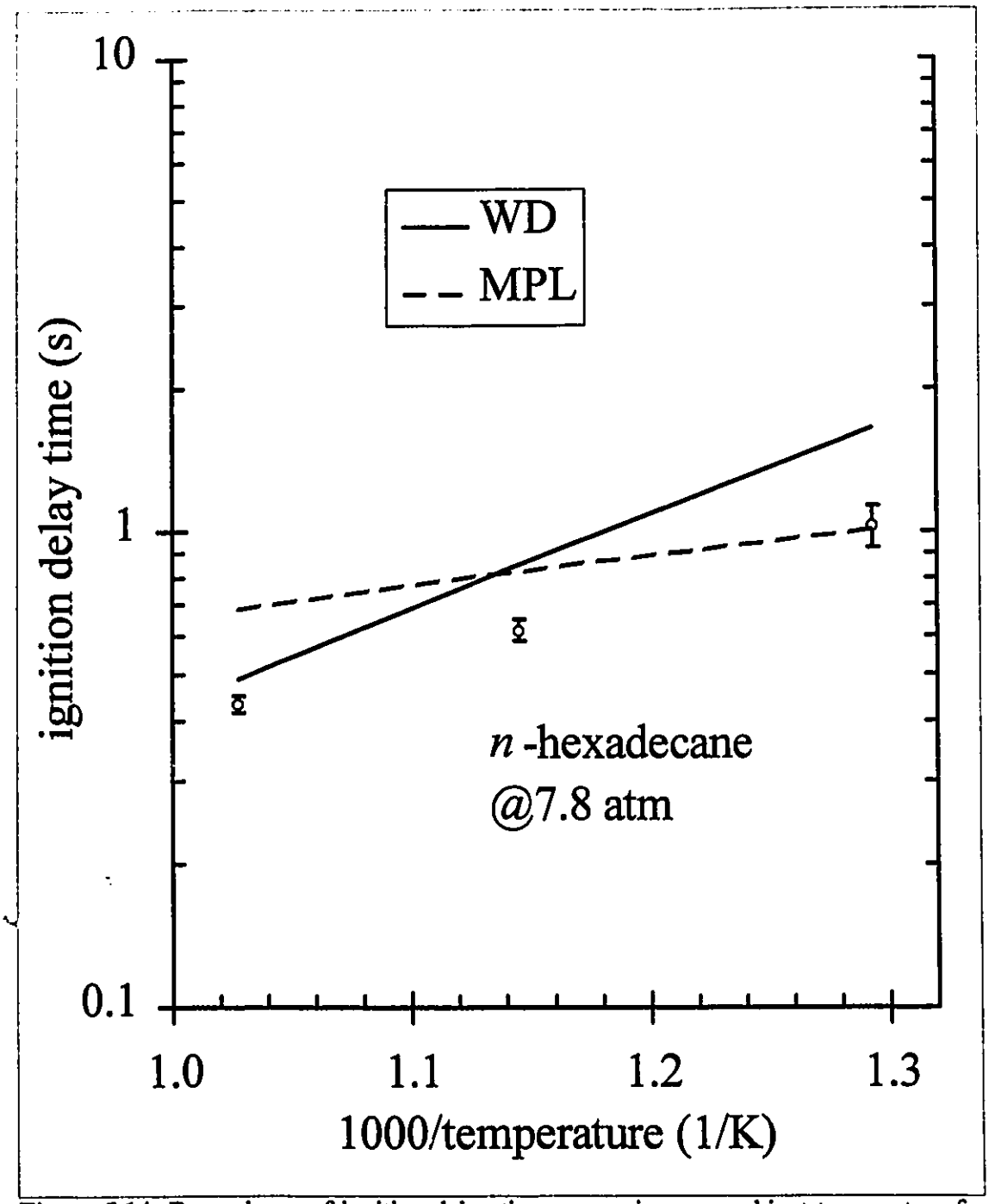

Figure 5.14: Dependence of ignition delay time versus inverse ambient temperature for *n*-hexadecane at a chamber pressure of 7.8 atm. Droplet diameter 1.40 mm. All data reduced to a uniform initial liquid temperature of 40°C. The error bars are at ± one standard deviation of the measurements. Solid line represents model predictions with modified Westbrook and Dryer reaction rate parameters: a = 0.25, b = 1.90, A = 4.30 × 10^5, and E = 78.24 kJ/mol. Dashed line represents model predictions with Müller *et al.* reaction rate parameters: A_1 = 9.75 × 10^8 s^{-1}, E_1 = 180.01 kJ/mol, A_{2OVL} = 1.54 × 10^9 $cm^6/(gmol^2 \cdot s)$, and E_{2OVL} = -19.71 kJ/mol.

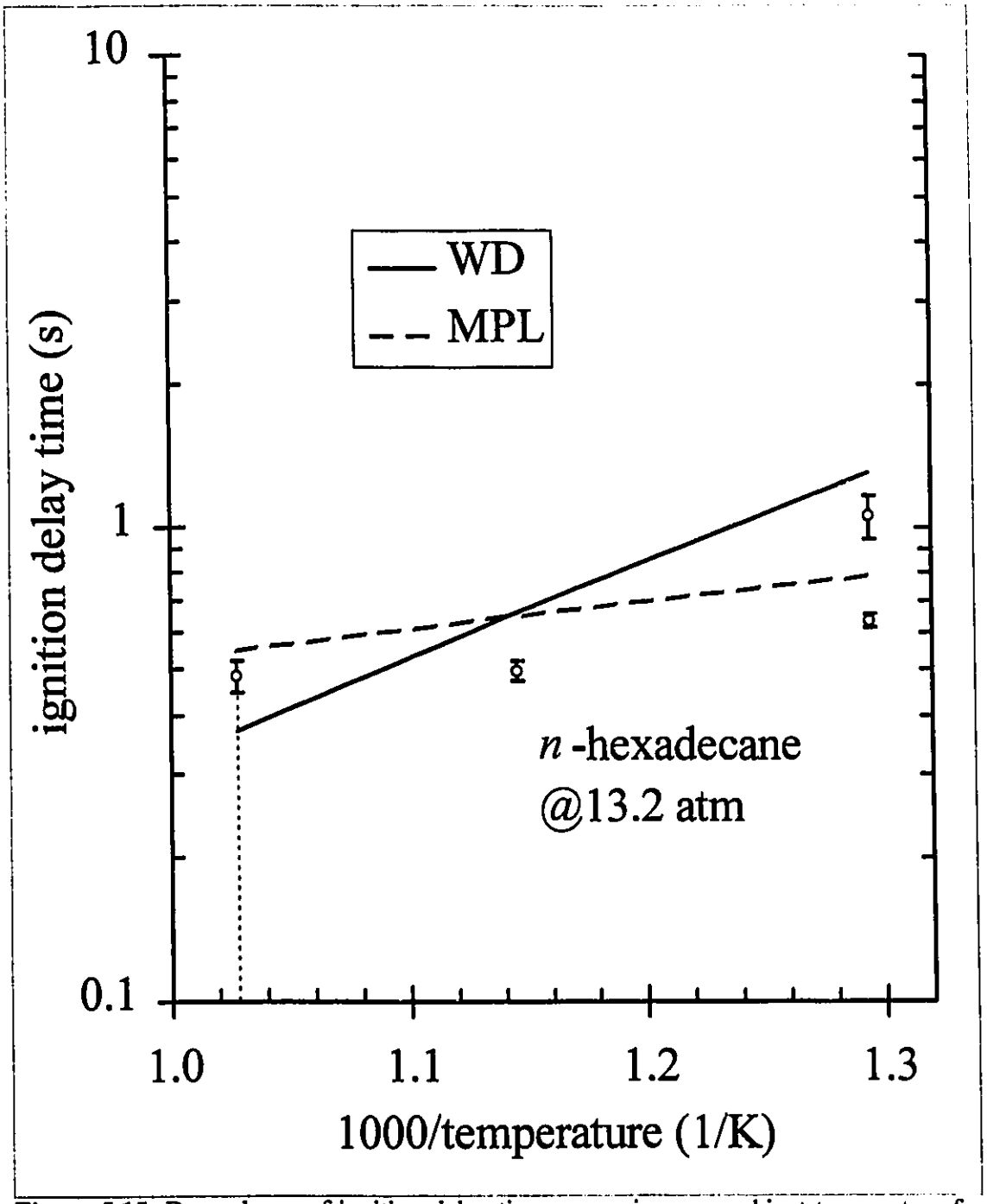

Figure 5.15: Dependence of ignition delay time versus inverse ambient temperature for *n*-hexadecane at a chamber pressure of 13.2 atm. Droplet diameter 1.40 mm. All data reduced to a uniform initial liquid temperature of 40°C. The error bars are at ± one standard deviation of the measurements. Solid line represents model predictions with modified Westbrook and Dryer reaction rate parameters: a = 0.25, b = 1.90, A = 4.30 × 10^5, and E = 78.24 kJ/mol. Dashed line represents model predictions with Müller *et al.* reaction rate parameters: A_1 = 9.75 × 10^8 s^{-1}, E_1 = 180.01 kJ/mol, A_{2OVL} = 1.54 × 10^9 $cm^6/(gmol^2 \cdot s)$, and E_{2OVL} = -19.71 kJ/mol.

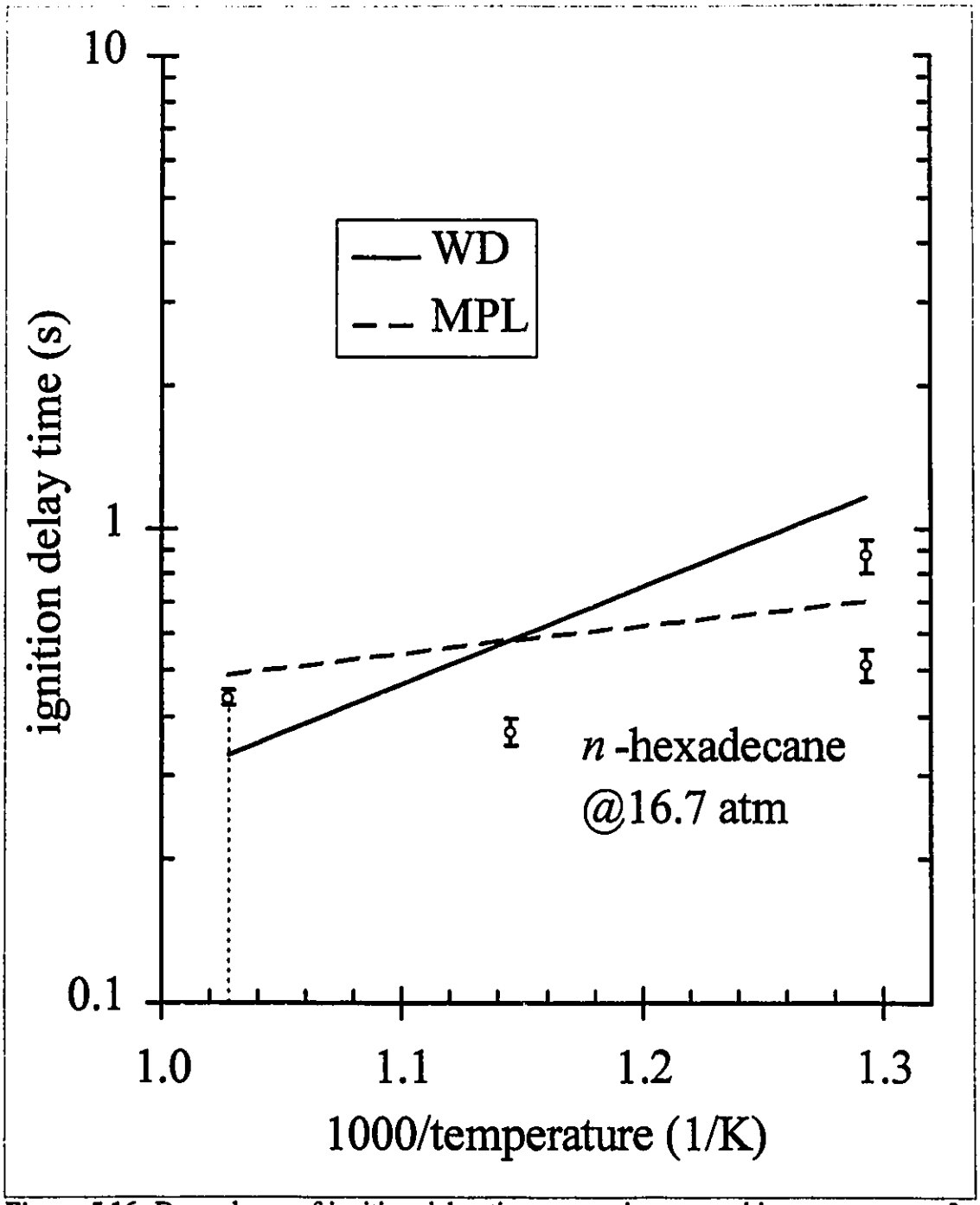

Figure 5.16: Dependence of ignition delay time versus inverse ambient temperature for *n*-hexadecane at a chamber pressure of 16.7 atm. Droplet diameter 1.40 mm. All data reduced to a uniform initial liquid temperature of 40°C. The error bars are at ± one standard deviation of the measurements. Solid line represents model predictions with modified Westbrook and Dryer reaction rate parameters: $a = 0.25$, $b = 1.90$, $A = 4.30 \times 10^5$, and $E = 78.24$ kJ/mol. Dashed line represents model predictions with Müller *et al.* reaction rate parameters: $A_1 = 9.75 \times 10^8$ s^{-1}, $E_1 = 180.01$ kJ/mol, $A_{2OVL} = 1.54 \times 10^9$ cm^6/(gmol^2·s), and $E_{2OVL} = -19.71$ kJ/mol.

5.2.2 Cycloparaffin hydrocarbons

Only one cycloparaffin hydrocarbon was studied, namely decalin (decahydronapthalene), chosen because its boiling point is similar to that of *n*-decane. Figures 5.17 to 5.19 show the dependence of ignition delay time on chamber pressure, for ambient temperatures of 973 K, 873 K, and 773 K, respectively. A change in chemical kinetics from two-stage ignition to one stage seems to occur at 11 atm for 973 K (see Figure 5.17). As discussed for *n*-paraffins, this also occurs over a range of pressures from 7 atm to 18 atm at temperatures below 973 K (Figures 5.18 and 5.19). The results suggest lower temperatures induce a higher occurrence of "twinned" ignition when pressures are 10 atm and above. The pressure dependence for decalin does not seem to be as strong as that observed for the *n*-paraffins family. The plot for 773 K starts at about 4 atm; this is the ignitable limit, and decalin droplets could not be ignited below this pressure.

Plots of ignition delay time versus inverse ambient temperature (Figures 5.20 to 5.23) reveal slight changes in effective activation energy for decalin under pressure, but not as much as for *n*-paraffins. This result suggests that the earlier assumption that pressure has little influence on activation energy may not be as valid as first presumed. Figures 5.22 and 5.23 might provide some insight into this matter. There are "twinned" data points in the upper half of the temperature ranges. The slower ignition points possess similar slopes (similar activation energies), whereas the faster ignition points have slopes that are less steep, suggesting a drop in effective activation energy with the effect of pressure. These "twinned" data points for the *n*-paraffin 1/T plots might be the apparent cause of the noticeable decrease in effective activation energies.

Overall, decalin behaves like *n*-paraffin hydrocarbons with only slightly slower ignition delay times. This is to be expected, since during the ignition process cycloparaffins resemble *n*-paraffins as the ring structure breaks into straight chain segments of hydrocarbons.

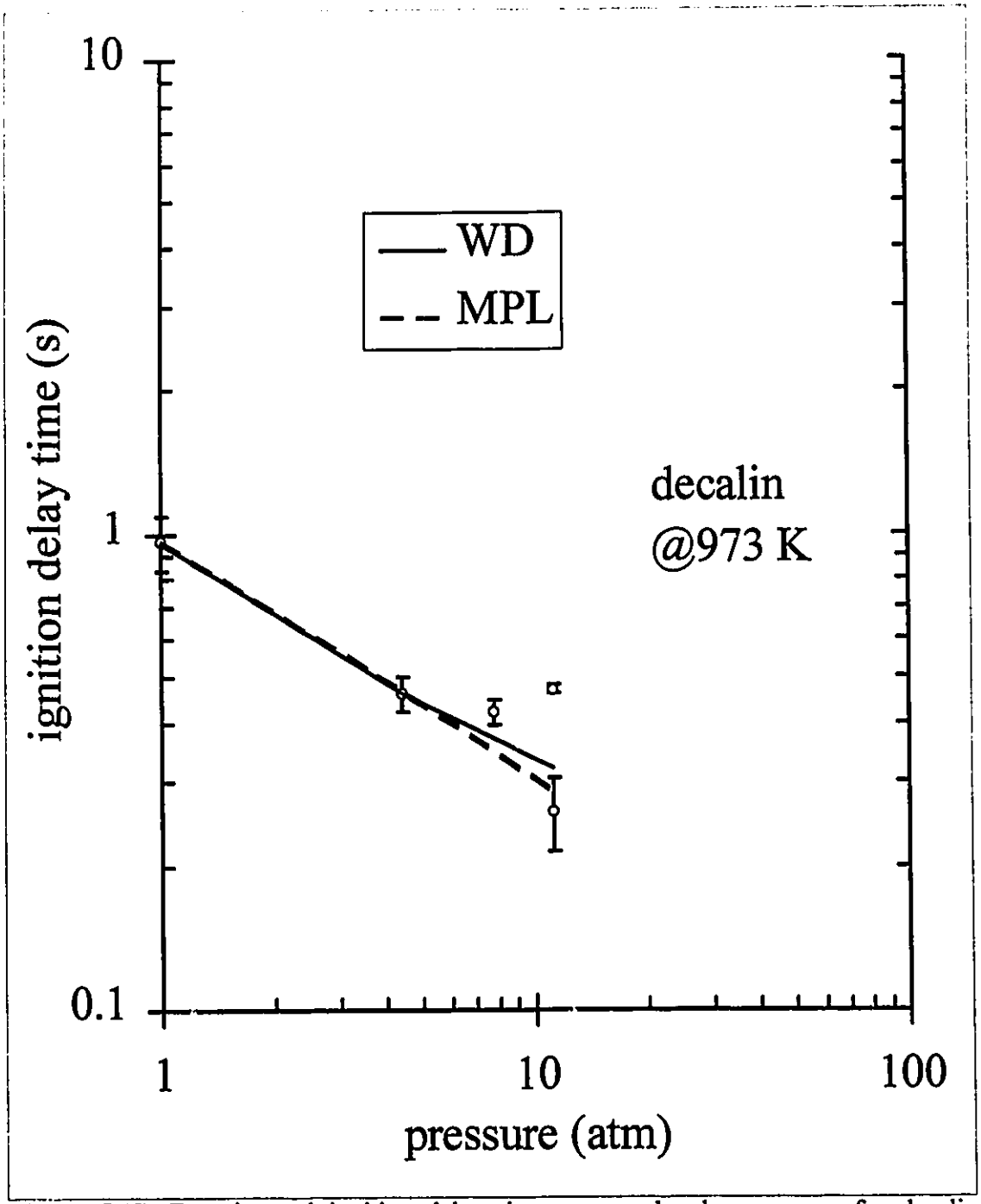

Figure 5.17: Experimental ignition delay time versus chamber pressure for decalin (decahydronaphthalene) at an ambient temperature of 973 K. Droplet diameter 1.40 mm. All data reduced to a uniform initial liquid temperature of 40°C. The error bars are at ± one standard deviation of the measurements. Solid line represents model predictions with modified Westbrook and Dryer reaction rate parameters: a = 0.25, b = 1.54, A = 1.07 × 10^5, and E = 81.59 kJ/mol. Dashed line represents model predictions with Müller *et al.* reaction rate parameters: A_1 = 1.15 × 10^8 s^{-1}, E_1 = 180.01 kJ/mol, A_{2OVL} = 1.09 × 10^9 $cm^6/(gmol^2 \cdot s)$, and E_{2OVL} = -19.71 kJ/mol.

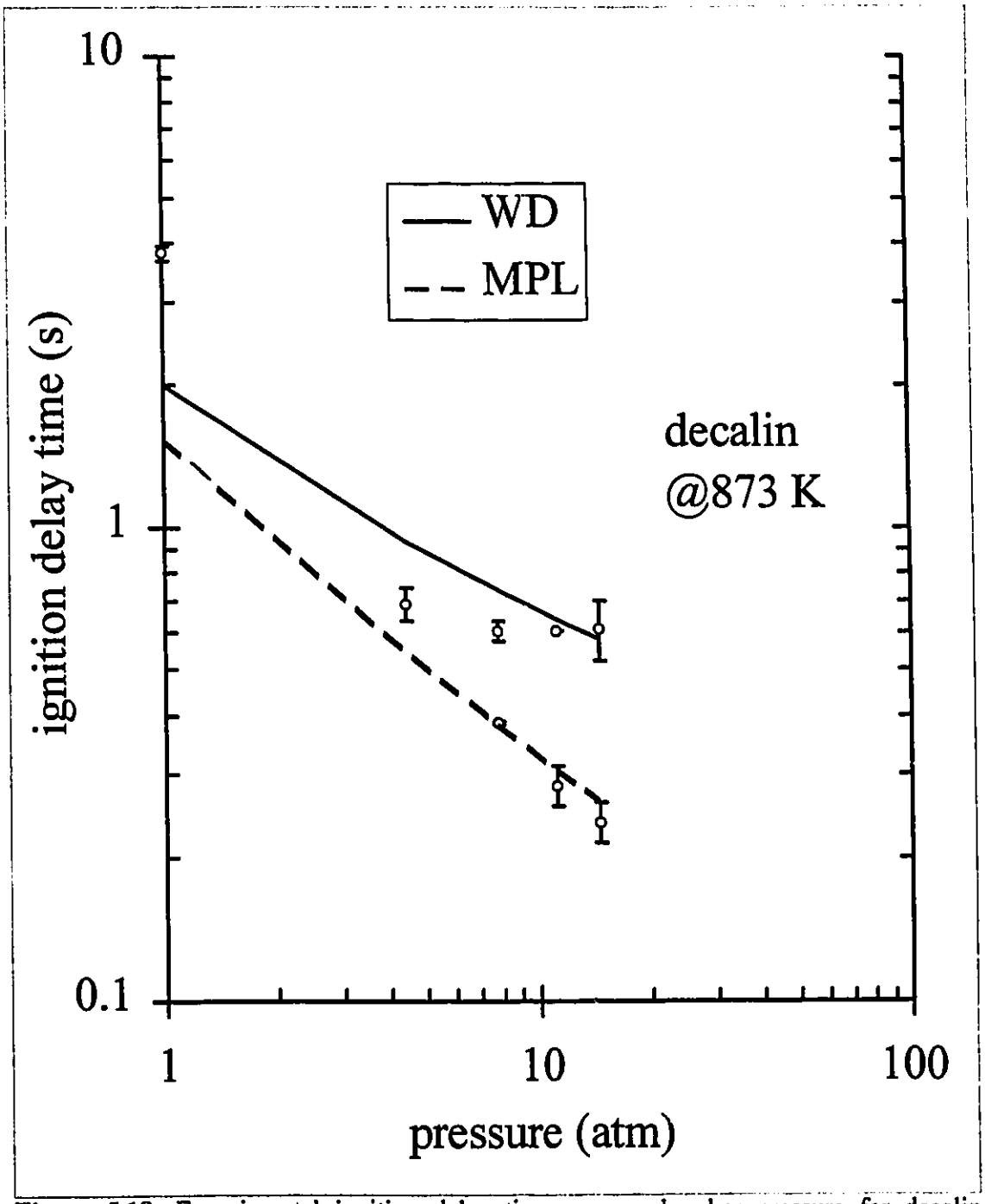

Figure 5.18: Experimental ignition delay time versus chamber pressure for decalin (decahydronaphthalene) at an ambient temperature of 873 K. Droplet diameter 1.40 mm. All data reduced to a uniform initial liquid temperature of 40°C. The error bars are at ± one standard deviation of the measurements. Solid line represents model predictions with modified Westbrook and Dryer reaction rate parameters: a = 0.25, b = 1.54, A = 1.07 × 10^5, and E = 81.59 kJ/mol. Dashed line represents model predictions with Müller *et al.* reaction rate parameters: A_1 = 1.15 × 10^8 s^{-1}, E_1 = 180.01 kJ/mol, A_{2OVL} = 1.09 × 10^9 $cm^6/(gmol^2 \cdot s)$, and E_{2OVL} = -19.71 kJ/mol.

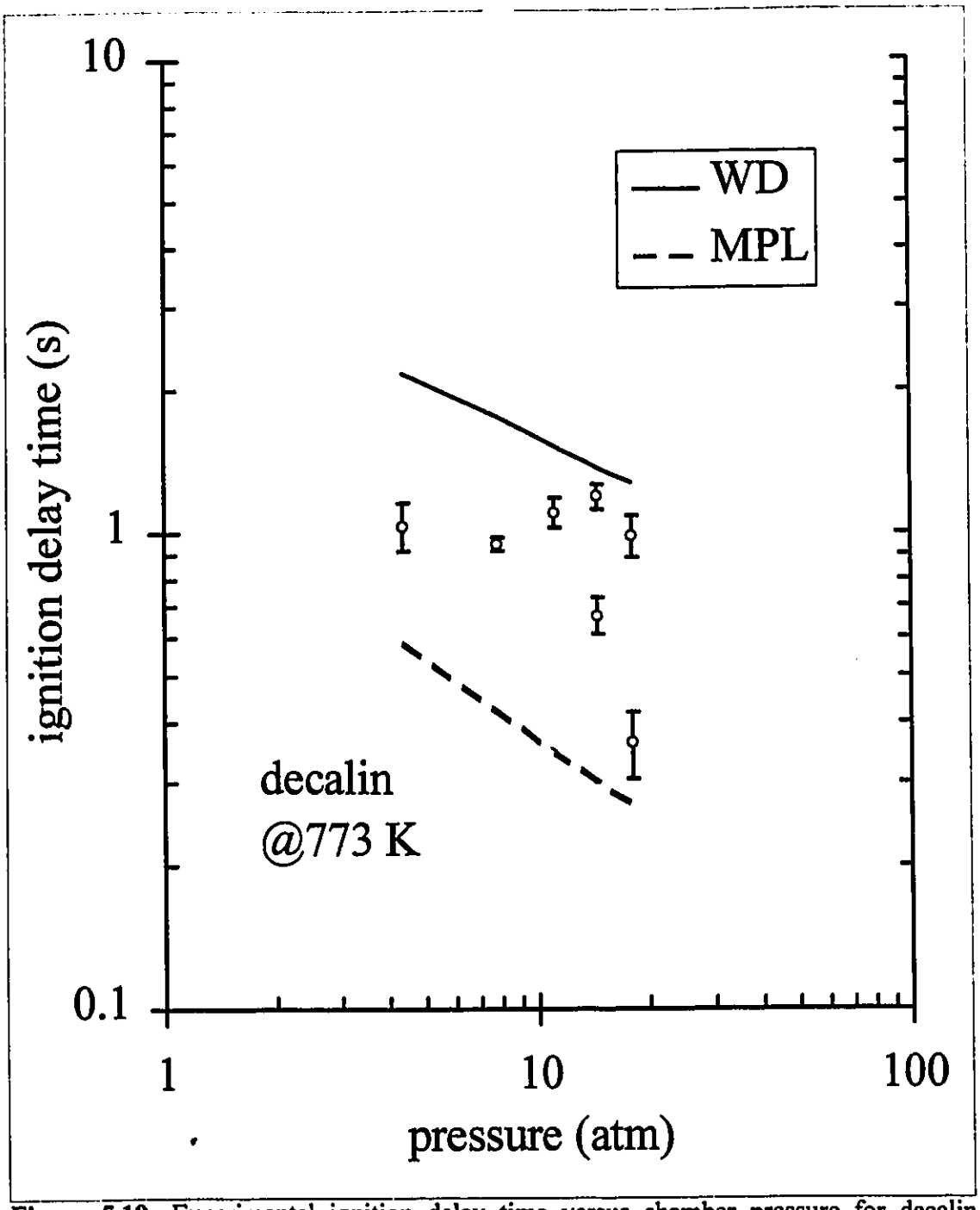

Figure 5.19: Experimental ignition delay time versus chamber pressure for decalin (decahydronaphthalene) at an ambient temperature of 773 K. Droplet diameter 1.40 mm. All data reduced to a uniform initial liquid temperature of 40°C. The error bars are at ± one standard deviation of the measurements. Solid line represents model predictions with modified Westbrook and Dryer reaction rate parameters: a = 0.25, b = 1.54, A = 1.07 × 10^5, and E = 81.59 kJ/mol. Dashed line represents model predictions with Müller *et al.* reaction rate parameters: A_1 = 1.15 × 10^8 s^{-1}, E_1 = 180.01 kJ/mol, A_{2OVL} = 1.09 × 10^9 $cm^6/(gmol^2 \cdot s)$, and E_{2OVL} = -19.71 kJ/mol.

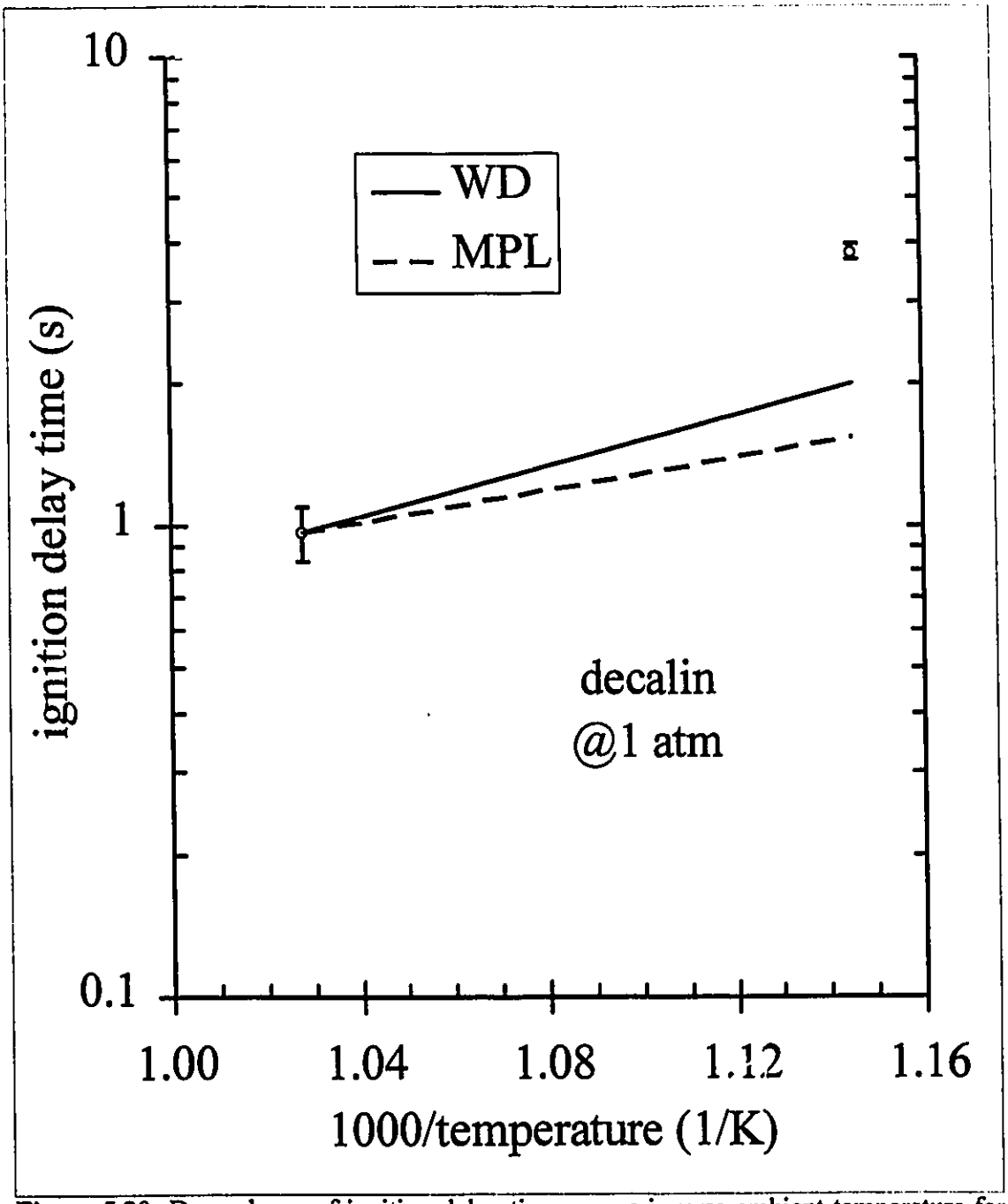

Figure 5.20: Dependence of ignition delay time versus inverse ambient temperature for decalin (decahydronaphthalene) at a chamber pressure of 1 atm. Droplet diameter 1.40 mm. All data reduced to a uniform initial liquid temperature of 40°C. The error bars are at ± one standard deviation of the measurements. Solid line represents model predictions with modified Westbrook and Dryer reaction rate parameters: $a = 0.25$, $b = 1.54$, $A = 1.07 \times 10^5$, and $E = 81.59$ kJ/mol. Dashed line represents model predictions with Müller *et al.* reaction rate parameters: $A_1 = 1.15 \times 10^8$ s^{-1}, $E_1 = 180.01$ kJ/mol, $A_{2OVL} = 1.09 \times 10^9$ $cm^6/(gmol^2 \cdot s)$, and $E_{2OVL} = -19.71$ kJ/mol.

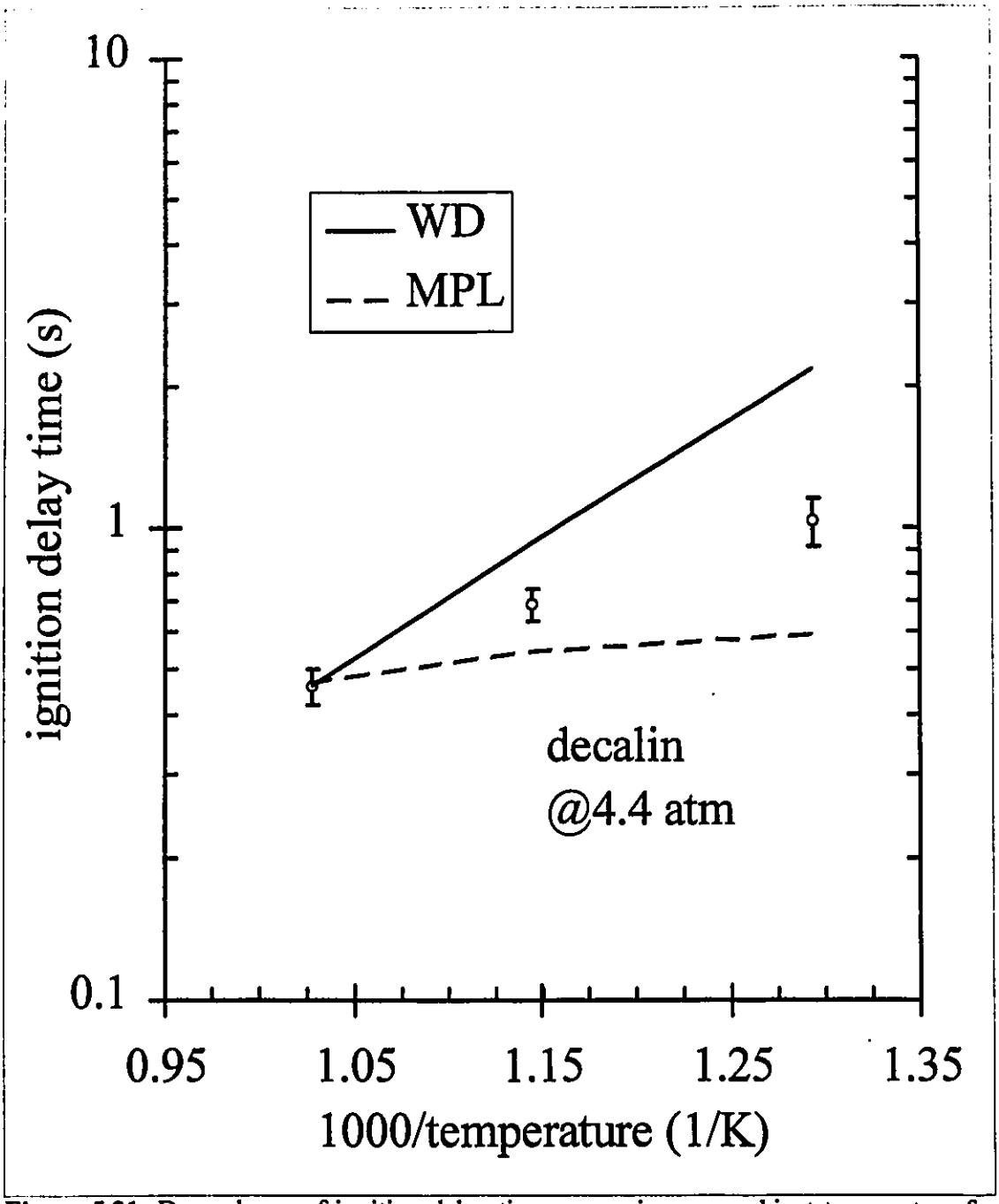

Figure 5.21: Dependence of ignition delay time versus inverse ambient temperature for decalin (decahydronaphthalene) at a chamber pressure of 4.4 atm. Droplet diameter 1.40 mm. All data reduced to a uniform initial liquid temperature of 40°C. The error bars are at ± one standard deviation of the measurements. Solid line represents :nodel predictions with modified Westbrook and Dryer reaction rate parameters: $a = 0.25$, $b = 1.54$, $A = 1.07 \times 10^5$, and $E = 81.59$ kJ/mol. Dashed line represents model predictions with Müller *et al.* reaction rate parameters: $A_1 = 1.15 \times 10^8$ s^{-1}, $E_1 = 180.01$ kJ/mol, $A_{2OVL} = 1.09 \times 10^9$ $cm^6/(gmol^2 \cdot s)$, and $E_{2OVL} = -19.71$ kJ/mol.

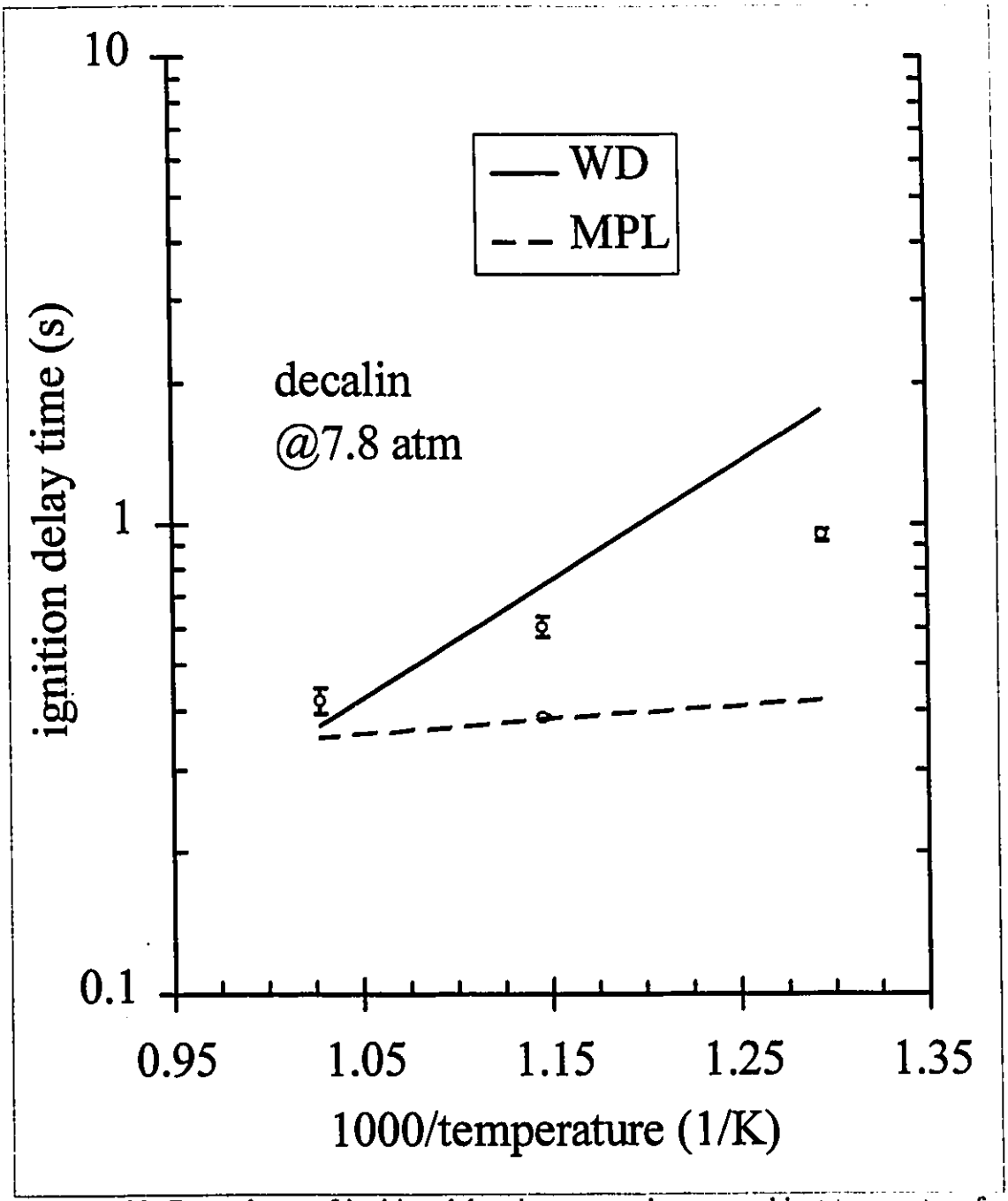

Figure 5.22: Dependence of ignition delay time versus inverse ambient temperature for decalin (decahydronaphthalene) at a chamber pressure of 7.8 atm. Droplet diameter 1.40 mm. All data reduced to a uniform initial liquid temperature of 40°C. The error bars are at ± one standard deviation of the measurements. Solid line represents model predictions with modified Westbrook and Dryer reaction rate parameters: $a = 0.25$, $b = 1.54$, $A = 1.07 \times 10^5$, and $E = 81.59$ kJ/mol. Dashed line represents model predictions with Müller *et al.* reaction rate parameters: $A_1 = 1.15 \times 10^8$ s^{-1}, $E_1 = 180.01$ kJ/mol, $A_{2OVL} = 1.09 \times 10^9$ cm^6/(gmol^2·s), and $E_{2OVL} = -19.71$ kJ/mol.

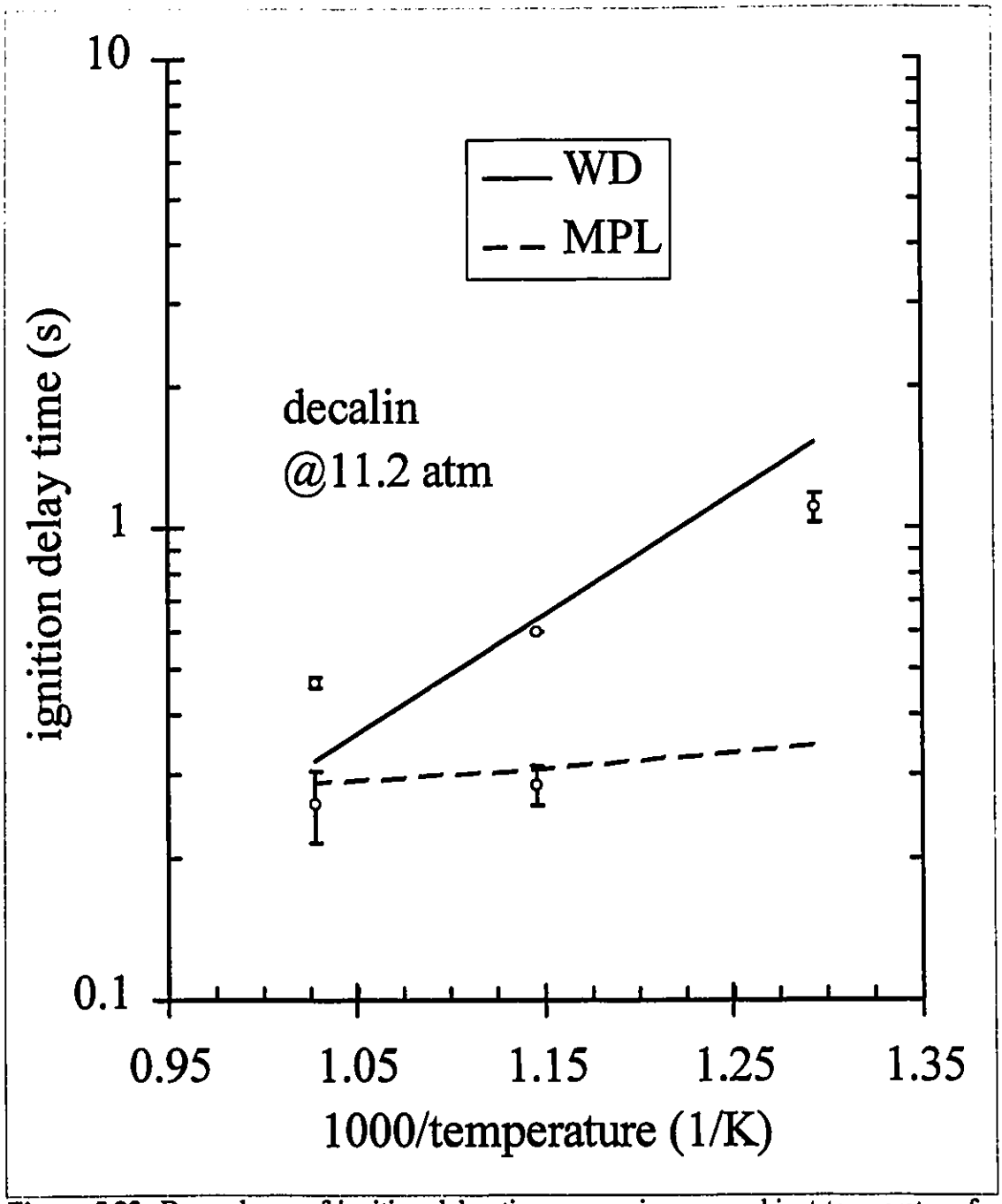

Figure 5.23: Dependence of ignition delay time versus inverse ambient temperature for decalin (decahydronaphthalene) at a chamber pressure of 11.2 atm. Droplet diameter 1.40 mm. All data reduced to a uniform initial liquid temperature of 40°C. The error bars are at ± one standard deviation of the measurements. Solid line represents model predictions with modified Westbrook and Dryer reaction rate parameters: $a = 0.25$, $b = 1.54$, $A = 1.07 \times 10^5$, and $E = 81.59$ kJ/mol. Dashed line represents model predictions with Müller *et al.* reaction rate parameters: $A_1 = 1.15 \times 10^8$ s^{-1}, $E_1 = 180.01$ kJ/mol, $A_{2OVL} = 1.09 \times 10^9$ cm^6/(gmol^2·s), and $E_{2OVL} = -19.71$ kJ/mol.

5.2.3 Aromatic hydrocarbons

The first aromatic compound chosen for experiments was mesitylene (1,3,5-trimethylbenzene). This fuel was chosen because its boiling point (437.9 K) is close to that of *n*-decane (447.3 K), making it well suited for mixture studies. The results for this compound (Figure 5.24) are remarkable. At atmospheric pressure, the data show considerable scatter, but the average value obtained agrees with that from earlier atmospheric pressure experiments (Bergeron and Hallett, 1989b). However, an increase in pressure to 2 atm results in a slightly *longer* ignition delay time, despite the increase in furnace power for sustaining the ambient temperature at 700°C. At pressures any higher than 2 atm, no ignition was possible. Earlier experiments at atmospheric pressure (Bergeron and Hallett, 1989b) showed that the ignitable limit for mesitylene droplets was about 660°C, or close to the experimental temperature. The large scatter observed in the present data is typical of droplets near the ignitable limit. However, one would expect that increasing the pressure would make the droplet more ignitable.

A review of ignition data under homogenous gaseous conditions for aromatic hydrocarbons (Salooja, 1965) showed that aromatics fall roughly into two groups of compounds of similar ignitability. Mesitylene and other methyl-benzenes, with the exception of *o*-xylene, belong to the less reactive group, while *o*-xylene and alkyl benzenes with two or more carbons in the side chain ignite more rapidly. Fuel-air mixtures of the less reactive compounds cease to be ignitable at about 650°C, while the limit for the other group of compounds is around 520°C to 550°C.

Having established that the failure to ignite mesitylene at higher pressures was at least partly due to its belonging to the less reactive group, it was decided to carry out subsequent aromatic experiments with an alkyl benzene, isobutylbenzene, whose boiling point (445.9 K) is virtually identical to that of *n*-decane (447.3 K).

Figure 5.25 shows remarkably that isobutylbenzene has the same ignition effect with chamber pressure as that observed with mesitylene. Ignition delay times showed

little or no influence of pressure. At 7.8 atm, ignition times actually increased from the previous data point at 4.4 atm. However, unlike *n*-paraffins, isobutylbenzene did not experience a change in the slope of the plots with 1/T under the influence of pressure (Figures 5.27 - 29). This suggests that the activation energy for this fuel does not change with pressure.

Experiments were also performed at 923 K for 4.4 atm and the ignition delay times obtained averaged 1.46 ± 0.09 seconds; however, at 7.8 atm and 923 K, the fuel was not ignitable for a wide range of droplet diameters (1.0 mm to 2.5 mm). With mesitylene and isobutylbenzene having similar effects, experiments were conducted with *o*-xylene and Figure 5.26 shows again no pressure dependence up to 2 atm, beyond which the fuel was not ignitable. In section §5.3.3 more will be said to provide an explanation for the ignition of aromatics by using the single-component numerical model to predict the mass flux of fuel evolving from the droplet surface.

It is interesting to note that none of the aromatics tested showed any sign of "twinned" data points. Recent measurements by Marchand (1995), at lower temperatures than those recorded here, have confirmed that experimental conditions which produce twinned points for paraffins do not do this for aromatics. This, together with the fact that the literature shows that aromatics do not undergo two-stage ignition, tends to support the hypothesis that the "twinned" points correspond to one- and two-stage ignition. It also shows that the measurements of two different ignition times for paraffins are not due to experimental error.

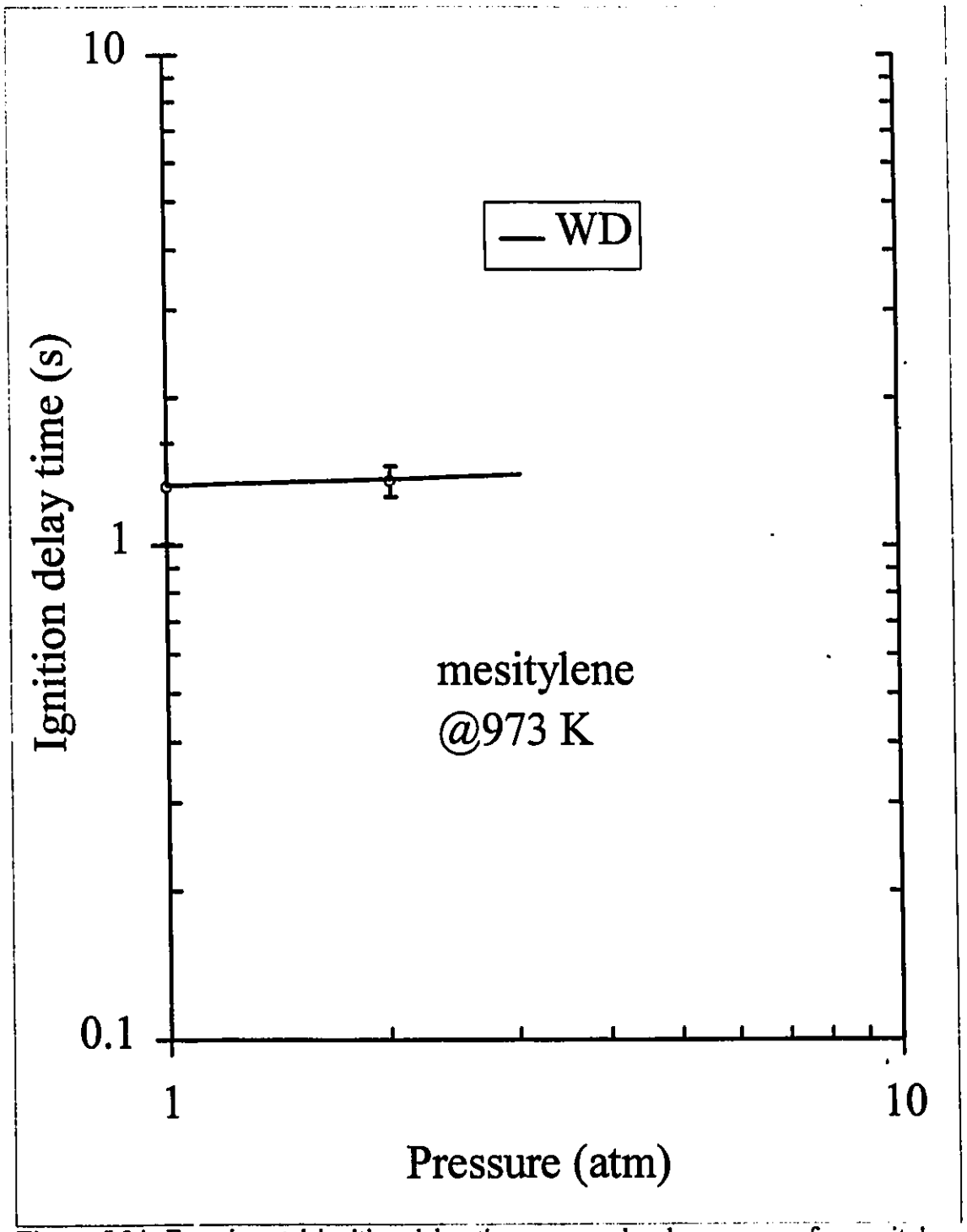

Figure 5.24: Experimental ignition delay time versus chamber pressure for mesitylene (1,3,5-trimethylbenzene) at an ambient temperature of 973 K. Droplet diameter 1.40 mm. All data reduced to a uniform initial liquid temperature of 40°C. The error bars are at ± one standard deviation of the measurements. Solid line represents model predictions with modified Westbrook and Dryer reaction rate parameters: $a = 0.25$, $b = 0.80$, $A = 4.14 \times 10^2$, and $E = 75.31$ kJ/mol.

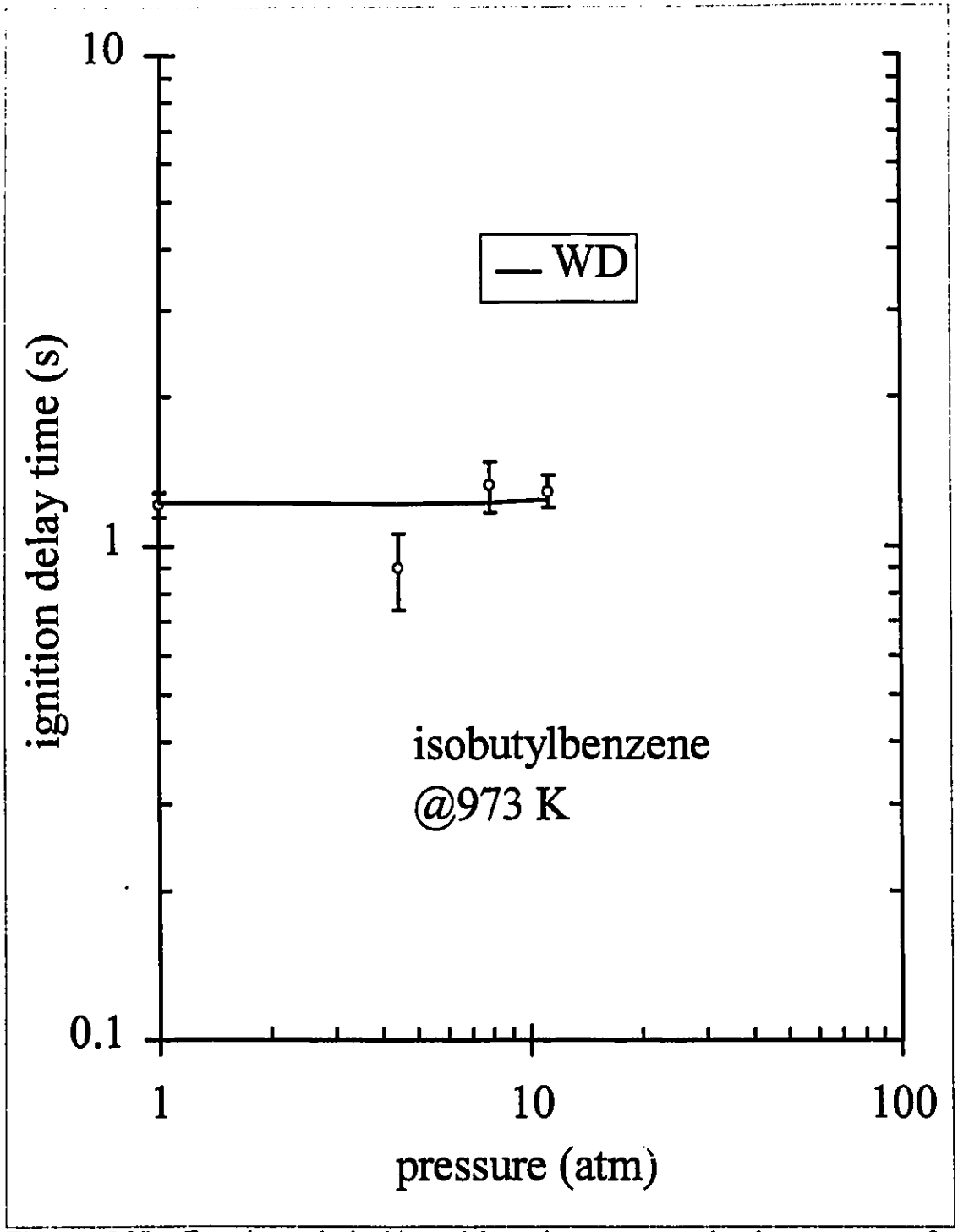

Figure 5.25: Experimental ignition delay time versus chamber pressure for isobutylbenzene at an ambient temperature of 973 K. Droplet diameter 1.40 mm. All data reduced to a uniform initial liquid temperature of 40°C. The error bars are at ± one standard deviation of the measurements. Solid line represents model predictions with modified Westbrook and Dryer reaction rate parameters: $a = 0.25$, $b = 0.90$, $A = 4.47 \times 10^3$, and $E = 90.58$ kJ/mol.

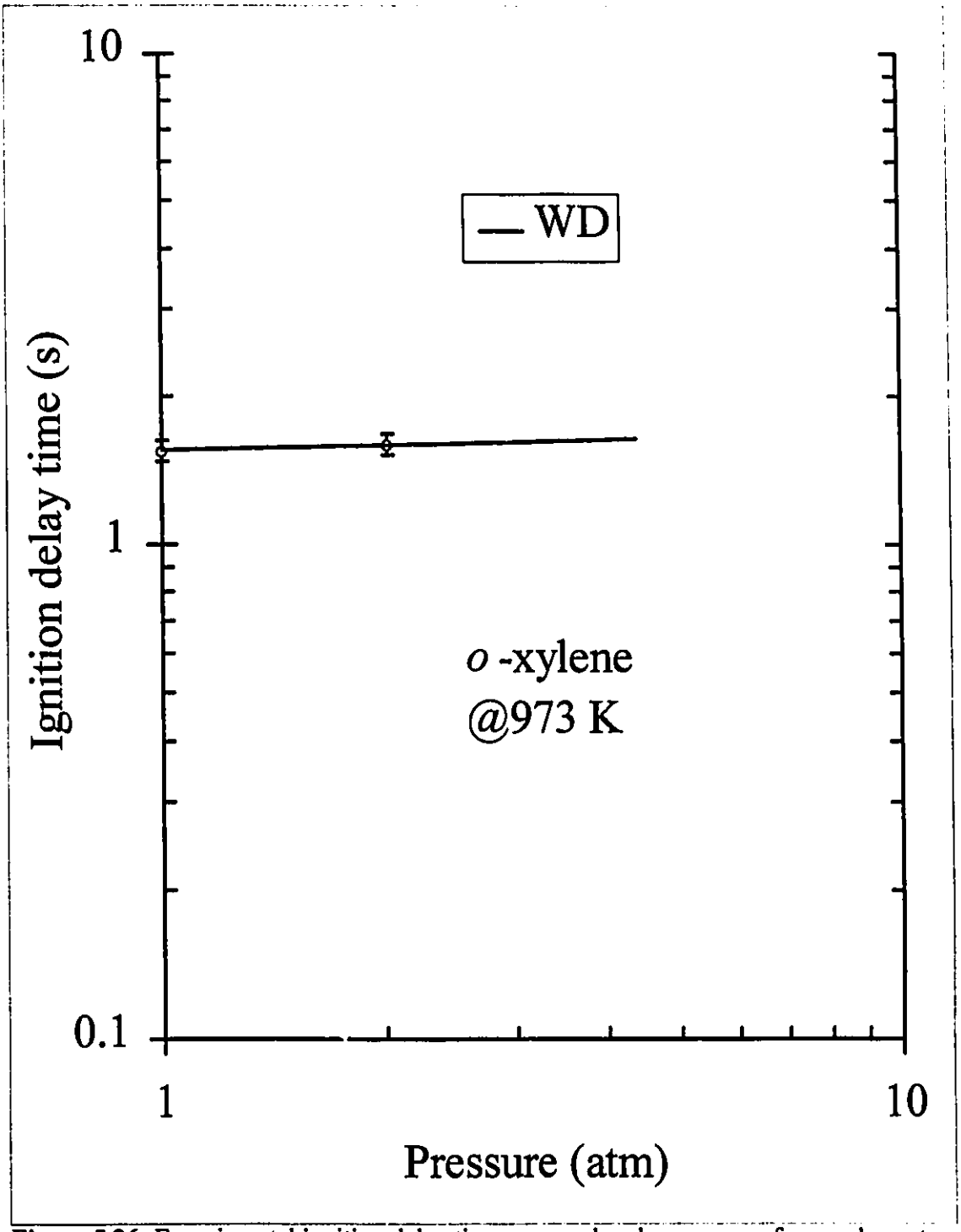

Figure 5.26: Experimental ignition delay time versus chamber pressure for *o*-xylene at an ambient temperature of 973 K. Droplet diameter 1.40 mm. All data reduced to a uniform initial liquid temperature of 40°C. The error bars are at ± one standard deviation of the measurements. Solid line represents model predictions with modified Westbrook and Dryer reaction rate parameters: $a = 0.25$, $b = 0.80$, $A = 1.77 \times 10^2$, and $E = 69.04$ kJ/mol.

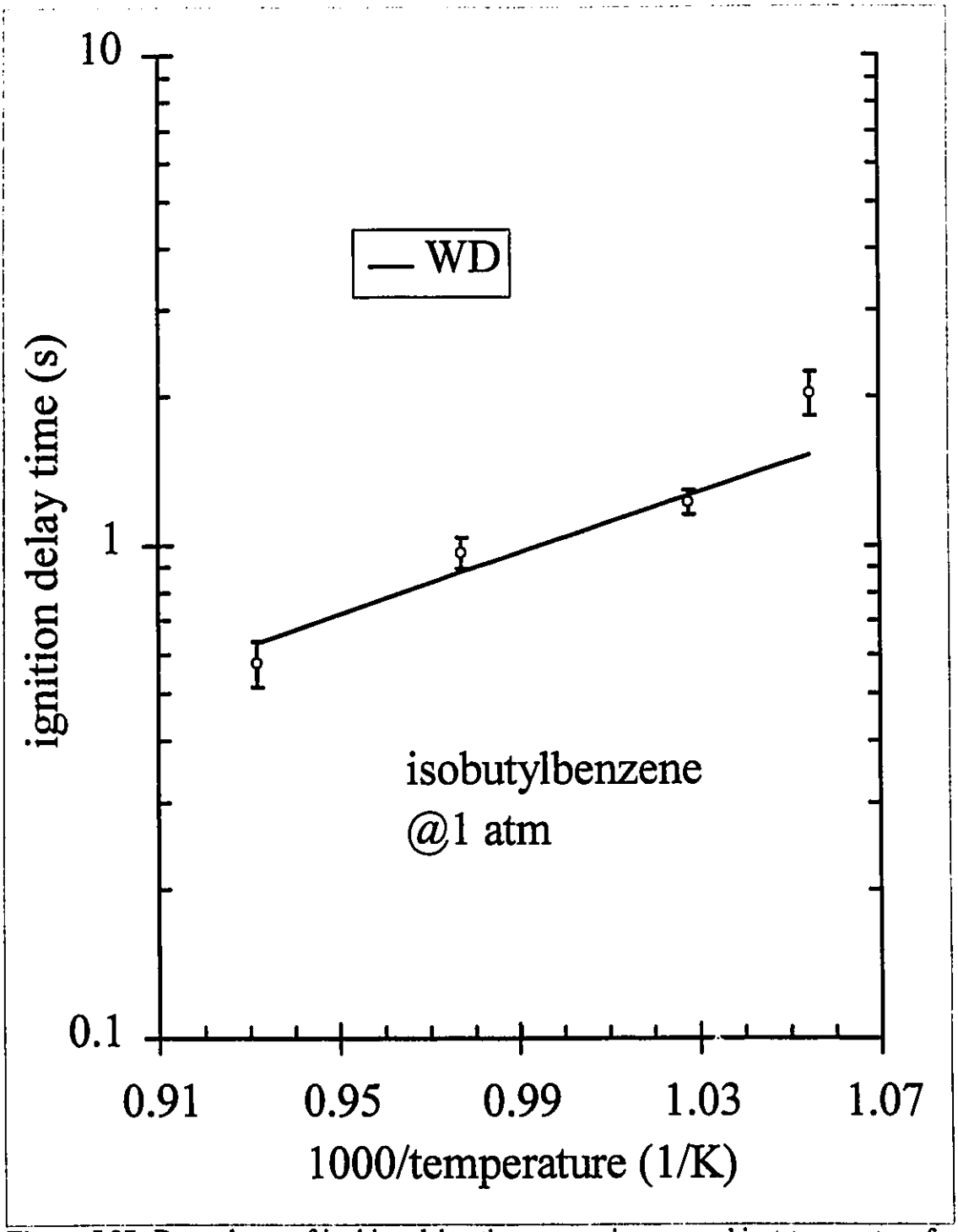

Figure 5.27: Dependence of ignition delay time versus inverse ambient temperature for isobutylbenzene at a chamber pressure of 1 atm. Droplet diameter 1.40 mm. All data reduced to a uniform initial liquid temperature of 40°C. The error bars are at ± one standard deviation of the measurements. Solid line represents model predictions with modified Westbrook and Dryer reaction rate parameters: $a = 0.25$, $b = 0.90$, $A = 4.47 \times 10^3$, and $E = 90.58$ kJ/mol.

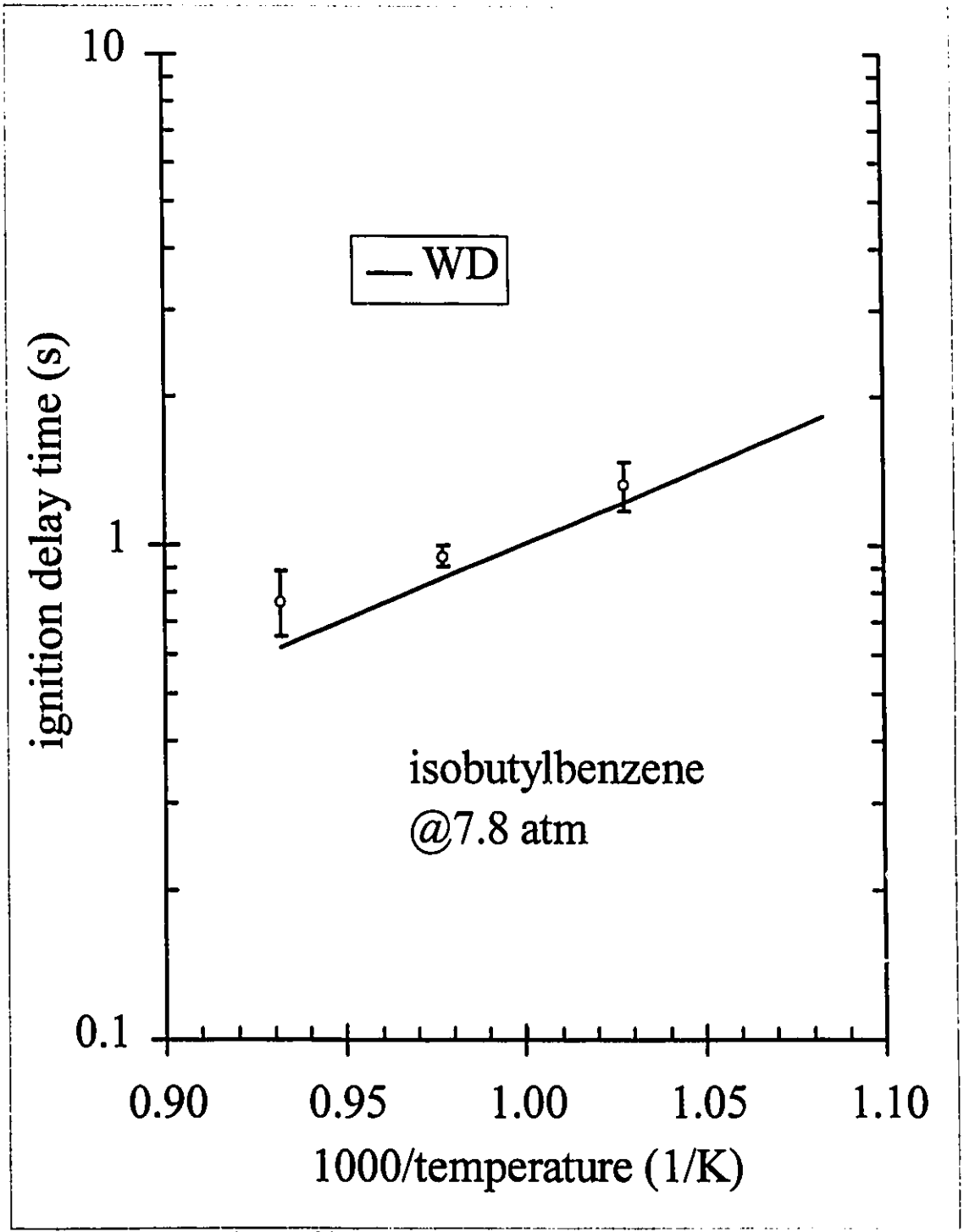

Figure 5.28: Dependence of ignition delay time versus inverse ambient temperature for isobutylbenzene at a chamber pressure of 7.8 atm. Droplet diameter 1.40 mm. All data reduced to a uniform initial liquid temperature of 40°C. The error bars are at ± one standard deviation of the measurements. Solid line represents model predictions with modified Westbrook and Dryer reaction rate parameters: $a = 0.25$, $b = 0.90$, $A = 4.47 \times 10^3$, and $E = 90.58$ kJ/mol.

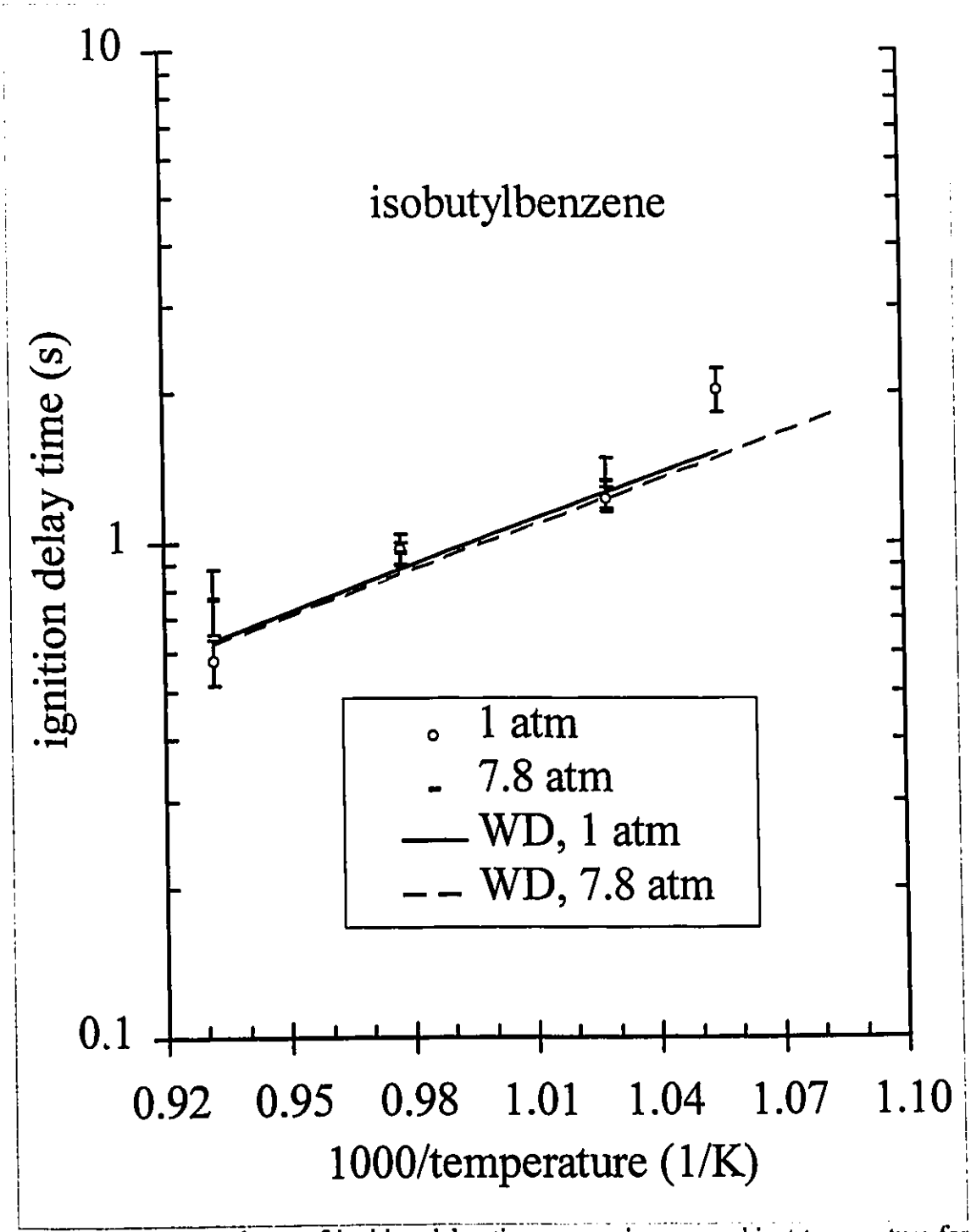

Figure 5.29: Dependence of ignition delay time versus inverse ambient temperature for isobutylbenzene at the chamber pressures of 1 and 7.8 atm. Droplet diameter 1.40 mm. All data reduced to a uniform initial liquid temperature of 40°C. The error bars are at ± one standard deviation of the measurements. Solid line represents model predictions with modified Westbrook and Dryer reaction rate parameters: $a = 0.25$, $b = 0.90$, $A = 4.47 \times 10^3$, and $E = 90.58$ kJ/mol.

5.3 Model predictions: single-component fuels

It was the original intention to derive chemical reaction rate parameters from these models so as to use this information for future mathematical modelling for Diesel engine ignition. However, it was found that the complex behaviour of the data - especially the "twinned" ignition points - could not be entirely reproduced by either model, so that the main purpose of this exercise was to explore the possibilities of these models for simulating various features of the data.

Numerical predictions of ignition delay times were achieved by using the single-component mathematical model with two different reaction models: modified Westbrook and Dryer (1981), and Müller *et al.* (1992). The Westbrook and Dryer rate model, Equation [2], has four parameters that affect the rate: a and b are fuel and oxygen exponents, E is the activation energy, and A is the pre-exponential. Of these, the experimental data only provides enough information to adjust three of these: $(a + b)$, E, and A. The fuel and oxygen exponents a and b are both unitless and they sum together to form the overall pressure dependence $(a + b)$. The behaviour of ignition time with temperature at constant pressure is controlled by E in units of kJ/mol, and the magnitude of the ignition time is determined by A. For the pressure dependence, it is not possible to separate the effects of a and b; thus, the exponent a is arbitrarily held constant at the value $a = 0.25$ as prescribed by Westbrook and Dryer, while b was allowed to vary. The Müller *et al.* model, Equation [8], required choosing the reaction rate parameters A_1, and A_{2OVL}. The E's in kJ/mol were not changed from Müller *et al.*'s, but rather held constant to values identical to their data for *n*-heptane.

The results shown thus far have two sets of model predictions represented, the first of which, labelled WD, are predictions with the modified Westbrook and Dryer reaction rate parameters, and the second, labelled MPL, are predictions with the Müller *et al.* reaction rate parameters. Figure captions have the values of the reaction parameters for the two models indicated.

5.3.1 *n*-Paraffin hydrocarbons

Model predictions using both reaction models are given in Figures 5.1 - 16. As stated in §4.2.1, the exponents a and b prescribed by Westbrook and Dryer were 0.25 and 1.50 respectively, giving an overall pressure dependence of $P^{a+b} = P^{1.75}$. The values b, E, and A. were originally correlated to experimental data at atmospheric pressure by Bergeron and Hallett (1989b). When these values were applied to the present data the pressure exponent was found to be too small and had to be increased. In selecting values, the fuel exponent a was held constant at the value prescribed by Westbrook and Dryer (1981) because they discovered the fuel exponent did not have a significant effect on the rate. The b parameter was varied to best represent the data. In view of the uncertainties associated with "twinned" data points and the fact that the model did not give a good representation of many of the data, no attempt was made to use a rigorous least-squares procedure for the fitting. The "best fit" for the current model was simply chosen by eye, selecting b such that the model would give a reasonable representation of the variation of ignition time with pressure at 973 K. The fit at lower temperatures (873 K and 773K) was not a concern; how the model performed at these temperatures depended on the fit at 973 K. This gave $a = 0.25$, $b = 1.80$, and an overall pressure dependence of $P^{a+b} = P^{2.05}$ for *n*-decane. For *n*-dodecane and *n*-hexadecane the fuel and oxygen exponents were determined to be the same with $a = 0.25$ and $b = 1.90$, and an overall pressure dependence of $P^{a+b} = P^{2.15}$. The pre-exponentials and activation energies chosen were respectively: 1.75×10^5 and 72.80 kJ/mol for *n*-decane, 4.05×10^5 and 76.15 kJ/mol for *n*-dodecane, and 4.30×10^5 and 78.24 kJ/mol for *n*-hexadecane. One of the weaknesses of the WD model is that it has a constant E, while the data indicate that the E of the reaction may be changing with pressure. Thus, while the model activation energy of each fuel was kept equal to the measured atmospheric pressure value, the true activation energies might be different under pressure from the atmospheric values.

After selecting parameters for the Westbrook and Dryer (WD) model for pressure and temperature dependence, it was found to be an inadequate description of ignition delay time in that it could not represent the whole realm of the data, especially at the lower temperatures. The model worked reasonably for data at 973 K, but for lower temperatures (873 K and 773 K), the WD model was on the high end of ignition times (refer to Figures 5.4 - 9), and it could not of course, reproduce the observed changes in effective activation energy with pressure (Figures 5.10 - 16). The poor performance of the WD model was the motivation for the implementation of the model by Müller, Peters, and Liñán (MPL). The adaptation of the MPL model to the specific *n*-paraffin fuel required modification of the two pre-exponential parameters, A_1 and A_{2OVL}, from the original values that were fitted for *n*-heptane by Müller *et al.* (1992). The pre-exponentials were respectively $A_1 = 6.00 \times 10^8$ s^{-1} and $A_{2OVL} = 1.09 \times 10^9$ $cm^6/(gmol^2 \cdot s)$ for *n*-decane, $A_1 = 7.25 \times 10^8$ s^{-1} and $A_{2OVL} = 1.24 \times 10^9$ $cm^6/(gmol^2 \cdot s)$ for *n*-dodecane, and $A_1 = 9.75 \times 10^8$ s^{-1} and $A_{2OVL} = 1.54 \times 10^9$ $cm^6/(gmol^2 \cdot s)$ for *n*-hexadecane. The activation energies, E_1 and E_{2OVL}, were not adjusted, but were kept the same as those obtained for *n*-heptane by Müller *et al.* (1992), the values of which were $E_1 = 180.01$ kJ/mol and $E_{2OVL} = -19.71$ kJ/mol. Activation energies should not vary too much for fuels within the *n*-paraffin family, which was why they were not changed for the present work.

The MPL predictions for all three *n*-paraffins showed ignition times slightly longer than those of the WD model at 973 K. However, at lower temperature (below 973 K) with two-stage ignition, the MPL model generally reproduced the faster of the "twinned" ignition times (see Figures 5.4 - 9). Because the MPL model involves two competing reaction pathways, it reproduces the trend of data with temperature a bit better, with the exception of *n*-dodecane (see Figures 5.10 - 16).

Some attempt was made to model the two-stage ignition using the MPL description. Figures 5.1, 5.4, and 5.7 show the MPL model with the high temperature

branch turned off by setting the rate $r_1 = 0$. The prediction is far from the data for the 973 K and 873 K plots, However, at 773 K the MPL model with $r_1 = 0$ approaches the slower of the ignition times, whereas the full MPL approximates the more rapid times. This suggests that a more complex kinetic model which takes into account two-stage ignition, as the multi-step Müller *et al.* (1992) model does, may be more successful here.

For all atmospheric pressure plots against (1/T) (Figures 5.10, 11 and 13), both models had similar predictions and represented the data reasonably well. At higher pressures, Figures 5.11 - 5.16 reveal that the model calculations differed significantly from each other. The WD with its constant value of activation energy no longer fits the trend with 1/T, suggesting that the real activation energy changes with P, while the MPL model is somewhat more representative of the data.

5.3.2 Cycloparaffin hydrocarbons

In §5.2.2 it was found that decalin behaves much like *n*-paraffins with only slightly higher ignition times. Numerical calculations using the WD and MPL models at 973 K (Figure 5.17) correlated good with the data, except for the high pressure end data at 11 atm. For the 873 K plot (Figure 5.18), the WD model is somewhat representative of the slower ignition times, whereas the MPL model was better at faster times. At 773 K (Figure 5.19) neither model fitted good. The WD model was a little high and the MPL model was low.

For decalin the 1/T plots (Figures 5.20 to 5.23) were very much like those for *n*-paraffins. Faster ignition times were better predicted by the MPL model and the slower times by the WD model. The results of the model predictions for decalin were: for WD reaction rate parameters a = 0.25, b =1.54, giving an overall pressure dependence of $P^{a+b} = P^{1.79}$, with $A = 1.07 \times 10^5$ and $E = 81.59$ kJ/mol; and for MPL reaction rate parameters $A_1 = 1.15 \times 10^9$ s^{-1}, $A_{2OVL} = 1.09 \times 10^9$ cm^6/(gmol^2·s), $E_1 = 180.01$ kJ/mol, and $E_{2OVL} = -19.71$ kJ/mol.

5.3.3 Aromatic hydrocarbons

The WD reaction rate parameters adjusted to represent isobutylbenzene data still show a strong positive dependence of rate on pressure (the fuel concentration exponent $a = 0.25$, and the oxygen exponent was chosen as $b = 0.90$, giving an overall pressure dependence of reaction rate of $P^{a+b} = P^{1.15}$), with $A = 4.47 \times 10^3$ and $E = 90.59$ kJ/mol, albeit a somewhat lesser dependence than for other fuels. A similar fit was obtained for mesitylene and *o*-xylene, giving $a = 0.25$, $b = 0.80$, $P^{a+b} = P^{1.05}$, $A = 4.14 \times 10^2$, and $E = 75.31$ kJ/mol for mesitylene; and $a = 0.25$, $b = 0.80$, $P^{a+b} = P^{1.05}$, $A = 1.77 \times 10^2$, and $E = 69.03$ kJ/mol for *o*-xylene.

Since the reaction kinetics of aromatics are quite different from paraffins, and since the Müller *et al.* (1992) model was designed specifically for paraffins, only the WD model was used for model predictions, as shown in Figures 5.24 - 29. The model results represent the experimental data reasonably well, and the plots against 1/T show no change in slope with pressure, suggesting that the activation energy for isobutylbenzene is constant (see Figure 5.29). However, since the reaction itself has a positive pressure exponent, the very small dependence of ignition time on pressure for the three aromatic fuels must therefore be the result of a competition between physical processes and chemical kinetics. At higher pressures, the droplet must be heated to higher temperatures to produce significant quantities of vapour, and thus undergoes a longer period of transient heating before reaction occurs. This counteracts the rise in reaction rate with pressure.

Using the numerical WD model, predicted histories of the mass flux of vapour evolved from the surface of the droplet for isobutylbenzene fuel at 973 K were computed for various pressures. Shown in Figure 5.30, the mass flux at atmospheric pressure is the largest followed by the flux histories at 5 and 10 atm of pressure. For comparison purposes, Figure 5.31 shows mass fluxes at the same pressure but for *n*-decane fuel. The plots are similar in shape, which means that mostly pressure and vapour-liquid

equilibrium affect the mass flux evolving from the surface of the liquid droplet. Since the pressure conditions are identical, and isobutylbenzene and *n*-decane have very similar normal boiling points, it is not surprising to find the mass fluxes of the fuels being similar. The only difference is the point of ignition on the time scale. Under pressure *n*-decane obviously ignites considerably faster than isobutylbenzene, and this is mainly the result of the greater dependence of reaction rate on pressure for *n*-paraffins. The processes of chemical reaction and the physical processes of mixing caused by diffusion driven by concentration differences and the state of the *VLE* compete during the ignition process. For isobutylbenzene the chemical reaction is too slow to cause significant heating until an appreciable concentration of fuel-air mixture is produced such that ignition can occur. This is not the case for *n*-decane and other straight paraffins and cycloparaffins because these particular fuels have reaction rates that accelerate faster with pressure. Physical processes are relatively the same for the fuels tested but it is the chemical properties of each fuel that has the greater influence and control on the fuel's ignition delay time.

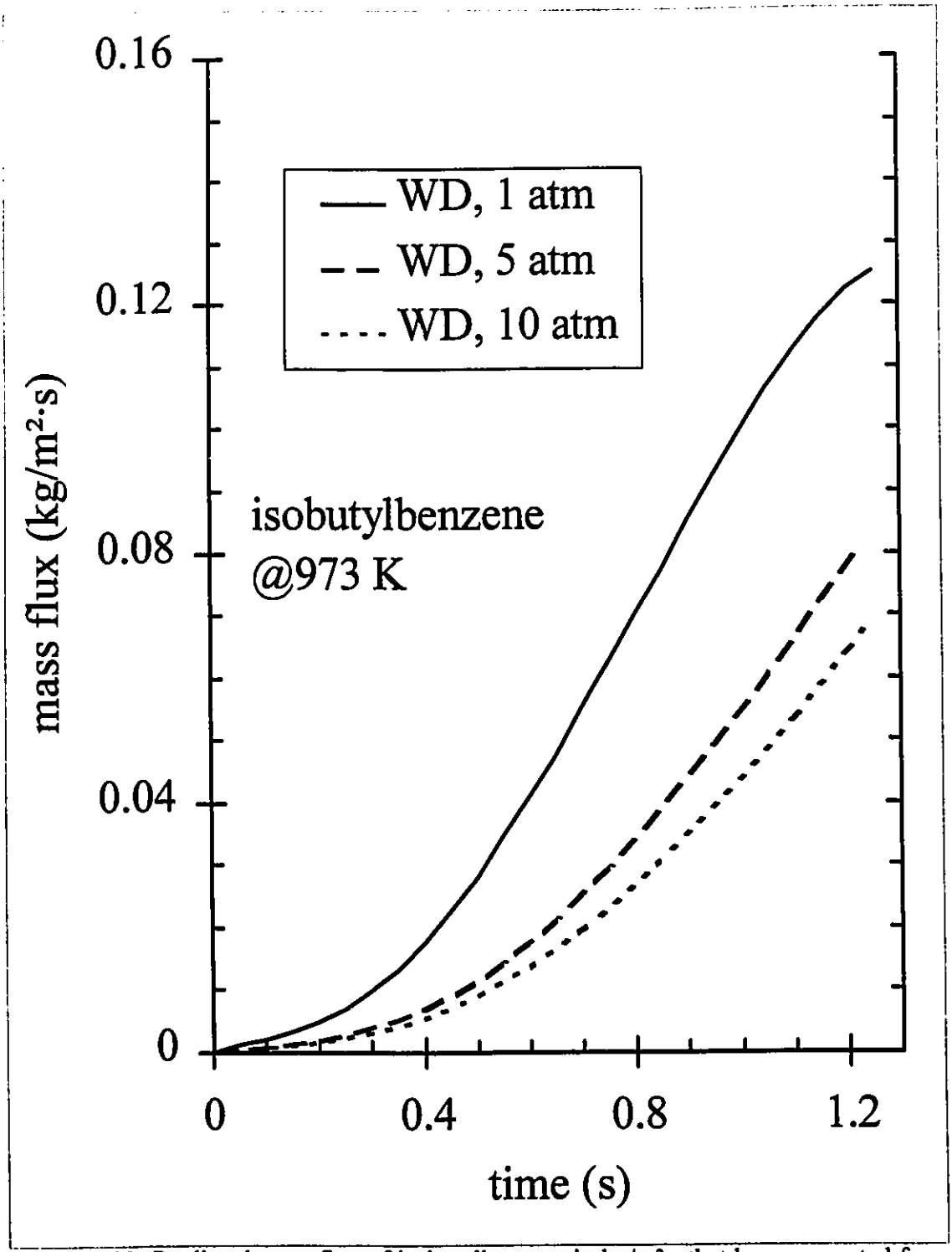

Figure 5.30: Predicted mass flux of isobutylbenzene in kg/m²·s that has evaporated from the surface of the droplet versus the time elapsed after initial exposed to the hot environment at an ambient temperature of 973 K. The mass fluxes shown are for chamber pressures of 1, 5, and 10 atm. The ignition delay times were predicted as 1.235 seconds at 1 atm, 1.215 seconds at 5 atm, and 1.230 seconds at 10 atm.

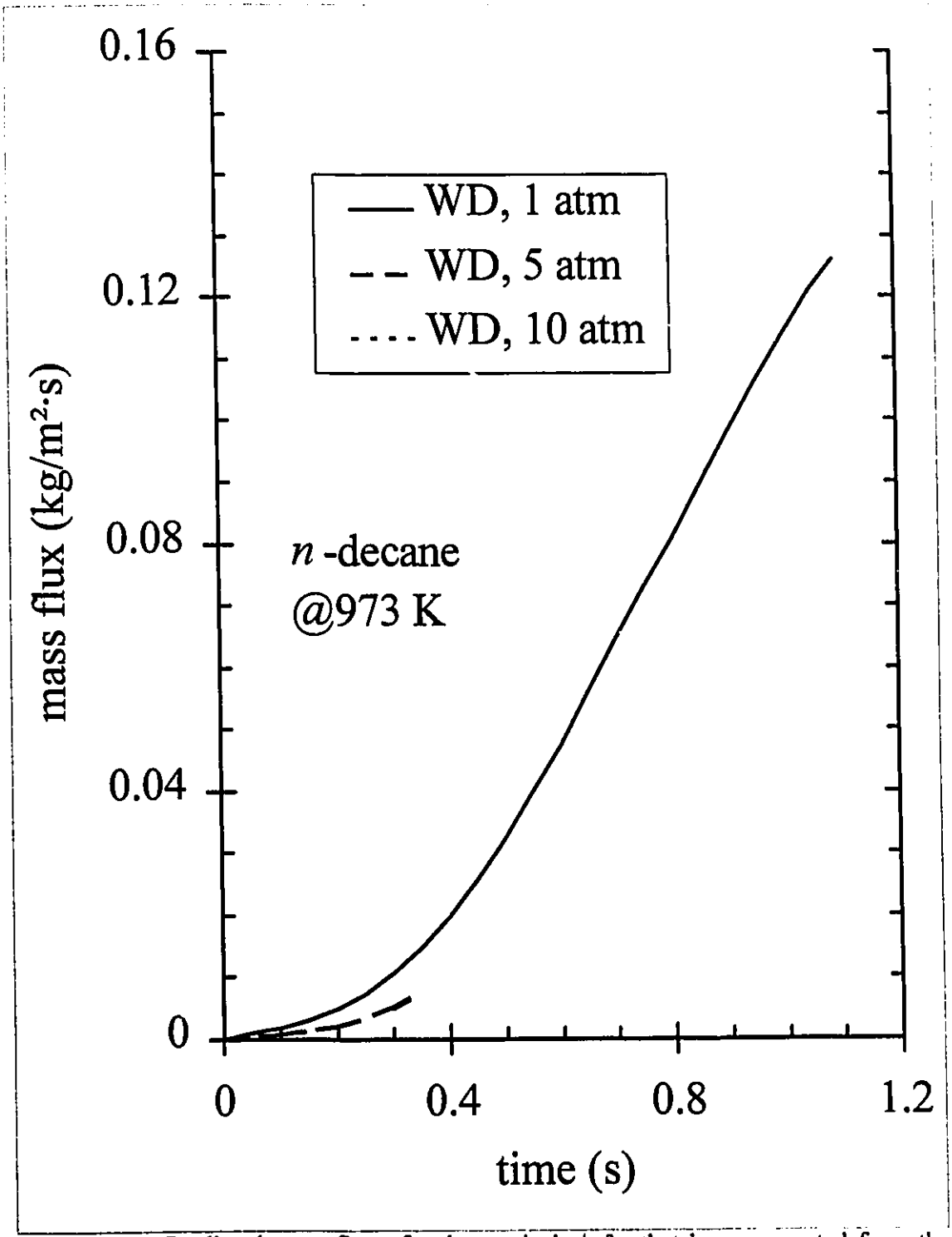

Figure 5.31: Predicted mass flux of *n*-decane in kg/m²·s that has evaporated from the surface of the droplet versus the time elapsed after initial exposed to the hot environment at an ambient temperature of 973 K. The mass fluxes shown are for chamber pressures of 1, 5, and 10 atm. The ignition delay times were predicted as 1.090 seconds at 1 atm, 0.330 seconds at 5 atm, and 0.215 seconds at 10 atm.

5.3.4 Summary of reaction rate parameters

This section summarizes the reaction rate parameters used for the predictions of the previous sections. Table 5.1 shows the modified Westbrook and Dryer parameters and Table 5.2 the Müller *et al.* parameters.

Table 5.1: Reaction rate parameters - Westbrook and Dryer model

Fuel	A	$E / \tilde{R}$ (K)	a	b
n-decane	$.75\times10^{5}$	8756	0.25	1.80
n-dodecane	4.05×10^{5}	9159	0.25	1.90
n-hexadecane	4.30×10^{5}	9410	0.25	1.90
decalin	$.07\times10^{5}$	9813	0.25	1.54
isobutylbenzene	4.47×10^{3}	10895	0.25	0.90
mesitylene	4.14×10^{2}	9058	0.25	0.80
o-xylene	$.77\times10^{2}$	8303	0.25	0.80

Table 5.2: Reaction rate parameters - Müller *et al.* model

Fuel	A (s^{-1})	$E_1 / \tilde{R}$ (K)	A_{2OVL} ($cm^6/(gmol^2 \cdot s)$)	$E_{2OVL} / \tilde{R}$ (K)
n-decane	6.00×10^{8}	21650	$.09\times10^{9}$	-2370
n-dodecane	7.25×10^{8}	21650	$.24\times10^{9}$	-2370
n-hexadecane	9.75×10^{8}	21650	$.54\times10^{9}$	-2370
decalin	$.15\times10^{9}$	21650	$.09\times10^{9}$	-2370

Since these reaction models did not fit much of the data at all, the use of these parameters for further modelling is not recommended unless one stays strictly in the regions of temperature and pressure for which reasonable agreement with the data was found. Therefore, the parameters reported above are only a rough approximation to the general trend of the real reaction rates with pressure, temperature, and fuel type.

5.3.5 Effect of pre-exponential parameter and liquid temperature on calculated ignition delay times

Since in all the numerical calculations the model behaviour was varied by changing the reaction rate parameters, it is of interest to see what the relative importance of chemical reaction is in the overall process of droplet ignition. This can be investigated by varying the pre-exponential factor A of the Westbrook and Dryer model. This model is the only model that will be used here to demonstrate this effect because a similar effect would be experienced with the MPL model.

Figure 5.32 reveals the changes produced by varying the pre-exponential factor to half the original fitted value (dashed line) or double the original fitted value (dotted line), from the original fitted value indicated by the solid line. The numbers shown are the pre-exponential parameter values in unit of s^{-1}. Halving the pre-exponential nearly doubles the predicted ignition times, and vice versa. This indicates a substantial degree of control of the overall process by chemical kinetics.

Figure 5.33 shows the effect of liquid temperature versus ignition delay time. The trend reveals that ignition times decrease about 15% from the value at 40°C if the liquid temperature is 60°C. This last value is roughly the highest liquid temperature encountered in the experiments, so that this gives an upper bound to the correction made in reducing data to a uniform initial liquid temperature of 40°C. It must be stated that the liquid temperature of the droplet is only approximate because no actual droplet temperature is measured by the present apparatus, the recorded measurements of ambient chamber temperature prior to droplet ignition being assumed equal to the liquid temperature.

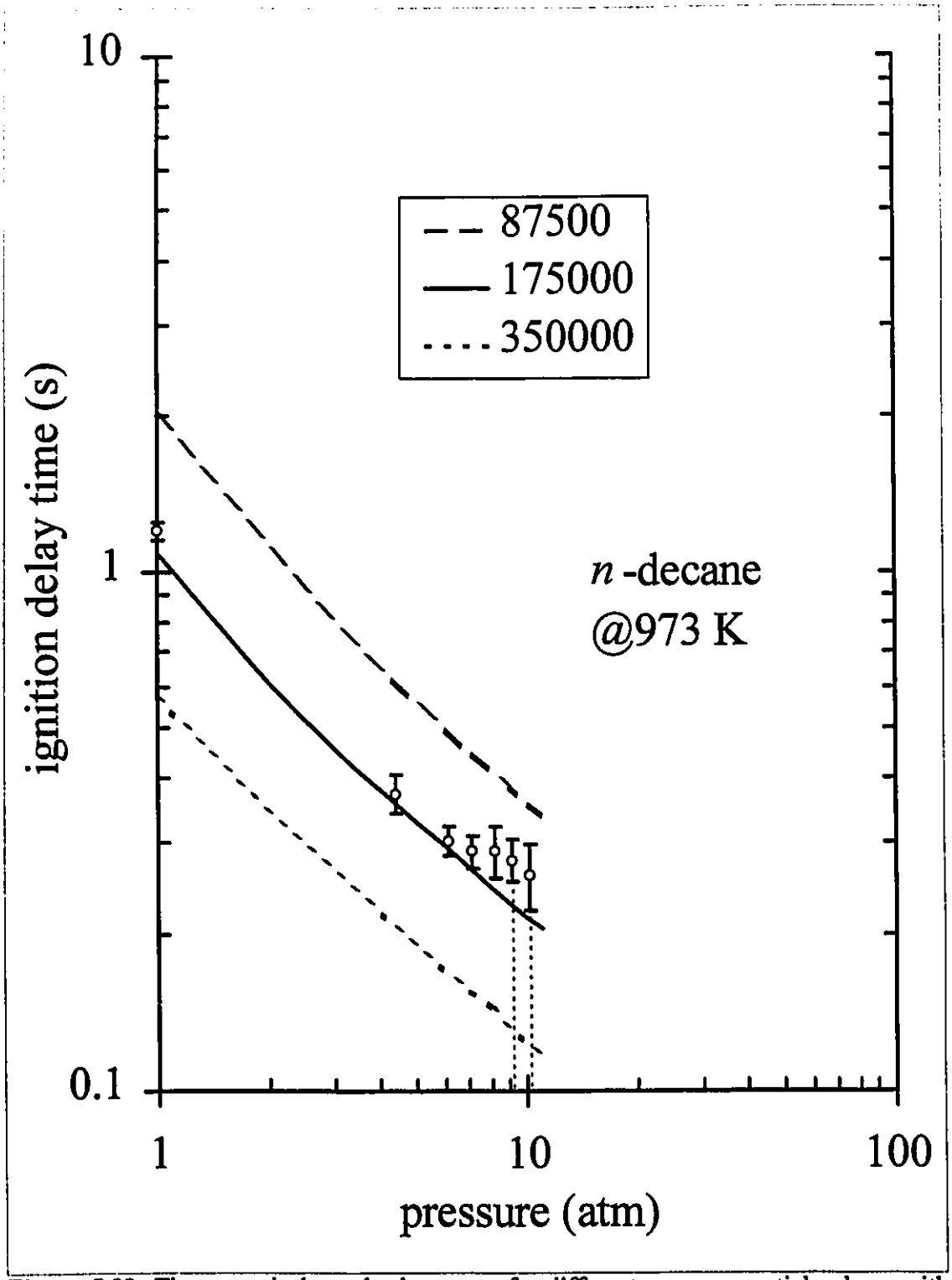

Figure 5.32: The numerical trends shown are for different pre-exponential values, with the values indicated. All other rate parameters were unchanged. Experimental data shown have been corrected to 40°C and the numerical ignition times have been computed at the 40°C liquid temperature.

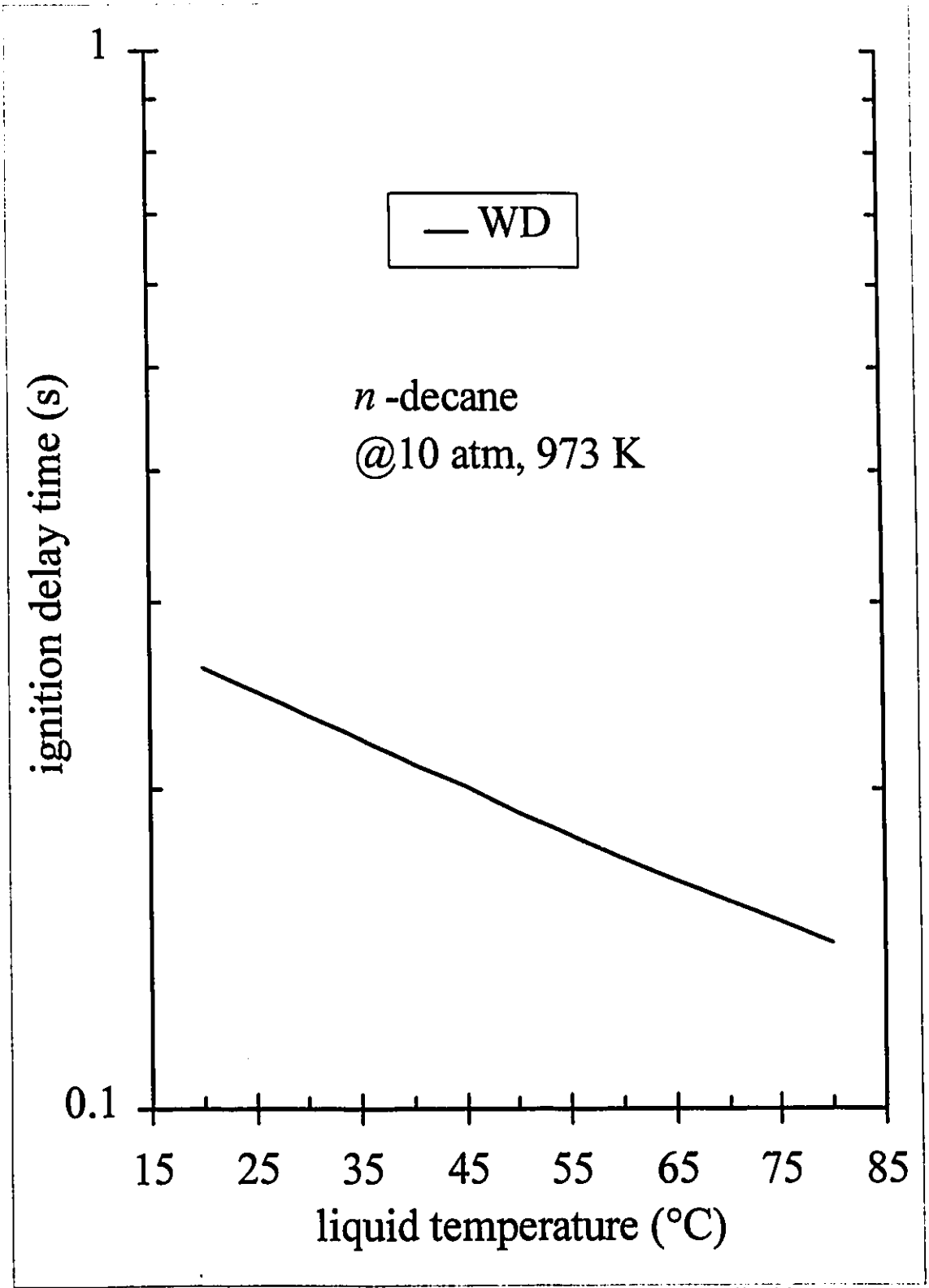

Figure 5.33: Plot of predicted ignition delay time (WD model) versus liquid temperature. The effect of liquid temperature on calculated ignition times of *n*-decane at 10 atm and 973 K.

5.4 Experimental data and model predictions: two-component fuels

Experiments were done for six binary mixtures, two of *n*-paraffin fuels (*n*-decane/*n*-dodecane and *n*-dodecane/*n*-hexadecane), one of an *n*-paraffin and a cycloparaffin (*n*-decane/decalin), and three of *n*-paraffins with aromatics (*n*-decane/isobutylbenzene, *n*-decane/mesitylene, and *n*-decane/*o*-xylene). These mixtures were tested at 10 atm absolute and 700°C. Because of the "twinned" data points encountered at lower temperatures, it was felt that mixture experiments below 973 K would be inconclusive. The results are shown in Figures 5.35 - 38. Figures 5.35 - 36 show the *n*-paraffin mixtures, Figure 5.37 the paraffin-cycloparaffin mixture, and Figures 5.38 - 40 the paraffin-aromatic mixtures. All data reported have been corrected to a uniform initial liquid temperature of 40°C.

As mentioned in §4.3, the state of mixing in the liquid is not a significant factor in determining the process of evaporation of a multi-component droplet. Numerical model runs, however, showed no significant difference in ignition delay times between well-mixed droplets and droplets with molecular diffusion as the only liquid-phase transport process. This agrees with earlier observations by Bergeron and Hallett (1989a).

As described in §4.4, two different reaction rate expressions were used for the two-component model calculations; these are denoted as "Model 1" (linear combination of component rates) and "Model 2" (linear combination of component rate parameters) in the figures. Both of these used the modified Westbrook and Dryer rate expressions for the pure components; no mixture calculations with the Müller *et al.* model were attempted.

5.4.1 Mixtures of *n*-paraffins

As the *n*-paraffins exhibit similar reaction behaviour, the main purpose of the paraffin mixture experiments and calculations was to explore the effects of component boiling point on mixture behaviour. Figure 5.35 shows data for a 50/50 by mass mixture of *n*-

decane and *n*-dodecane. The two fuels do differ somewhat in normal boiling point (174°C and 216°C, respectively). Ignition delay times were slightly higher than both model predictions. For *n*-dodecane/*n*-hexadecane mixtures (Figure 5.36), these fuels have a greater disparity in normal boiling point (216°C and 287°C, respectively). The experimental results are much higher than model values except for one grouping. It is believed that this is the same effect as that observed in atmospheric pressure experiments on mixtures (Bergeron and Hallett, 1989a). The higher ignition delay times are believed to be due to an "aging" effect on the droplet during transient heating. Referring to the Figure 5.34, the more volatile component vaporizes more quickly, depleting the concentration of this component near the droplet surface. At the top of the droplet, only a thin layer of fuel covers the "shoulder" of the supporting bead. This region will be quickly stripped of the volatile component, and, unlike the surface layer around the rest of the droplet, will not be replenished by diffusion and internal circulation. The vapour produced by this "shoulder" will hence become nearly pure *n*-hexadecane shortly after the start of vaporization. This vapour, falling downward in the natural convection flow around the droplet, will tend to "blanket" the fuel diffusing out from the lower regions of the droplet. Hence it will be the least volatile component which comes first in contact with the air, causing ignition to behave as if the droplet were almost pure *n*-hexadecane. Because of this, the experimental points for this mixture must be regarded as spurious. In work at atmospheric pressure, this effect occurred only when a large difference in boiling point existed between components (for example, it was observed for *n*-heptane/*n*-hexadecane mixtures, but not for *n*-dodecane/*n*-hexadecane). Evidently increased natural convection at higher pressures causes this to occur for smaller differences in boiling point as well. There was no significant difference between the performance of the two different mixture reaction rate models for these mixtures.

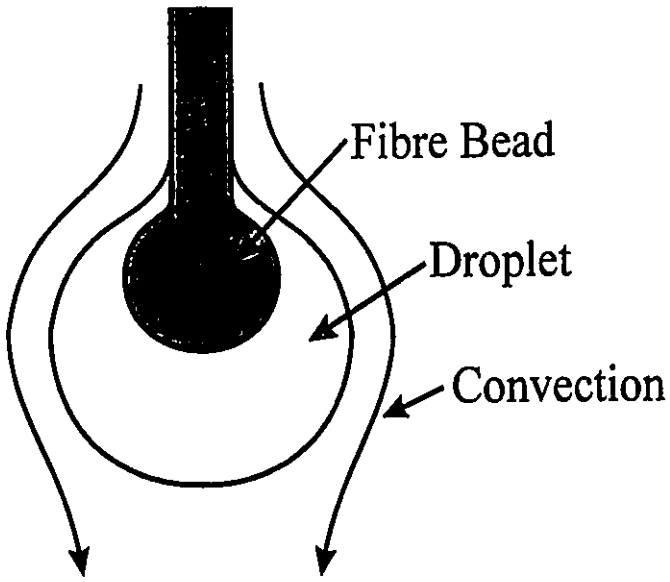

Figure 5.34: Effect of natural convection on mixture droplet during transient heating. Convection is additive by presence of air flow (downward pass droplet region) caused by upward air flow from hot walls of furnace.

The mixture predictions reflect the fact that the more volatile component of the mixture dominates the ignition behaviour, as even at small concentrations in the liquid phase it will be present in large quantities in the vapour. Hence, ignition times for the mixtures are close to those for the more volatile pure component except at very small concentrations of the latter.

The mixture models (1 and 2) at the concentration extremes give identical results as the WD model for the respective pure components.

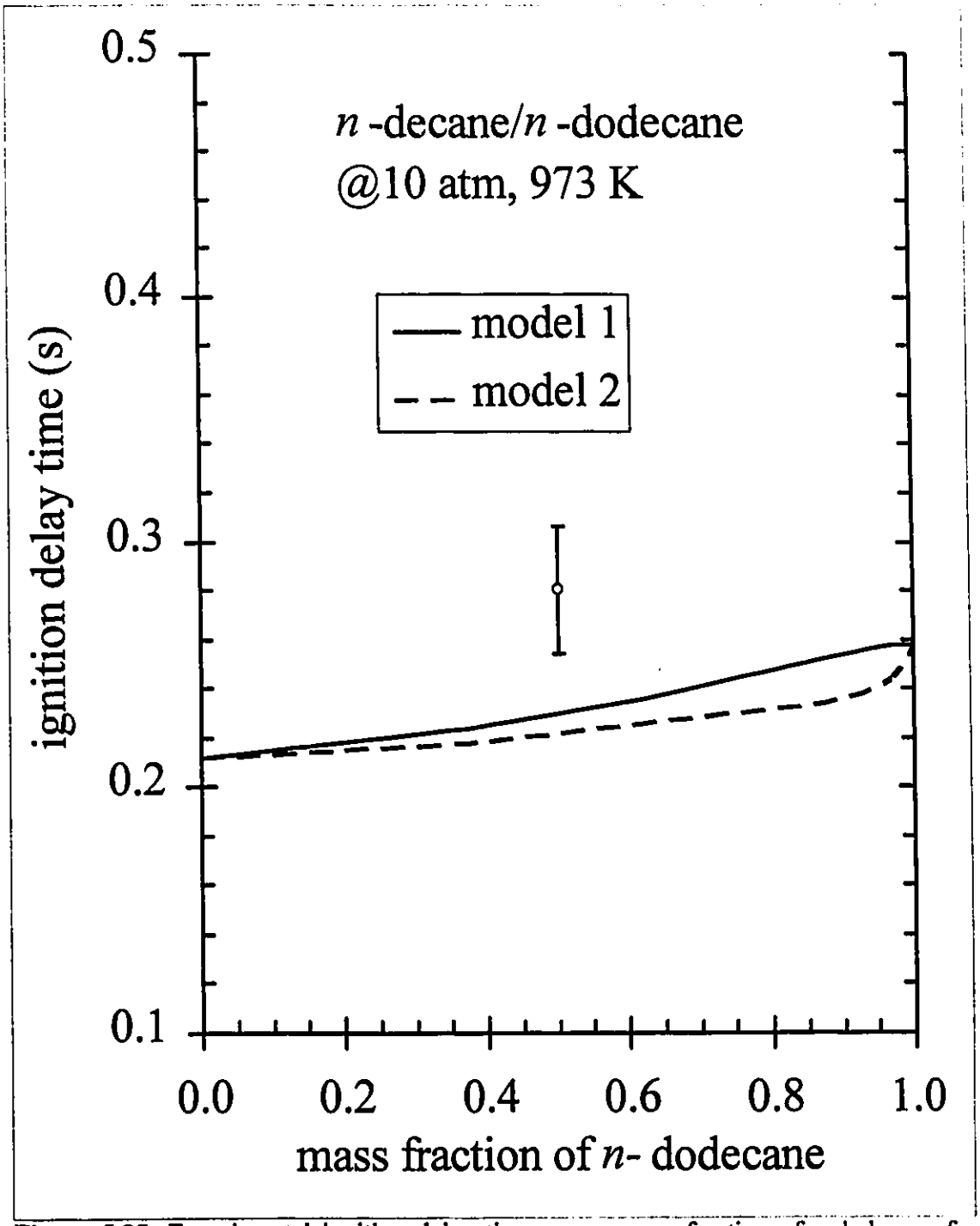

Figure 5.35: Experimental ignition delay time versus mass fraction of *n*-dodecane for binary mixture of *n*-decane/*n*-dodecane at pressure of 10 atm and at ambient temperature of 973 K. Droplet diameter 1.40 mm. All data reduced to a uniform initial liquid temperature of 40°C. The error bars are at ± one standard deviation of the measurements. Solid line represents model 1 predictions using a linear combination of component rates. Dashed line represents model 2 predictions using linear combinations of component parameters.

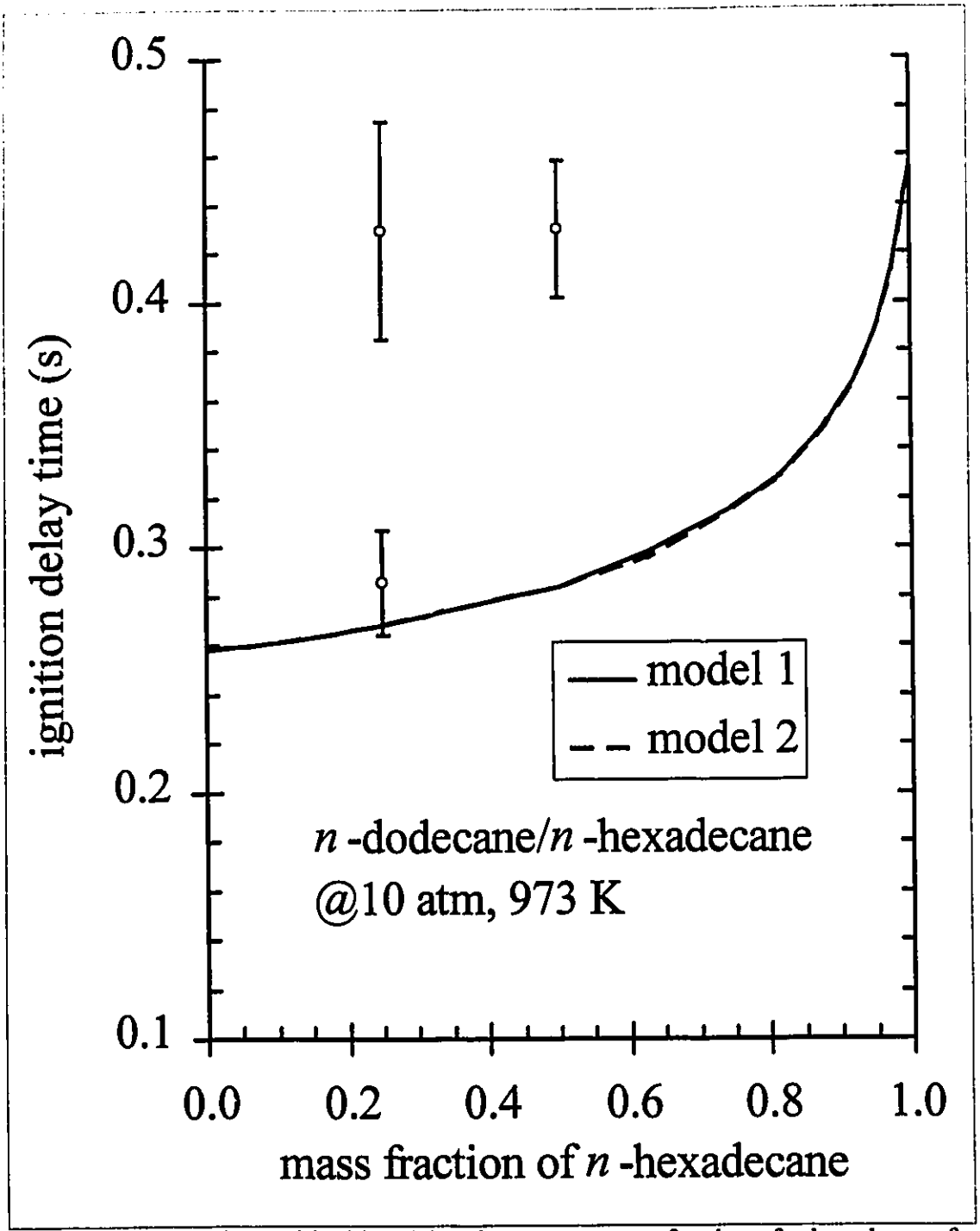

Figure 5.36: Experimental ignition delay time versus mass fraction of *n*-hexadecane for binary mixture of *n*-dodecane/*n*-hexadecane at pressure of 10 atm and at ambient temperature of 973 K. Droplet diameter 1.40 mm. All data reduced to a uniform initial liquid temperature of 40°C. The error bars are at ± one standard deviation of the measurements. Solid line represents model 1 predictions using a linear combination of component rates. Dashed line represents model 2 predictions using linear combinations of component parameters.

5.4.2 Mixture of *n*-paraffin and cycloparaffin

The normal boiling point of decalin is 190°C and is similar to *n*-decane. Hence the results in Figure 5.37 mainly reflect the effects of chemical kinetics. The reaction behaviour of decalin was found in single component experiments to be similar to that of *n*-paraffins, but somewhat slower. The predicted results show a nearly linear dependence of ignition delay on decalin concentration, and both reaction models agree with the mixture data, most likely because of the similarity between the rate expressions for the two fuels. It is believed the ring de-coupling of cycloparaffins is a fast process which leads to *n*-paraffin behaviour.

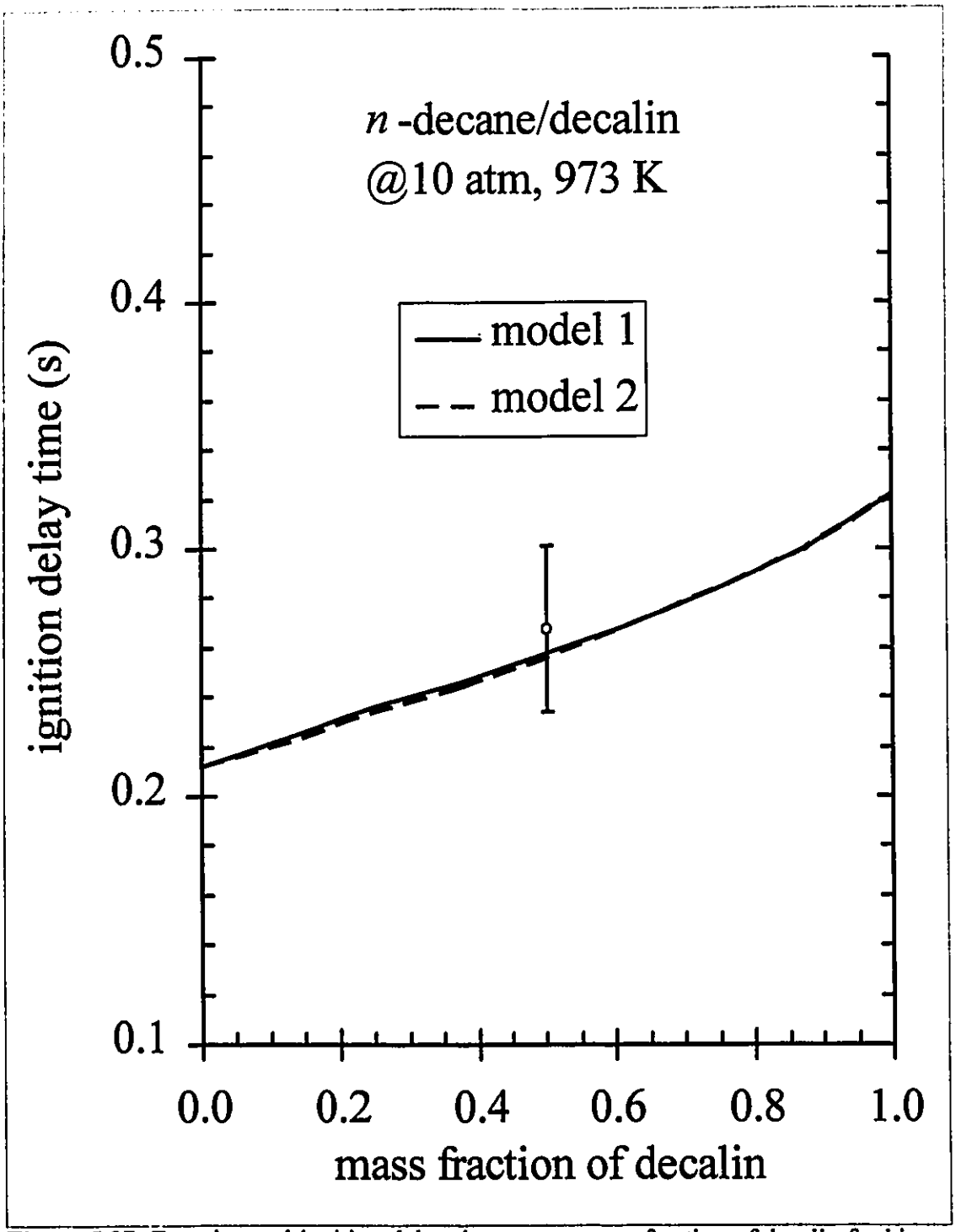

Figure 5.37: Experimental ignition delay time versus mass fraction of decalin for binary mixture of *n*-decane/decalin at pressure of 10 atm and at ambient temperature of 973 K. Droplet diameter 1.40 mm. All data reduced to a uniform initial liquid temperature of 40°C. The error bars are at ± one standard deviation of the measurements. Solid line represents model 1 predictions using a linear combination of component rates. Dashed line represents model 2 predictions using linear combinations of component parameters.

5.4.3 Mixture of *n*-paraffin and aromatics

The aromatics used (isobutylbenzene, mesitylene, and *o*-xylene) have normal boiling points of 170°C, 163°C, and 144°C, respectively; these components were chosen because their boiling points are all close to *n*-decane, allowing the experiments to more or less isolate the effect of chemical kinetics. These mixtures show more complex variations in ignition time with composition, and according to model 2 can actually ignite more rapidly than either pure component at some concentrations.

Model results were reasonably representative of the data. Model 2 seems to be a better predictor than model 1 for the *n*-decane/isobutylbenzene mixture (Figure 5.38). However, the opposite may be true for *n*-decane/mesitylene (Figure 5.39) where model 1 is better. Mixtures of *n*-decane/*o*-xylene fall between both models (Figure 5.40). The results do not discriminate clearly which model best represents the experimental data. An explanation to the outcome lies in how aromatics respond under pressure. Both mesitylene and *o*-xylene do not ignite beyond 2 atm absolute as pure species. However, addition of the much more ignitable *n*-decane considerably changes this limitation. Since the rate expressions for mesitylene and *o*-xylene have to be extrapolated well beyond the 2 atm ignitable limit in making these calculations, they may not be particularly reliable, and this will affect the performance of the model quite strongly. The model obviously becomes unrealistic in predicting that mixtures of these two components continues to occur as one approaches very high aromatic concentrations.

It must be noted that no two-stage ignition was observed for any mixture tested. One might suggest the two regimes (in Figure 5.36) of ignition delay times represent the "twinned" ignition, but the effect of "aging" is the more likely explanation of what is actually occurring.

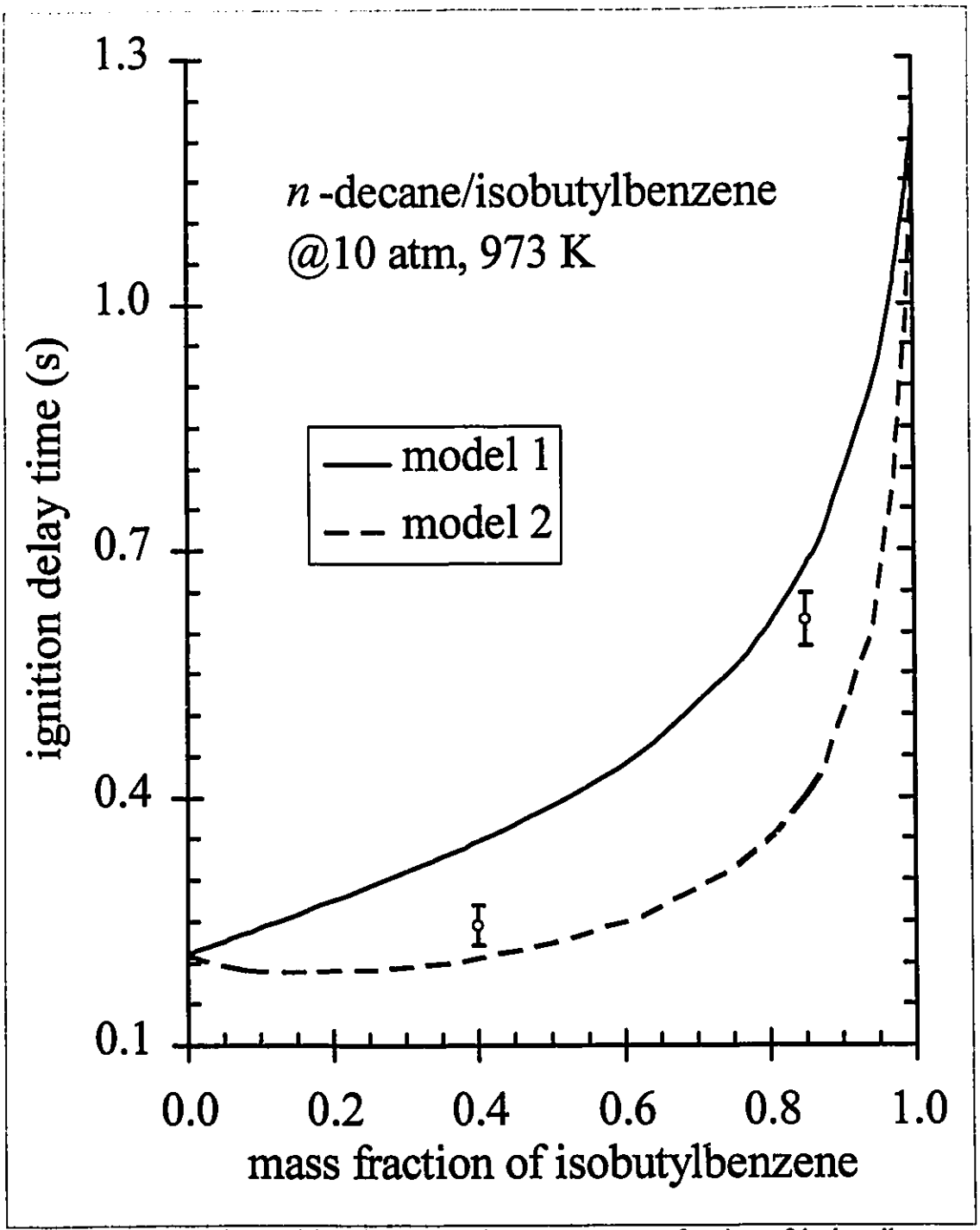

Figure 5.38: Experimental ignition delay time versus mass fraction of isobutylbenzene for binary mixture of *n*-decane/isobutylbenzene at pressure of 10 atm and at ambient temperature of 973 K. Droplet diameter 1.40 mm. All data reduced to a uniform initial liquid temperature of 40°C. The error bars are at ± one standard deviation of the measurements. Solid line represents model 1 predictions using a linear combination of component rates. Dashed line represents model 2 predictions using linear combinations of component parameters.

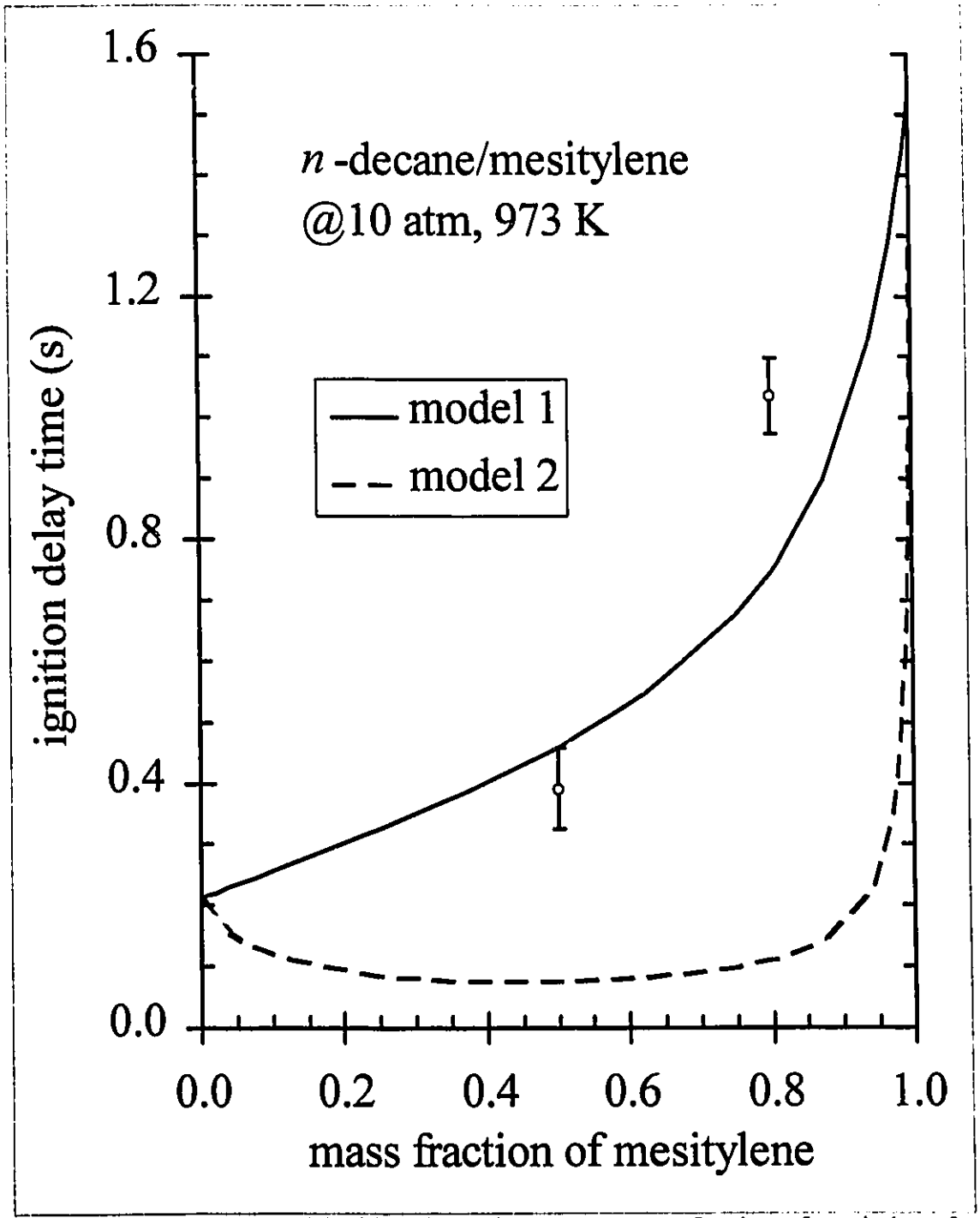

Figure 5.39: Experimental ignition delay time versus mass fraction of mesitylene for binary mixture of *n*-decane/mesitylene at pressure of 10 atm and at ambient temperature of 973 K. Droplet diameter 1.40 mm. All data reduced to a uniform initial liquid temperature of 40°C. The error bars are at ± one standard deviation of the measurements. Solid line represents model 1 predictions using a linear combination of component rates. Dashed line represents model 2 predictions using linear combinations of component parameters.

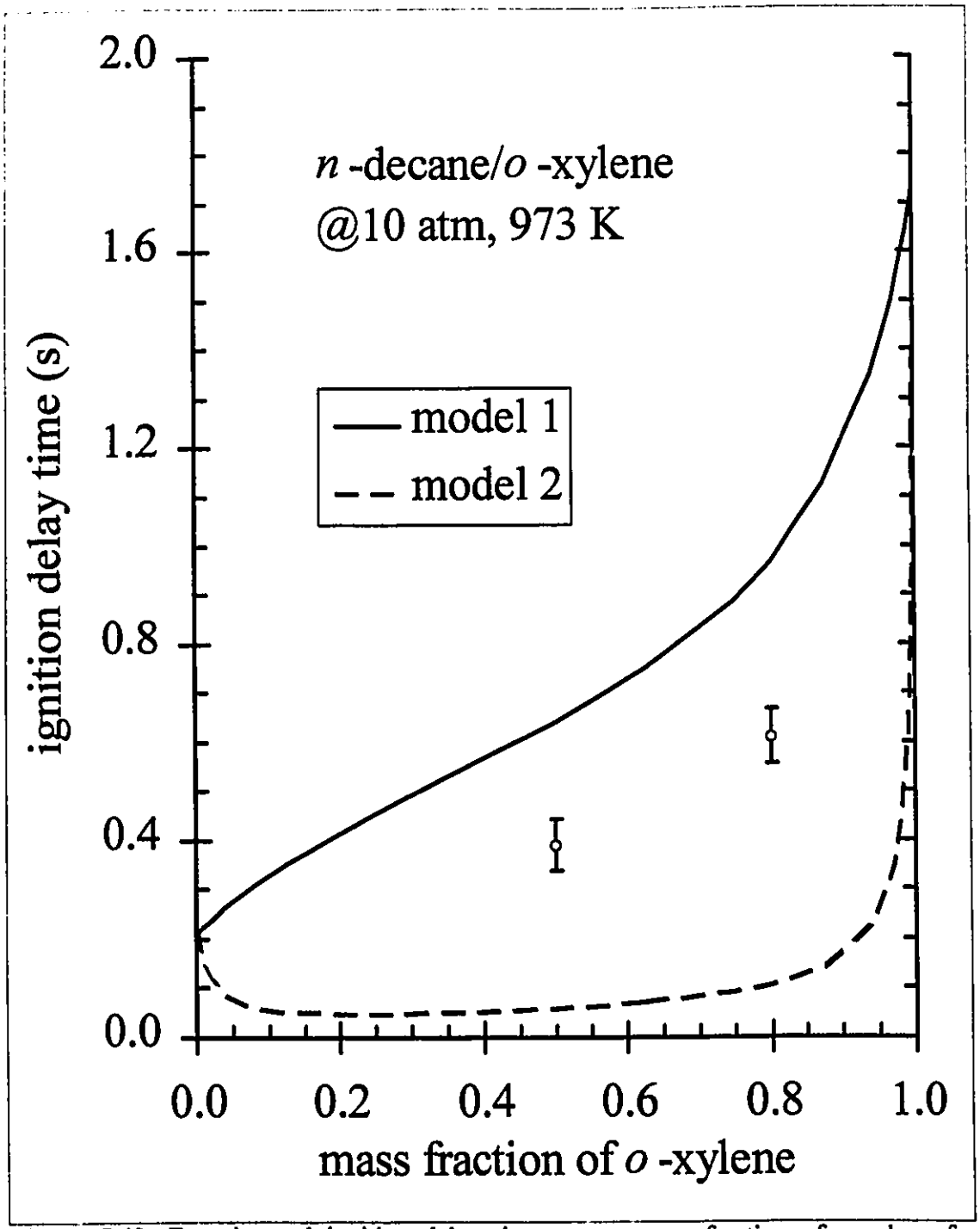

Figure 5.40: Experimental ignition delay time versus mass fraction of *o*-xylene for binary mixture of *n*-decane/*o*-xylene at pressure of 10 atm and at ambient temperature of 973 K. Droplet diameter 1.40 mm. All data reduced to a uniform initial liquid temperature of 40°C. The error bars are at ± one standard deviation of the measurements. Solid line represents model 1 predictions using a linear combination of component rates. Dashed line represents model 2 predictions using linear combinations of component parameters.

CHAPTER SIX

Conclusions and Recommendations

This thesis discussed experiments on the auto-ignition of single hydrocarbons droplets and its binary mixtures that were carried out at pressures ranging up to 18 atm and at temperatures between 773 K and 973 K. The fuels that were tested included *n*-paraffins (decane, dodecane, and hexadecane), aromatics (mesitylene, *o*-xylene, and isobutylbenzene) and a cycloparaffin (decalin), as well as selected binary combinations: *n*-decane/*n*-dodecane, *n*-dodecane/*n*-hexadecane, *n*-decane/decalin, *n*-decane/isobutylbenzene, *n*-decane/mesitylene, and *n*-decane/*o*-xylene. An existing numerical model was used to model the droplet ignition process, including all the physical processes of heat transfer, droplet evaporation, vapour diffusion, and chemical reaction. Two different chemical reaction models (WD - a single-step rate model from Westbrook and Dryer, 1981, and MPL - a simplified form of the four-step global model from Müller *et al.*, 1992) were explored because the chemical reaction section was the only part of the numerical model which can be adjusted to fit the model to the measured data.

6.1 Conclusions

The following conclusions were drawn:

1. ***n*-Paraffin fuels:** At the highest temperature of experiments (973 K), *n*-paraffins showed a strongly dependence on pressure, in which ignition delay times decreased monotonically with pressure. However, at lower temperatures and at elevated pressure

more complex ignition behaviour was clearly evident. Over a large range of pressures and temperatures, two distinct ignition times could be obtained at given operating conditions. The measured points seemed to organize themselves into two branches, one of slow ignition delay times and the other faster ones. High to low temperature ignitions performed under increasing pressures revealed more of these "twinned" ignition delayed times at the higher pressure regions. At these pressure regions, the pressure dependence of ignition delay time becomes less apparent. It is believed that this is an indication of the existence of two different possible reaction pathways, probably associated with two-stage ignition.

2. **Aromatic Fuels:** In contrast to the *n*-paraffins, the aromatics showed no or very little dependence of ignition delay on pressure, and in fact sometimes showed, surprisingly, a slight increase of ignition delay with pressure. Model reaction rate parameters derived from the data showed that aromatics have a much lower (although still positive) dependence of reaction rate on pressure than the *n*-paraffin family. Experimental results for aromatics showed no evidence of "twinned" data points. This corresponds to the fact from the literature that aromatics do not undergo two-stage ignition. It is also evidence that the twinned data points are not simply the result of deficiencies in experimental techniques.
3. **Cycloparaffin fuels:** The only cycloparaffin tested, decalin, resembled the ignition behaviour with respect to temperature and pressure of *n*-paraffins.
4. **Binary mixture fuels:** The ignition behaviour is governed by the more volatile of the pure fuel components. For mixtures of similar boiling points, the ignition behaviour resembled more closely that of the more reactive component.
5. **Reaction rate models:** The Westbrook and Dryer model (with modified reaction rate parameters) reproduced the data at 1 atm and at 973 K reasonably well for the *n*-paraffin fuels and the cycloparaffin. However, the model did not fit the low temperature ignition data. The Müller *et al.* model, which was applied only to *n*-

paraffin fuels and decalin, gave poorer model fits to 1 atm data and to the pressure dependence at 973 K. In the lower temperature region where most of the "twinned" points occurred, the MPL model followed roughly the trend of the faster ignition times.

6. **Binary mixture models:** Of the two simple mixture models proposed for determining mixture reaction rates (linear combination of pure component rates or linear combination of pure component rate parameters), both numerical models gave reasonable approximations to the data. However, neither model fitted the data very well.
7. **Experimental Significance:** This work was only the second experimental investigation of static droplet ignition under pressure, and it was the first to test fuels other than *n*-paraffins or to deal with mixtures. The most important findings of this work were the disclosure of the two distinct ignition delay times at particular pressures and temperatures and the unusual behaviour of the aromatics under pressure.

In summary, the ignition behaviour of hydrocarbons under pressure appear to be an extremely complex process comprising many reactions, and to model these reactions with a simple reaction description is not adequate. Therefore, more sophisticated models are necessary to better predict hydrocarbon ignition under pressure.

6.2 Recommendations

1. **Chemical reaction modelling:** Clearly the model results have demonstrated that although single and two-step rate models can simulate some of the experimental data, the current models are not capable of making reliable predictions of ignition delay times of hydrocarbons under pressure. Therefore, it is a recommendation that a more detailed and complex reaction model is required. For starters, implementation of the full Müller *et al.* model would be interesting to predict two-stage to one-stage ignition behaviour. The complexity of this model would be substantial, requiring a kinetics solver, and the introduction of several chemical species into the model and not just fuel, oxygen, and air as in the current description.
2. **Higher pressure ignition time data:** Limitations in the apparatus prevented measurements beyond pressures of 18 atm at temperatures as low as 773K. Data at higher pressures are necessary to confirm the phenomena discovered in this research. It is recommended that an improved furnace design may lower heat losses to permit experiments to be conducted at the pressures desired.
3. **Mixture modelling:** Experiments and modelling on mixtures should be conducted under conditions which produce "twinned" ignition times in the pure components.

REFERENCES

Bathie, W. W., "Fundamentals of Gas Turbines", John Wiley and Sons, New York, NY (1984).

Benson, R. S., and N. D. Whitehouse, "Internal Combustion Engines", Pergamon Press, New York, NY (1979).

Bergeron, C. A., and W. L. H. Hallett, "Auto-ignition of Single Droplets of Two-component Liquid Fuels", Combust. Sci. and Tech. **65**, 181-194 (1989a).

Bergeron, C. A., and W. L. H. Hallett, "Ignition Characteristics of Liquid Hydrocarbon Fuels as Single Droplets", Can. J. Chem. Eng. **67**, 142-149 (1989b).

Canada, G. S., and G. M. Faeth, "Fuel Droplet Burning Rates at High Pressure", 14th Symp. (Int.) on Combustion, 1345-1354 (1972).

Canada, G. S., and G. M. Faeth, "Combustion of Liquid Fuels in a Flowing Combustion Gas Environment at High Pressures", 15th Symp. (Int.) on Combustion, 419-428 (1974).

Curtis, E. W., and P. V. Farrell, "A Numerical Study of High Pressure Droplet Vaporization", Combustion and Flame **90**, 85-102 (1992).

Drisdelle, L., "The Effects of Convection on the Auto-ignition of Liquid Droplets", M. Eng. Thesis, Dept. of Chemical Eng., University of Ottawa, (1990).

El-Wakil, M. M., and M. I. Abdou, "The Self-ignition of Fuel Drops in Heated Air Streams I - Experimental Data", Fuel **45**, 177-188 (1966).

El-Wakil, M. M., and M. I. Abdou, "The Self-ignition of Fuel Drops in Heated Air Streams II - Physical Ignition Delay", Fuel **45**, 189-205 (1966).

Faeth, G. M., D. P. Dominicis, J. F. Tulpinsky, and D. R. Olson, "Supercritical Bipropellant Droplet Combustion", 12th Symp. (Int.) on Combustion, 9-18 (1972).

Faeth, G. M., and D. R. Olson, "The Ignition of Hydrocarbon Fuel Droplets in Air", Soc. of Auto Engineers Paper No. 680465 (1968).

Goodger, E. M., and A. F. M. Eissa, "Spontaneous Ignition of Falling Droplets in the Cranfield Pressure Rig", J. of the Inst. of Energy **60**, 199-208 (1987).

Goodger, E. M., and A. F. M. Eissa, "Spontaneous Ignition Research: Review of Experimental Data", J. of the Inst. of Energy **60**, 84-94 (1987).

Hall, A. R., and J. Diederichsen, An Experimental Study of the Burning of Single Drops of Fuel in Air at Pressures up to Twenty Atmospheres", 4th Symp. (Int.) on Combustion, 837-846 (1953).

Hallett, W. L. H., and M. A. Ricard, "Calculations of the Auto-ignition of Liquid Hydrocarbons Mixtures as Single Droplets", Fuel **71**, 225-229 (1992).

Halstead, M. P., L. J. Kirsch, and C. P. Quinn, The Auto-ignition of Hydrocarbons Fuels at High Temperatures and Pressures - Fitting of a Mathematical Model", Combustion and Flame **30**, 45-60 (1977).

Hsieh, K. C., J. S. Shuen, and V. Yang, "Multi-component Droplet Vaporization in a High Pressure Environment", The Combustion Institute (Central States Section). 1988 Spring Technical Meeting, Indianapolis, Indiana, 27-34 (1988).

Jin, J. D., and G. L. Borman, "A Model for Multi-component Droplet Vaporization at High Ambient Pressures", Soc. of Auto Engineers Paper No. 850264 (1985).

Kadota, T., and H. Hiroyasu, "Evaporation of a Single Droplet at Elevated", Bulletin of the JSME **19**, No. 138, 1515-1521 (1976).

Kadota, T., H. Hiroyasu, and H. Oya, "Spontaneous Ignition Delay of a Fuel Droplet in High Pressure and Temperature Gaseous Environments", Bulletin of the JSME **19**, No.130, 437-445 (1976).

Kadota, T., H. and Hiroyasu, "Combustion of a Fuel Droplet in Supercritical Gaseous Environments", 18th Symp. (Int.) on Combustion, 275-282. (1980).

Kumagai, S., "Combustion of a Fuel Sprays", 6th Symp. (Int.) on Combustion, 668-674 (1956).

Lafrenière, J. A., "Unpublished measurements", Dept. of Mechanical Eng., University of Ottawa, (1989).

Lazar, R. S., and G. M. Faeth, "Bipropellant Droplet Combustion in the Vicinity of the Critical Point", 13th Symp. (Int.) on Combustion, 801-811 (1970).

Lee, H. S., and A. C. Fernandez-Pello, "A Model of Diffusionally Controlled Near and Supercritical Droplet Vaporization", The Combustion Institute (Central States Section) 1986 Spring Technical Meeting, Cleveland, Ohio, May 5-6 (1986).

Lefebvre, A. H., "Gas Turbine Combustion", Hemisphere Publishing Corporation, McGraw-Hill Book Company, New York, NY (1983).

Manrique, J. A., and G. L. Borman, "Calculations of Steady-state Droplet Vaporization at High Ambient Pressures", Int. J. of Heat and Mass Transfer **12**, 1081-1095 (1969).

Marchand, C., "Unpublished measurements", Dept. of Chemical Eng., University of Ottawa, (1995).

Matlosz, R. L., S. Leipziger, and T. P. Torda, "Investigation of Liquid Drop Evaporation in a High Temperature and High Pressure Environment", Int. J. of Heat and Mass Transfer **15**, 831-850 (1972).

Müller, U. C., N. Peters, and A. Liñán, "Global Kinetics for *n*-Heptane Ignition at High Pressure", 24th Symp. (Int.) on Combustion, 777-784 (1992).

Mullins, B. P., "Development of a Combustion Test Rig for Measuring the Ignition Delay of Fuels", Fuel **32**, 218-223 (1953).

Mullins, B. P., "Studies on the Spontaneous Ignition of Fuels Injected into a Hot Air Stream - Ignition Delay Measurements on Hydrocarbons", Fuel **32**, 363-379 (1953).

Mullins, B. P., and S. J. Penner, "Explosions and Detonations, Flammability and Ignition", AGARDograph **31**, 192-217 (1959).

Natarajan, R., and T. A. Brzustowski, "Some New Observations on the Combustion of Hydrocarbon Droplets at Elevated Pressures", Combust. Sci. and Tech. **2**, 259-269 (1970).

Pischinger, F., U. Reuter, and E. Scheid, "Self-ignition of Diesel Sprays and Its Dependence on Fuel Properties and Injection Parameters", J. of Eng. for Gas Turbines and Power **110**, 399-404 (1988).

Reid, R. C., J. M. Prausnitz, and T. K. Sherwood, "The Properties of Gases and Liquids", 4th edition, McGraw-Hill Inc., New York, NY (1976).

Rosner, D. E., "On Liquid Droplet Combustion at High Pressure", AIAA Journal **5**, No. 1, 163-166 (1967).

Rosner, D. E., and W. S. Chang, "Transient Evaporation and Combustion of a Fuel Droplet Near its Critical Temperature", Combust. Sci. and Tech. **7**, 145-158 (1973).

Ruszalo, R., and W. L. H. Hallett, "A Model for the Auto-ignition of Single Liquid at High Pressure", Combust. Sci. and Tech. **86**, 183-197 (1992).

Ryan, T. W., and B. Stapper, "Diesel Fuel Ignition Quality as Determined in a Constant Volume Combustion Bomb", Soc. of Auto Engineers Paper No. 870586 (1987).

Salooja, K. C., "Studies of Combustion Processes Leading to Ignition of Aromatic Hydrocarbons", Combustion and Flame **9**, 121-129 (1965).

Sangiovanni, J. J., "A Model for the Non-steady Ignition and Combustion of a Fuel Droplet", Evaporation and Combustion of Fuels, J.T. Zung editor, Advances in Chemistry Series **166**, 27-53 (1978).

Satcunanathan, S., "Spontaneous Ignition of Liquid Fuel Droplets Falling Through a Hot Air Column", Ind. Eng. Chem. Process Des. Develop. **9**, 359-362 (1970).

Satcunanathan, S., "Ignition Delay of Individual Liquid Fuel Droplets", Ind. Eng. Chem. Process Des. Develop. **10**, 297-304 (1971).

Sato, J., M. Tsue, M. Niwa, and M. Kono, "Effects of Natural Convection on High Pressure Droplet Combustion", Combustion and Flame **82**, 142-150 (1990).

Savery, W., and G. L. Borman, "Experiments on Droplet Vaporization at Supercritical Pressures", AIAA Paper No. 70-6 (1970).

Shuen, J. S., V. Yang, and C. C. Hsiao, "Combustion of Liquid Fuel Droplets in Supercritical Conditions", Combustion and Flame **89**, 299-319 (1992).

Spalding, D. B., "Theory of Particle Combustion at High Pressure", ARS Journal, 828-835 (1959).

Talley, D. G., and S. C. Yao, "A Semi-empirical Approach to Thermal and Composition Transients Inside Vaporizing Fuel Droplets", 21th Symp. (Int.) on Combustion, 609-616 (1986).

Tong, A. Y., and W. A. Sirignano, "Multi-component Droplet Vaporization in a High Temperature Gas", Combustion and Flame **66**, 221-235 (1986).

Weast, R. C. (Editor), and M. J. Astle (Associate Editor), "CRC Handbook of Chemistry and Physics", CRC Press Inc, F-65 (1982).

Westbrook, C. K., and F. L. Dryer, "Simplified Reaction Mechanisms for the Oxidation of Hydrocarbon Fuels in Flames", Combust. Sci. and Tech. **27**, 31-43 (1981).

Wieber, P. R., "Calculated Temperature Histories of Vaporizing Droplets to the Critical Point", AIAA Journal **1**, No. 12, 2764-2770 (1963).

APPENDICES

As an input to the ignition model, properties for isobutylbenzene had to be computed using standard correlations in Reid *et al.* (1976). Properties for all other fuels were already in the existing data banks of the model.

Appendix 1 - Property calculations for liquid hydrocarbon fuels

SAMPLE CALCULATIONS[4] (fuel: isobutylbenzene)

Rihani and Doraiswamy's group contributions for ideal-gas heat capacity (cal/mol·K):

group	no.	a	b	c	d
$cb-(H)$	5	-1.4572	$.915\times10^{-2}$	-1.233×10^{-5}	2.985×10^{-9}
$cb-(C)$	1	-1.3883	$.516\times10^{-2}$	-1.069×10^{-5}	2.659×10^{-9}
$c-(C)_2(H)_2$	1	0.3945	2.136×10^{-2}	-1.197×10^{-5}	2.596×10^{-9}
$c-(C)_3(H)$	1	-3.5232	3.416×10^{-2}	-2.816×10^{-5}	8.015×10^{-9}
$c-(C)_3(H)$	2	0.6087	2.143×10^{-2}	-8.520×10^{-6}	$.135\times10^{-8}$
		$\sum$no.×a	$\sum$no.×b	$\sum$no.×c	$\sum$no.×d
		-10.586	2.093×10^{-1}	-1.295×10^{-4}	5.090×10^{-8}

$$\therefore\ C_{P,g} = -10.586 + 2.093\times10^{-1}(T) - 1.295\times10^{-4}(T^2) + 5.090\times10^{-8}(T^3)\ \text{cal/mol·K.}$$

[4]All calculations and property values for the hydrocarbon fuels were taken from Reid *et al.* (1976).

Compressibility factor: $z_c = \frac{P_c V_c}{R T_c} = \frac{31\ \text{atm} \cdot \frac{481.8\ \text{cm}^3}{\text{gmol}} \cdot \frac{1000\ \text{l}}{\text{m}^3} \cdot \frac{\text{m}^3}{100^3\ \text{cm}^3}}{\frac{0.0820562\ \text{l} \cdot \text{atm}}{\text{gmol} \cdot \text{K}} \cdot 650\ \text{K}} = 0.280$

Luria and Benson's group contributions for liquid heat capacity (cal/mol·K):

group	no.	a	b	c	d
cb – (H)	5	-1.842	5.778×10^{-2}	-1.716×10^{-4}	$.995 \times 10^{-7}$
cb – (C)	1	28.807	-2.824×10^{-1}	9.779×10^{-4}	-1.103×10^{-6}
c – $(C)_2(H)_2$	1	-1.383	7.049×10^{-2}	-2.063×10^{-4}	2.269×10^{-7}
c – $(C)_3(H)$	1	2.489	-4.617×10^{-2}	3.181×10^{-4}	-4.565×10^{-7}
c – $(C)_3(H)$	2	8.459	2.113×10^{-3}	-5.605×10^{-5}	$.723 \times 10^{-7}$
		$\sum$no.×a	$\sum$no.×b	$\sum$no.×c	$\sum$no.×d
		37.621	3.505×10^{-2}	$.196 \times 10^{-4}$	9.500×10^{-9}

$\therefore\ C_{P,l} = 37.621 + 3.505 \times 10^{-2}(T) + 1.196 \times 10^{-4}(T^2) + 9.500 \times 10^{-9}(T^3)$ cal/mol·K.

Verma-Doraiswamy's group contributions for heat of formation @298 K (J/kg):

group	no.	dH°_{f298}	group	no.	dH°_{f298}
cb – (H)	5	3.27	$(C)(O)_2$	10	-393.9
cb – (C)	1	5.55	$(H)_2(O)$	7	-285.8
c – $(C)_2(H)_2$	1	-4.94	$(C)_{10}(H)_{14}$	1	-23.40
c – $(C)_3(H)$	1	-1.29			
c – $(C)_3(H)$	2	-10.25			
c6 ring correction		-0.76			
		$\sum$no.×dH°_{f298}	Heat of reaction = 4.4050×10^7 J/kg		

Heat of formation =-23.40 kJ/mol Heat of combustion = -4.4050×10^7 J/kg

Chen method for enthalpy of vaporization at normal boiling point (J/kg):

$T_c = 650.0$ K $T_{br} = T_b / T_c = 445.9 / 650.0 = 0.686$ $P_c = 31.0$ atm

$$dH_{vb} = \frac{1.987 \cdot T_c \cdot T_{br}(3.978 \cdot T_{br} - 3.938 + 1.555\ln(P_c))}{1.07 - T_{br}} = 297.24 \times 10^3\ \text{J/kg}$$

Chueh and Swanson 's group contributions for liquid heat capacity (J/kg·K):

$$C_{P,l@20°C} = 5(-CH=) + 1(--C=) + 1(-CH_2) + 1(--CH-) + 2(--CH_3) + 2.5$$

$$C_{P,l@20°C} = 5(5.3) + 2.9 + 7.26 + 4.4 + 2(8.8) + 2.5 = 1906.49 \text{ J / kg} \cdot \text{K}$$

All other fuel properties are read off tables and charts in Reid *et al.* (1976).

Appendix 2 - Furnace and chamber purge calculations

The purpose of this calculation is to determine the total purging air quantity required to make up most of the oxygen that was consumed by the ignition experiments. The basis is to take a complete stoichiometric combustion of two 1.5 mm droplets of a hydrocarbon fuel. Two droplets are taken because they represent the ignition of a fuel and an alcohol droplet.

The strategy of purging is to purge the furnace gases first, then exhaust the gases through the vessel. A mass balance on products in the furnace with the vessel in series

$$m_F \frac{dY_F}{dt} = -\dot{m} Y_F, \qquad [20]$$

solving at $Y_F = Y_{F0}$ at $t = 0$

$$Y_F = Y_{F0} \exp\left(\frac{-\dot{m}t}{m_F}\right); \qquad [21]$$

followed by a mass balance on products in the vessel

$$m_F \frac{dY_V}{dt} = \dot{m}\left(Y_{F0} \exp\left(\frac{-\dot{m}t}{m_F}\right) - Y_V\right) \qquad [22]$$

solving at $Y_V = 0$ at $t = 0$

$$Y_V = \frac{m_F Y_{F0}}{m_V + m_F}\left(\exp\left(\frac{-\dot{m}t}{m_F}\right) - \exp\left(\frac{-\dot{m}t}{m_V}\right)\right). \qquad [23]$$

Equation [21] is the lumped sum mass fraction of products in the furnace and Equation [23] is the lumped sum mass fraction of products in the vessel after furnace purging.

If the vessel was to be purged alone, from Equation [21] solving at $Y_V = Y_{V0}$ at the end of furnace purging

$$Y_v = Y_{v0} \exp\left(\frac{-\dot{m}t}{m_v}\right). \qquad [24]$$

Equations [21], [23], and [24] give the mass fractions of products in either the furnace and/or vessel with respect to time. Figure A.1 shows the furnace and vessel oxygen mass with respect to purge time of each compartment. The total void volume of the apparatus is 0.037 m^3, the purge flow rate is 64 l/min, and the air density and molecular weight are respectively 1.204 kg/m^3 and 28.97 g/mol.

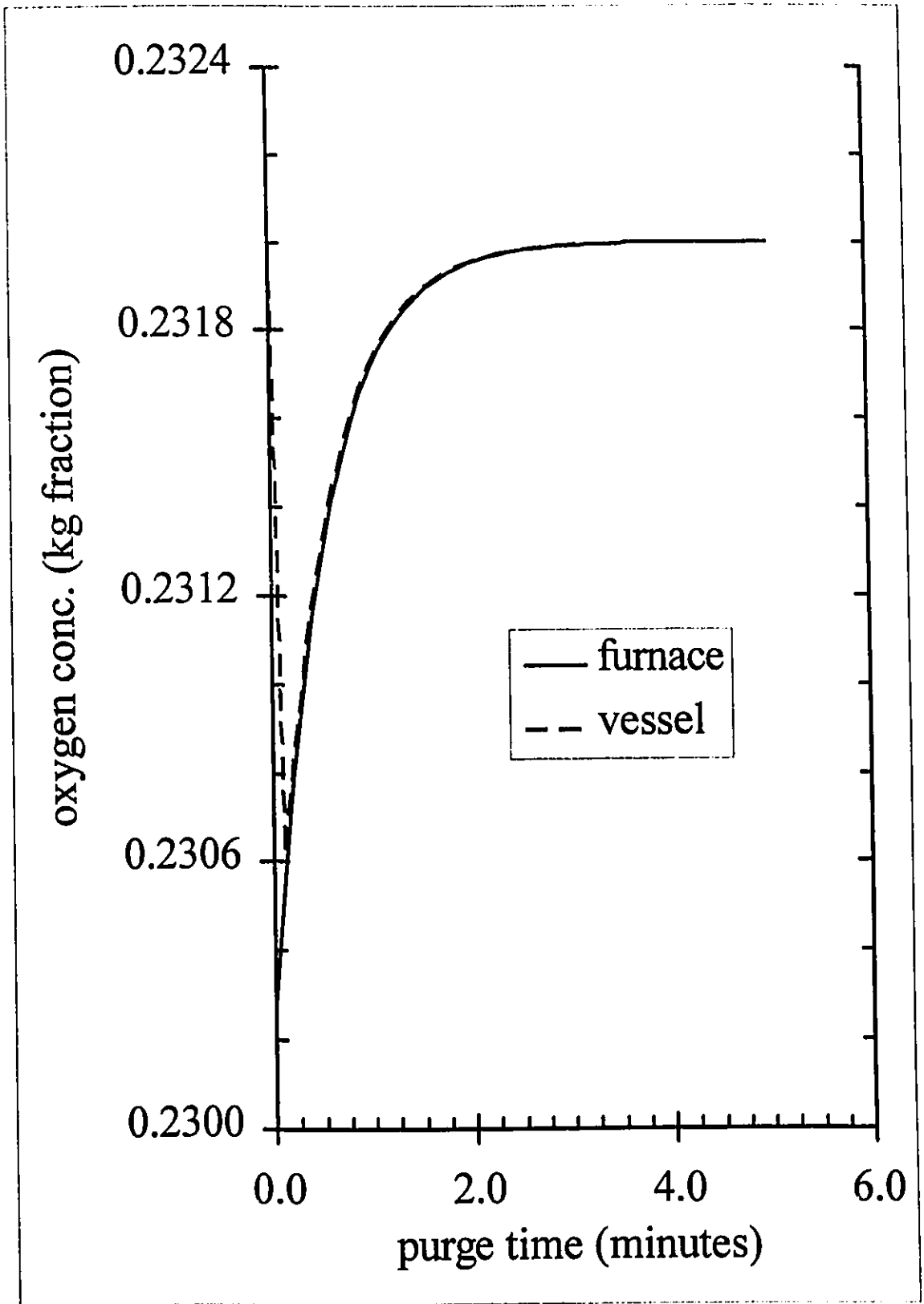

Figure A.1: Oxygen mass fraction versus purge time at 1 atm and an ambient chamber temperature of 20°C.